SHIRSHOV INSTITUTE OF OCEANOLOGY

CRUISE REPORT No. 51

RV *AKADEMIK IOFFE* CRUISE 3 June – 12 July 2016

North Atlantic Repeat Hydrography of WOCE section along 59.5 N and sill sections between Iceland - Faroe Islands and Shetlands

Principal Scientist **S. Gladyshev**[1]

2016

Shirshov Institute of Oceanology
36 Nakhimovskii prospect
Moscow 117997 RUSSIA
Tel: +7(495) 719 0255 Fax: +7(499) 124 6342
Email :sgladyshev@ocean.ru

[1]**Shirshov Institute of Oceanology**

DOCUMENT DATA SHEET

AUTHOR	*PUBLICATION DATE*
GLADYSHEV, S	2016
TITLE	
RV ***Akademik Ioffe*** Cruise 51 , 3 June – 12 July 2016.	
REFERENCE	
Shirshov Institute of Oceanology, Akademik Ioffe Cruise Report, No. 51, 84pp. tables & figs.	

ABSTRACT

RV ***Akademik Ioffe*** Cruise 51 was a contribution to the Russian CLIVAR and WORLD OCEAN Research Programmes. CTD section was designed to enable the ocean circulation in the Subpolar gyre of the North Atlantic to be mapped and in particular the course of the North Atlantic, Irminger and East Greenland Currents within the region to be determined. The main goal is to continue annual monitoring of the North Atlantic large-scale circulation and climate changes in the North Atlantic. The sections over North Atlantic sills between Iceland - Faroe Islands and Shetlands were carried out to estimate variability of the meridional fluxes and water mass exchange between the North Atlantic and the Arctic Ocean.

During the cruise 27 sta. were made in Labrador Sea.

KEYWORDS

CRUISE 51 2016, *AKADEMIK IOFFE,* **CLIVAR, TRANSATLANTIC SECTION, EAST GREENLAND CURRENT, IRMINGER BASIN, NORTH ATLANTIC SUBPOLAR GYRE, CLIVAR, CTD OBSERVATIONS, LADCP, VMADCP, SILLS, LABRADOR SEA**

ISSUING ORGANISATION

Shirshov Institute of Oceanology
36 Nakhimovskii prospect
Moscow 117997 RUSSIA

Director: Academician Robert Nigmatulin

Copies of this report are available from: **Department of Marine Operations,** Tel: +7(495)7190255 Fax: +7(499)124 6342

Email: sgladyshev@**ocean.ru**

Contents
Scientific Personnel

Scientific Personnel

GLADYSHEV, S.	Principal Scientist	Shirshov
PYATAKOV, V.	Chief of CTD group	Shirshov Atlantic Branch
GLADYSHEV, V.	CTD, LADCP, Sampling	Shirshov
ZAPOTYL'KO, V.	CTD, LADCP	Shirshov
AGARKOV, A.	CTD, LADCP, Sampling	Shirshov
KRYUKOV, D.	CTD, LADCP, Sampling	Shirshov Atlantic Branch
TUZOV, F.	CTD, LADCP, Sampling	MGU
LUKASHIN, S.	Winch	Shirshov Atlantic Branch
		Shirshov
BULYCHEV, V.	Oxygen	Shirshov Atlantic Branch
AVDIEVA, A.	Nutrients	Shirshov
ALYUKAEVA, A.	Chief of Chemistry group	Shirshov
BUBNOVA E.	Nutrients	Shirshov Atlantic Branch
PARFENOVA, M.	Sampling	
SANTANA, M.	CO_2	University of Las Palmas
GONZÁLEZ, M.	CO_2	University of Las Palmas
GONZÁLEZ, K.	CO_2	University of Las Palmas
ALAMO, A.	CO_2	University of Las Palmas
KLYUVITKIN, A.	Ghief of geological group	Shirshov
POLITOVA, N.	Suspended Sediment matter	Shirshov
NOVICHKOVA, E.	Bottom sediment treatment	Shirshov
NOVIGATSKII A.	Moorings, Multi corer	Shirshov
KOZINA, N.	Bottom sediment treatment	Shirshov
BUDKO, D.	Moorings, Grab corer	Shirshov
SAVVICHEV, A.	Microbiology	Shirshov
ISACHENKO, S.	Geological Winch	Shirshov
AMBROSIMOV, A.	Moorings, Gravity corer	Shirshov
TIKHONOVA, A.	Foraminifer analysis	Shirshov
STARODYMOVA, D.	Bottom sediment treatment	Shirshov
BULOKHOV, A.	Moorings, Gravity Corer	Shirshov

1. CRUISE NARRATIVE

1.1 Cruise Details

Expedition Designation: R/V ***Akademik Ioffe*** Cruise 51, RUSSIA CLIVAR

Principal Scientist: Dr. Sergey V. Gladyshev (Shirshov).

Ship: RV ***Akademik Ioffe.***

Ports of Call: Gdansk (Poland) to Halifax (Canada).

Cruise Dates: 3th June to 12th July 2015.

1.2 Cruise Summary

1.2.1 Cruise Track and Stations

The cruise track with station positions is shown in **Fig. l**. Only small volume samples were taken, details are listed in **Table 1**.

1.2.2. Equipment

The principal instruments used during the cruise were a SBE 9P-1277 CTD with dual temperature and conductivity sensors (SBE 3 SN 03P6082, SBE 4 SN 044580, SBE 3 SN 03P6088, SBE 4 SN 044581), oxygen sensor (SBE 43, SN 433321), fluorimeter-turbidity sensor (WET Labs, SN 4237), Benthos altimeter model PSA-900D, LADCP WHS-300 kHz down-looking (S/N 6393), LADCP WHS-300 kHz up-looking (S/N 14151). These were mounted together with a multisampler Carousel SBE 32 equipped with 22 5-litre Niskin bottles. Upon recovery each bottle was sampled in turn for dissolved oxygen, nutrients, salinity. All sampling was done on deck. Currents were measured using vessel mounted ADCP (VMADCP) TRDI OS38 kHz (S/N 1185) installed at the central point of the ship hall.

Navigation information was provided by a Trimble SPSx50/SPSx51 - Modular GPS receiver and every second was recorded on the PC. Additional measurements were made with an ELAC 12 kHz, Aanderaa meteorological package.

1.2.3 Sampling

Nominal depths sampled were: bottom, 3100, 3000, 2750, 2500, 2250, 2000, 1750, 1500, 1250, 1100, 1000, 900, 800, 700, 600, 500, 400, 300, 200, 150, 100, 50, 30, 20, 10 m. On deep casts fewer shallow and intermediate bottles were fired. The actual bottle depths are shown in **Fig. 2**.

1.2.4 Number of Stations Occupied

203 stations (91 casts) were occupied during the cruise along North-Atlantic sills, transatlantic section along 59.5 N and in the Labrador Sea (**Fig. l**).

1.3 Scientific Objectives

The cruise objectives were to:

1. To complete a CTD section from the Great Britain to Greenland.
2. To complete CTD sections from Shetlands to Iceland
3. To carry out section in the Labrador Sea
4. To survey the North Atlantic Subpolar Gyre with high-resolution CTD and LADCP/VMADCP data to determine the circulation and meridional fluxes.

1.4 Narrative

1.4.1 Introduction

The Meridional overturning circulation (MOC) in the North Atlantic is one of the main drivers of the widely known global oceanic "conveyor belt" – an important element of the Earth's climate system [e.g., van Aken, 2007]. Warm upper-ocean waters transported northward by the North Atlantic Current release heat to the atmosphere, gain density due to cooling and eventually sink in the subpolar North Atlantic and adjacent Arctic seas thereby generating the return southward flow of colder waters at depths (**Fig. 3**) [Dickson and Brown, 1994; Koltermann et al., 1999]. Temporal variability of the large-scale circulation and associated heat transport in the subpolar North Atlantic is one of the principal factors behind the high-latitude climate anomalies in the Northern Hemisphere.

Progress in understanding the causes of the ongoing climate change and forecasting climate variability in the Arctic and over European part of Russia for the next decades require reliable observation-based estimates of the variability of the North Atlantic circulation and the Atlantic–Arctic heat and freshwater fluxes, as well as elucidation of the underlying mechanisms. In a number of recent studies, radical changes in the thermohaline regime and large-scale circulation in the Atlantic Ocean have been suggested to occur under global warming. For instance, the long-term freshening of the subpolar North Atlantic deep waters since the mid-1960s [Dickson et al., 2002] has been (cautiously) attributed to climate change-related factors [Curry et al., 2003; Hansen et al., 2004]. Hypothetically, under global warming, an increased evaporation in the tropics and increased precipitation at high latitudes, coupled with an intensified melting of Arctic ice, lead to the upper-ocean freshening in the regions of deep water formation and, hence, to the deep water freshening in the Atlantic Ocean. At the same time, milder winters along with the upper-ocean freshening lead to a decrease in the deep water production rates, which results in slowing of the Atlantic Meridional Overturning Circulation [e.g., Hansen et al., 2004; Bryden et al., 2005].

To better understand the past and present changes in the ocean-atmosphere dynamical system, as well as their causes and consequences, data on the full-depth oceanic variability are needed. An indispensable effective tool for assessing the large-scale circulation and thermohaline changes in the deep ocean and investigating mechanisms governing these changes are repeated full-depth transoceanic observations.

Since 1997, the P.P. Shirshov Institute of Oceanology has carried out the long-term monitoring of the North Atlantic circulation and water mass properties in the 59.5°N hydrographic section between Cape Farewell (Greenland) and Scotland (**Fig. 3**). Since 2002, the section has been repeated yearly on board the Russian research vessels, providing high precision data on temperature, salinity, oxygen and nutrients concentrations, and current velocities in the entire water column – “from shore to shore”, from the sea surface to the bottom. In 2011, in addition to annual repeat measurements at 59.5°N, the P.P. Shirshov Institute of Oceanology started full-depth repeat observations of the oceanic exchange between the Atlantic and Arctic oceans through the straits between Greenland, Iceland, Faeroe and Shetland Islands (**Fig. 3**). The full-depth observations – of the same oceanic quantities as at 59.5°N – are performed in the straits from research vessels twice a year, in summer and fall. Based on the unique data set thus

collected, a number of fundamental findings have already been achieved. Below, we briefly summarize the main subjects and results of our research.

The 59.5°N transatlantic section (**Fig. 3**) was designed for monitoring the large-scale circulation and thermohaline / chemical properties of oceanic waters at the northern periphery of the NA – the region where the warm upper-ocean waters are transformed by deep convection and mixing into the colder intermediate and deep waters – the Labrador Sea Water (LSW), Iceland Scotland Overflow Water (ISOW) and Denmark Strait Overflow Water (DSOW) (**Fig. 3**) – transported southward in the lower limb of the Atlantic MOC. Hydrographic data collected at 59.5°N along with those obtained within the framework of the kindred projects, primarily the French OVIDE (http://www.ifremer.fr/lpo/ovide), and historical data sets have been used for studying the dense water production [Falina et al., 2007; Falina et al., 2012], decadal temperature and salinity changes in the intermediate–deep water column [Sarafanov et al., 2007; Sarafanov et al., 2008; Sarafanov et al., 2010b], causes of these changes [Sarafanov, 2009; Sarafanov et al., 2010b], the mean state [Sarafanov et al, 2012] and long-term variability of the large-scale circulation in the region [Sarafanov et al., 2009; Sarafanov et al, 2010a; Våge et al., 2011].

1.4.2 Deep convection in the Irminger Sea

The oxygen data collected in 1997 in the northern North Atlantic in several sections ending nearby the southern tip of Greenland provided the observation-based support for the hypothesis [Pickart et al., 2003] that winter convection in the Irminger Sea may penetrate deep into the LSW layer (1000 – 2000 m) thus causing local renewal of this water mass. A separate lateral maximum of oxygen concentrations in the deep LSW layer was detected east of Cape Farewell (59.5°N, 36–40°W): the concentrations increased (by ~0.1 ml/l) from the Labrador Sea eastern edge toward the Irminger Sea (**Fig. 4**) rather than the reverse, as would be expected if LSW observed in the Irminger Sea interior in 1997 were solely of advective origin [Falina et al., 2007].

1.4.3. Reversal of the deep-water freshening

The LSW and Nordic Seas overflow-derived deep waters, ISOW and DSOW, freshened in the northern North Atlantic during the last three–four decades of the 20th century [Dickson et

al., 2002]. Between the 1960s and 1990s, the water column in the region freshened on average by about 0.03 [Curry et al., 2003].

The long-term freshening reversed in the mid-1990s [Sarafanov et al., 2007; Sarafanov et al., 2008; Sarafanov et al., 2010b]. The salinification (and warming) of the intermediate and deep waters since the mid-1990s (**Fig. 5**) was much more intense than the preceding freshening. Over nearly a decade (1997–2006), temperature / salinity in the intermediate–deep water column ($\sigma_0 \geq 27.45$, depths > 500–1000 m) at 59.5°N increased by ~0.3°C / 0.03–0.04 [Sarafanov et al., 2008].

In the Irminger Sea, the long-term freshening in the deep water column (σ_0>27.80, depths > ~2000 m) reversed in the early 2000s [Sarafanov et al., 2010b]. The observed freshening reversal was a lagged consequence of the persistent ISOW salinification that occurred upstream, in the Iceland Basin, after 1996 due to salinification of the northeast Atlantic waters entrained into the overflow. It was demonstrated [Sarafanov et al., 2010b] that the entrainment salinity increase was associated with the North Atlantic Oscillation (NAO)-induced weakening and contraction of the Subpolar Gyre and corresponding northwestward advance of subtropical waters that followed the NAO decline in the mid-1990s and continued through the mid-2000s. Remarkably, the deep water freshening reversal was not related to changes in the overflow water salinity.

1.4.4. Deep-ocean salinity changes and the NAO

Close relationship between the thermohaline properties of the northern North Atlantic intermediate and deep waters and the winter NAO index on a decadal time scale ($r^2 \approx 0.65$, 1950s–2000s, **Fig. 6b** and **6c**) was revealed [Sarafanov, 2009] from the observation-based salinity time series for LSW in the Labrador Sea [Yashayaev, 2007] and ISOW in the Iceland basin [Boessenkool et al., 2007; Sarafanov et al., 2007]. Persistent NAO decline (amplification) leads to warming and salinification (cooling and freshening) in the intermediate–deep water column.

An explanation for the close link between the NAO and the coherent decadal changes in the intermediate and deep water properties in the region was proposed [Sarafanov, 2009]. The two factors dominate this link (**Fig. 6d**): (i) intensity of convection in the Labrador Sea

controlling injection of relatively cold fresh waters into the intermediate layer and (ii) zonal extent of the Subpolar Gyre that regulates the relative contributions of cold fresh subpolar waters and warm saline subtropical waters to the entrainment into the Norwegian Sea overflow south of the Iceland–Scotland Ridge and to the Atlantic inflow to the Nordic Seas. These factors act in phase leading to the observed coherent thermohaline changes in the intermediate–deep water column.

Due to weakening of the surface forcing associated with the NAO transition into neutral to low phase (1950s to mid-1960s, mid-1990s to mid-2000s), convection in the Labrador Sea weakens diminishing cold fresh water penetration into the intermediate layer. This results in warming and salinification at the intermediate depths in the Subpolar Gyre. Concurrently, the Subpolar Gyre contracts allowing northward advance of warm saline upper-ocean and intermediate subtropical waters in the northeastern North Atlantic. Northward progression of subtropical waters increases temperature and salinity at the upper intermediate levels and, correspondingly, increases temperature and salinity of the northeast Atlantic waters entrained into the Iceland–Scotland overflow along its pathway to the deep Iceland basin. As a result, temperature and salinity at the deep levels increase. The contrary changes – intensification of deep convection in the Labrador Sea and expansion of the Subpolar Gyre – caused by amplifying surface forcing (mid-1960s to mid-1990s) lead to cooling and freshening at the intermediate–deep levels. Additionally, under high-NAO conditions, deep convection may occur in the Irminger Sea potentially contributing to cooling and freshening at the intermediate (LSW) levels. The two regimes of convection and large-scale circulation corresponding to stronger (early 1990s) and weaker (mid-1960s, mid-2000s) NAO-related atmospheric forcing are schematically visualized in **Fig. 7**.

1.4.5 Deep-ocean salinity changes and climate change

There are increasing concerns that in the warmer climate, the MOC may substantially decline due to a decrease in the convective activity in the northern North Atlantic and Nordic Seas [e.g., Meehl et al., 2007]. The long-term freshening in the Nordic Seas and freshening of the northern North Atlantic deep waters in the 1960s–1990s have been considered as a likely indicator or precursor of the dramatic change in the MOC [e.g., Hansen et al., 2004]. The freshening has been attributed to a combination of factors potentially associated with the global

warming: the increasing ice melt and net precipitation at high latitudes [e.g., Curry et al., 2003]. A probable causality between the climate change and the decreasing North Atlantic deep water salinity has supported the concerns and unfavorable predictions, thus 'warming up' the reasonable scientific debate on climate change and overblown speculations in media.

Despite the long-term increase in freshwater input to the Arctic, freshening in the northern North Atlantic had reversed in the mid-1990s, as we demonstrated above. This reversal forces us to revise the hypotheses on the mechanisms behind the deep-water thermohaline anomalies. It seems doubtful that the persistent global temperature growth may lead to the opposite decadal trends (positive-then-negative-then-positive, **Fig. 6**) in the deep water salinity.

Our results [Sarafanov et al., 2008; Sarafanov, 2009; Sarafanov et al., 2010b] suggest that natural atmospheric variability over the North Atlantic plays the major role in the deep-water thermohaline variability on a decadal time scale. There are no reasons to associate the deep-water freshening in the 1960s–1990s with climate change, unless the 3-decade-long surface forcing amplification is evidently shown to be a consequence of the latter. Having said that, the net 1950s–2000s trends in the water mass salinities are negative implying that the global factors (e.g., probable intensification of hydrological cycle [Curry et al., 2003]) may act on longer time scales.

1.4.6 Decadal variability of the Deep Western Boundary Current at Cape Farewell

Recent decadal changes in the Deep Western Boundary Current (DWBC) transport southeast of Cape Farewell were assessed from hydrographic data (1991–2007, **Fig. 7a**), direct velocity measurements (2002–2006) and satellite altimetry (1992–2007). Following the approach used in earlier studies [e.g., Bacon, 1998], we first determined that the DWBC (σ_0>27.80) baroclinic transport (T_{BC}) referenced to 1000 m depth increased by ~2 Sv between the mid-1990s (1994–1997) and 2000s (2000–2007) (**Fig. 8b**) [Sarafanov et al., 2009]. In the next step, we quantified velocity changes at the reference level (1000 m) by combining estimates of the hydrography-derived velocity changes in the water column and the altimetry-derived velocity changes at the sea surface [see Sarafanov et al., 2010a]. The inferred increase in the southward velocity at 1000 m above the DWBC in 1994–2007 indicates that the increase in the DWBC absolute transport was larger but very close to the 2-Sv increase in the DWBC T_{BC}. This result along with the observed coherence of the DWBC absolute and baroclinic transport changes

between individual observations [Sarafanov et al., 2010a] imply that the DWBC absolute transport variability in the region is well represented by its baroclinic component on decadal and shorter time scales.

The historical record of the DWBC T_{BC} (1955–2007, **Fig. 8c**) updated after Bacon [1998] shows distinct decadal variability (±2–2.5 Sv) with the transport minima in the 1950s and mid-1990s, maximum in the early 1980s and moderate-to-high transport in the 2000s. The DWBC T_{BC} decadal variability is consistent with the general pattern of the recent decadal hydrographic and circulation changes in the northern North Atlantic. The DWBC T_{BC} anomalies negatively correlate (R = –0.80, 1955–2007) with thickness anomalies of the Labrador Sea Water (LSW) at its origin implying a close link between the DWBC transport southeast of Cape Farewell and the LSW production in the Labrador Sea (**Fig. 8d**). During the recent three decades (late 1970s – late 2000s), the DWBC T_{BC} changes were also in-phase with changes in the strength and zonal extent of the Subpolar Gyre [see Sarafanov et al., 2010a]. In particular, the Gyre weakening at shallow levels in the mid-1990s – mid-2000s was accompanied by the DWBC strengthening in the Irminger Sea [Sarafanov et al., 2009; Sarafanov et al., 2010a; Våge et al., 2011]. The results imply that the decadal changes in the (i) LSW production, (ii) SPG strength and (iii) DWBC transport in the Irminger Sea are linked, representing a complex coherent oceanic response to the decadal variability of the surface forcing.

1.4.7 Mean state of the full-depth circulation in the 2000s

A mean state of the full-depth summer circulation in the Atlantic Ocean in the region in between Cape Farewell (Greenland), Scotland and the Greenland-Scotland Ridge (see **Fig. 3**) was assessed by combining 2002–2008 yearly hydrographic measurements at 59.5°N, mean dynamic topography, satellite altimetry data and available estimates of the Atlantic–Nordic Seas exchange [see Sarafanov et al., 2012]. The mean absolute transports by the upper-ocean, mid-depth and deep currents and the MOC (MOCσ=16.5±2.2 Sv, at σ_0=27.55) at 59.5°N were quantified in the density space. Inter-basin and diapycnal volume fluxes in between the 59.5°N section and the Greenland-Scotland Ridge were then estimated from a box model.

The estimated meridional and diapycnal volume fluxes contributing to the MOC are schematically visualized in **Fig. 9**. The dominant components of the meridional exchange across 59.5°N are the North Atlantic Current (NAC, 15.5±0.8 Sv, σ_0<27.55) east of the Reykjanes

Ridge, the northward Irminger Current (IC, 12.0±3.0 Sv) and southward Western Boundary Current (WBC, 32.1±5.9 Sv) in the Irminger Sea and the deep water export from the northern Iceland Basin (3.7±0.8 Sv, σ_0>27.80). About 60% (12.7±1.4 Sv) of waters carried in the MOCσ upper limb (σ_0<27.55) by the NAC/IC across 59.5°N (21.1±1.0 Sv) recirculates westwards south of the Greenland-Scotland Ridge and feeds the WBC. 80% (10.2±1.7 Sv) of the recirculating NAC/IC-derived upper-ocean waters gains density of σ_0>27.55 and contributes to the MOCσ lower limb. Accordingly, the contribution of light-to-dense water conversion south of the Greenland-Scotland Ridge (~10 Sv) to the MOCσ lower limb at 59.5°N is one and a half times larger than the contribution of dense water production in the Nordic Seas (~6 Sv).

1.4.8 Cascading of dense shelf waters in the Irminger Sea

Based on the hydrographic data collected at 59.5°N, 64.3°N and 65–66°N in the western Irminger Sea in the 1990s – 2000s, an observational evidence for the deep-reaching cascading of dense shelf waters south of the Denmark Strait was found [Falina et al., 2012]. The data collected in the northwestern Irminger Sea (65–66°N) indicate that the East Greenland Current ~200 km south of the Denmark Strait occasionally carries shelf waters as dense as the overflow-derived deep waters transported by the DWBC (σ_0 > 27.80). Hydrographic traces of cascading of dense shelf waters down the East Greenland slope were found from repeat measurements at 64.3ºN, where the densest fresh plumes were observed within the DWBC (σ_0 > 27.80) (**Fig. 10**). Using the data collected at 59.5°N, we showed that the fresh 'signals' originating from the shelf can be traced in the DWBC as far downstream as the latitude of Cape Farewell, where the anomalously fresh oxygenated plumes are repeatedly observed in the ISOW and DSOW density classes.

The results of our analysis along with the results from earlier studies [e.g., Rudels et al., 1999; Rudels et al., 2002] indicate that shelf water cascading in the northern Irminger Sea is an intermittent process occurring in all seasons of the year. This implies that, despite the apparent short duration of a particular cascading event, the cumulative contribution of such events to the thermohaline variability and southward export of the deep waters in the WBC can be considerable. Our tentative estimate based on data from two synoptic surveys at ~59.5°N suggests that the transient contribution of a cascading event in the northern Irminger Sea to the DWBC transport at Cape Farewell can be as large as ~25%.

References

1. Bacon, S. (1998), Decadal variability in the outflow from the Nordic seas to the deep Atlantic Ocean, *Nature*, *394*, 871–874.
2. Dickson, R. R., and J. Brown (1994), The production of North Atlantic Deep Water: Sources, rates and pathways, *J. Geophys. Res.*, *99*, C6, 12319–12341.
3. Dickson, R., Yashayaev, I., Meincke, J., Turrell, B., Dye, S., and J. Holfort (2002), Rapid freshening of the deep North Atlantic Ocean over the past four decades, *Nature*, *416*, 832–837.
4. Boessenkool, K. P., Hall, I. R., Elderfield, H., and I. Yashayaev (2007), North Atlantic climate and deep-ocean flow speed changes during the last 230 years, *Geophys. Res. Lett.*, *34*, L13614, doi:10.1029/2007GL030285.
5. Curry, R., Dickson, R., and I. Yashayaev (2003), A change in the freshwater balance of the Atlantic Ocean over the past four decades, *Nature*, *426*, 826–829.
6. Falina, A., A. Sarafanov, and A. Sokov (2007), Variability and renewal of Labrador Sea Water in the Irminger Basin in 1991–2004, *J. Geophys. Res.*, *112*, C01006, doi: 10.1029/2005JC003348.
7. Falina A., A. Sarafanov, H. Mercier, P. Lherminier, A. Sokov, and N. Daniault (2012), On the cascading of dense shelf waters in the Irminger Sea, *J. Phys. Oceanogr.*, doi:http://dx.doi.org/10.1175/JPO-D-12-012.1 (in press)
8. Hansen, B., Osterhus S., Quadfasel D., and W. Turrell (2004), Already the day after tomorrow?, *Science*, *305*, 953–954.
9. Hurrell, J. W. (1995), Decadal trends in the North Atlantic Oscillation: regional temperatures and precipitation, *Science*, *269*, 676–679.
10. Koltermann, K. P., A. Sokov, V. Tereschenkov, S. Dobroliubov, K. Lorbacher, and A. Sy (1999), Decadal changes in the thermohaline circulation of the North Atlantic, *Deep Sea Res.*, *Part II*, *46*, 109–138, doi:10.1016/S0967-0645(98)00115-5.
11. Lherminier, P., H. Mercier, T. Huck, C. Gourcuff, F. F. Perez, P. Morin, A. Sarafanov, and A. Falina (2010), The Atlantic Meridional Overturning Circulation and the subpolar gyre observed at the A25–Ovide section in June 2002 and 2004, *Deep-Sea Res.*, *Part I*, *57*, 1374–1391, doi:10.1016/ j.dsr.2010.07.009.

12. Meehl, G. A., (2007), Global climate projections. Climate Change 2007: The Physical Science Basis, S. Solomon et al., Eds., Cambridge University Press, 747–847.
13. Pickart, R. S., Spall, M., Ribergaard, M. H., Moore, G. W. K. and R. Milliff (2003), Deep convection in the Irminger Sea forced by the Greenland tip jet, *Nature*, *424*, 152–156.
14. Rudels B., Eriksson P., Grönvall H., Hietala R. and Launiainen J. (1999), Hydrographic Observations in Denmark Strait in Fall 1997, and their Implications for the Entrainment into the Overflow Plume, *Geophys. Res. Lett.*, *26*, 1325–1328.
15. Rudels, B., E. Fahrbach, J. Meincke, G. Budeus, and P. Eriksson (2002), The East Greeenland Current and its contribution to the Denmark Strait overflow, *ICES J. Marine Science*, *59*, 1133–1154.
16. Sarafanov, A., A. Sokov, A. Demidov, and A. Falina (2007), Warming and salinification of intermediate and deep waters in the Irminger Sea and Iceland Basin in 1997–2006, *Geophys. Res. Lett.*, *34*, L23609, doi:10.1029/2007GL031074.
17. Sarafanov, A., A. Falina, A. Sokov, and A. Demidov (2008), Intense warming and salinification of intermediate waters of southern origin in the eastern subpolar North Atlantic in the 1990s to mid-2000s, *J. Geophys. Res.*, *113*, C12022, doi:10.1029/2008JC004975.
18. Sarafanov, A. (2009), On the effect of the North Atlantic Oscillation on temperature and salinity of the subpolar North Atlantic intermediate and deep waters, *ICES J. Marine Science*, *66 (7),* 1448–1454, doi:10.1093/icesjms/fsp094.
19. Sarafanov, A., A. Falina, H. Mercier, P. Lherminier, and A. Sokov (2009), Recent changes in the Greenland–Scotland overflow-derived water transport inferred from hydrographic observations in the southern Irminger Sea, *Geophys. Res. Lett.*, *36*, L13606, doi:10.1029/2009GL038385.
20. Sarafanov A., A. Falina, P. Lherminier, H. Mercier, A. Sokov, and C. Gourcuff (2010a), Assessing decadal changes in the Deep Western Boundary Current absolute transport southeast of Cape Farewell (Greenland) from hydrography and altimetry, *J. Geophys. Res.*, *115*, C11003, doi:10.1029/2009JC005811.
21. Sarafanov A., H. Mercier, A. Falina, A. Sokov, and P. Lherminier (2010b), Cessation and partial reversal of deep water freshening in the northern North Atlantic: observation-

based estimates and attribution, *Tellus*, *62A*, 80–90, doi:10.1111/j.1600-0870.2009.00418.x.

22. Sarafanov A., A. Falina, H. Mercier, A. Sokov, P. Lherminier, C. Gourcuff, S. Gladyshev, F. Gaillard, and N. Daniault (2012) Mean full-depth summer circulation and transports at the northern periphery of the Atlantic Ocean in the 2000s, *J. Geophys. Res., 117,* C01014, doi:10.1029/2011JC007572.
23. Schmitz, W. J., Jr., and M. S. McCartney (1993), On the North Atlantic Circulation, *Rev. Geophys.*, *31*, 29–49.
24. Schott, F. A., and P. Brandt (2007), Circulation and deep water export of the subpolar North Atlantic during the 1990s, *in Ocean Circulation: Mechanisms and Impacts*, *Geophys. Monograph Series*, *173*, Eds. A. Schmittner, J. Chiang, and S. Hemmings, 91–118, doi:10.1029/173GM08.
25. Sutherland, D. A., and R. S. Pickart (2008), The East Greenland Coastal Current: structure, variability, and forcing, *Prog. Oceanogr.*, *78*, 58–77, doi:10.1016/j.pocean.2007.09.006.
26. Våge K., R. Pickart, A. Sarafanov, Ø. Knutsen, H. Mercier, P. Lherminier, H. van Aken, J. Meincke, D. Quadfasel, and S. Bacon (2011a), The Irminger Gyre: circulation, convection, and interannual variability, *Deep-Sea Res. Part I*, *58*, 590–614, doi:10.1016/j.dsr.2011.03.001.
27. van Aken, H. M. (2007), The oceanic thermohaline circulation: An introduction, New York, Springer, 326 p., ISBN 978-0-387-36637-1.
28. Yashayaev, I. (2007), Hydrographic changes in the Labrador Sea, 1960–2005, *Prog. Oceanogr.*, *73*, 242–276.

.

1.5 Preliminary Results

The upper-ocean, mid-depth and deep water circulation patterns, merging the results of the present analysis with those from the earlier studies [e.g., *Macrander et al.*, 2005; *Østerhus et al.*, 2005, 2008; *Schott and Brandt*, 2007; *Sutherland and Pickart*, 2008; *Lherminier et al.*, 2010; *Våge et al.*, 2011], are schematically visualized Figures 12–14. A schematic diagram of the meridional overturning circulation in the Atlantic Ocean north of 59.5°N is displayed in Fig. 9.

The results provide the following conceptual view of the gyre / overturning circulation at the northern periphery of the Atlantic Ocean in the 2000s.

The NAC and IC collectively carry 21.1 ± 1.0 Sv of warm upper-ocean waters across 59.5°N northwards within the MOCσ upper limb ($\sigma_0 < 27.55$). About 40% of this flow forms the Atlantic Inflow to the Nordic Seas, and 60% (12.7 ± 1.4 Sv) recirculates westwards in the subpolar gyre northern limb south of Iceland to feed the WBC in the Irminger Sea. Only 20% (2.4 ± 1.2 Sv) of the recirculating NAC/IC-derived waters exits the Irminger Sea in the WBC at shallow levels ($\sigma_0 < 27.55$), while 80% (10.2 ± 1.7 Sv, a half of the NAC/IC northward flow across 59.5°N) gains density of $\sigma_0 > 27.55$ and enters the MOCσ lower limb. The resulting net southward transport in the MOCσ lower limb at the latitude of Cape Farewell is 16.5 ± 2.2 Sv, of which ~60% (~10.2 Sv) is due to light-to-dense water transformation south of the GSR.

As no dense-to-light water re-conversion is expected to occur in the subpolar gyre, the NAC/IC-derived waters, once entering the MOCσ lower limb in the Irminger Sea, will eventually contribute to the MOCz lower limb (~11 Sv at 59.5°N) at the southern margin of the subpolar region. There, at ~48°N, the MOCσ and MOCz are of nearly the same magnitude, 16 ± 2 Sv, as estimated from data collected in the 1990s [see *Schott and Brandt*, 2007; *Lumpkin et al.*, 2008]. This is very close to our estimate of the mean MOCσ at 59.5°N. The comparison is tentative, though, because it does take into account the decadal variability of the MOC [*Koltermann et al.*, 1999; *Willis*, 2010]. With this caveat in mind, our results imply a minor contribution to the MOCσ by the net dense water formation in the subpolar gyre between ~48°N and 59.5°N. This inference concurs with the results by *Pickart and Spall* [2007] suggesting a

minor contribution to the Atlantic MOC by the net water mass transformation in the Labrador Sea.

To conclude, the results of the present study, verified with independent estimates where possible, provide the first observation-based quantitative view of a mean state of the gyre / overturning circulation at the northern periphery of the Atlantic Ocean. The most interesting features of the obtain circulation pattern are as follows:

• Nearly half of volume of the upper-ocean waters transported northward across 59.5°N in the eastern limb of the subpolar gyre (NAC and IC, $\sigma_0 < 27.55$) overturns in the density plane south of the GSR and feeds the lower limb of the Atlantic MOCσ.

• The contribution to the MOCσ lower limb at 59.5°N by overturning (light-to-dense transformation) of the NAC / IC-derived upper-ocean waters south of the GSR is one and a half times as large as the contribution of the Nordic Seas overflows.

• The net southward flow in MOCσ lower limb at 59.5°N is associated primarily with the deep water ($\sigma_0 > 27.80$) export. Nearly half of the net southward flow of deep waters across 59.5°N is due to entrainment of the Atlantic waters in the Irminger Sea.

• The DWBC at 59.5°N is fed primarily by the Denmark Strait Overflow and by the diapycnal flux / entrainment from the mid-depth layer, while the contribution to the DWBC transport from the ISOW flow is minor. A major part of the ISOW transported into the Irminger Sea from the Charlie-Gibbs Fracture Zone recirculates southward in the eastern Irminger Sea and exits the basin via an interior pathway rather than along the western boundary. The results can be used for validation of numerical models. From this perspective, multi-year mean transports have an obvious advantage over individual section-based synoptic estimates, which bear the impress of vigorous variability occurring on a variety of spatial and temporal scales. The methodological outcome is that the combined use of repeat hydrography, the MDT by *Rio and Hernandez* [2004] and satellite altimetry data can provide a useful estimate of the mean full-depth circulation across a transatlantic section without imposing *a priori* constraints.

1.6 Major Problems and Goals Not Achieved

Bottle ## 17 and 18 leaked at the first two stations. Seasave did not work properly on sta. 3383.

2. CONTINUOUS MEASUREMENTS (on station and underway)

2.1 Navigation

Navigation data from Trimble SPSx50/SPSx51 GPS was recorded every 1 second and was stored on the PC in binary format.

2.2 Meteorological Measurements

The standard mean meteorological measurements were stored in the separate files on the same PC with navigation data. Recording were running immediately after departure from Gdansk (Poland) on 3rd June, and worked reliably until completion of the cruise in Halifax (Canada) on 12th July. Variability of the atmospheric pressure, air temperature relative humidity and winds during this time are shown in **Figures 11-14**.

2.3 Thermosalinograph

SBE 21 S/N 3254 data were collected along the section lines starting on June 7th.

2.4 Echosounding

The bathymetric equipment aboard during RV Akademik Ioffe Cruise 51 consists of an ELAC 12 kHz hydrographic echosounder. Data were collected for most of the cruise. The Hull mounted transducer is located 5.8 metres below the sea surface and this value was entered to estimate the depth.

Depth was indicated on the echosounder display and stored on the PC together with the navigation.

Two files with extension NAV and MET with maximum size 256032 b were created. File name corresponded to GMT time when the file was opened for records.

2.5 Vessel Mounted Acoustic Doppler Current Profiler (VMADCP) OS 38 kHz

The Ocean Surveyor 38 kHz is designed for vessel-mount current profile measurement in the upper ocean water from depths greater than 40-50 meters. The system consists of a transducer and electronics chassis connected to PC. Data are transmitted in binary format through the I/O cable. GPS data in NMEA format are transmitted separately to another PC COM – port. The VMADCP can operate in two regimes (Narrow Bandwith and Broad Bandwith Profiling). Its main specifications are shown below.

To collect OS 38 kHz data we used *VmDas* software (version 1.46). The NMEA messages *VmDas* reads are standard GGA, HDG, HDT, VTG messages.

	Bin size	Maximum range	Accuracy $(cm/s)^2$
Narrow Band (long-range mode)	16 m	800 - 1000 m	30
	24 m	900 - 1200 m	23
Broad Band (high-precision mode)	16 m	520 - 730 m	12
	24 m	730 – 780 m	9

We used a following configuration to collect the data.

WP00001 – Broad Bandwidth profiling
WN045 – number of bins 45
WS2400– cell size 24 m
WF1600 – blanking size 16 m
BP00 – no bottom track (BP),

VmDas saves data in a few files with extension ENX, ENS, ENR (raw data with and without navigation), NR – NMEA messages, STA and LTA averaged data. Misalignment angle was introduced in configuration file and was used by VmDas for data correction.

Data processing performed STA files with 40-profile averaging. Taking into account that single ping takes about 3 seconds, one 40-profile ensemble lasts near 120 seconds in Narrow Bandwidth regime.

Data processing consists of data conversion in NetCDF format with extension NC and further cleaning, filtering, tide removing (using barotropic tidal model TPXO 7.2) and averaging. The standard averaging was 3 km. IFREMER software was used to process OS 38 kHz data.

3. ON-STATION MEASUREMENTS

3.1 CTD

3.1.1 Equipment

The deep profiler system used during the cruise included the following components: SBE 32 painted aluminum 24 bottle multisampler frame, SBE 9P-1227 CTD, Up and Down looking RD Instruments WHS – 300 kHz Acoustic Doppler Current Profiler (LADCP), Separate Battery pack pressure case ext. 6000 m connected to LADCPs with star cable, 24 x 5 liter Test Oceanic Niskin bottles, Benthos altimeter PSA-900D.

Lab equipment for data acquisition and archiving of CTD/LADCP data consisted of the following items mounted on the deck.

Pentium IV – Intel 2.2 GHz, PC Intel Core 2 Duo 2.4GHz Personal Computers. APC Back-UPS 550VA/330W, SBE 11p Deck Unit.

Cruise Preparation

Equipment and sensors were assembled when the ship crossed the Baltic and North Seas (3-7th June). Water bottles were checked for integrity of seals, taps, stoppers and lanyards before being fitted and roped to the multisampler frame.

Deployment

The CTD was deployed with a lowering rate of 60 meters/min (30-40 meters/min in the upper 200 meters or deeper if the conditions are rough). It is recovered at a rate of 60 meters/min.

The LADCPs fitted within the frame with a separate battery pressure case performed well. These units contain a compass and tilt sensors which could possibly provide useful information on the attitude and rotation of the whole profiler package throughout deployments.

Bottle firing using the deck unit and pylon was very reliable during the cruise.

Operationally this has been a successful cruise with virtually no time being lost due to mechanical or equipment failure.

3.1.2 Data processing and calibration

CTD data were logged at 24 scans per second and passed from the CTD deck unit to the PC.

The CTD data was recorded onto disk by the PC using SEABIRD SEASOFT-Win 32: Seasave 7, Software Release 7.21d. A screen display of temperature, oxygen, salinity and density profiles vs pressure are used to decide the depths at which bottles are to be tripped on the up cast. The bottles are tripped using the enable and fire buttons on the PC screen. During post-processing, the SEASAVE software stores 35 scans at each bottle trip within a separate file. At the end of the station, all the data and header files associated with the station are transferred immediately via ethernet to the second PC. The SBE data processing software is used to create 1 dbar processed data files.

The data processing takes the following steps:

DATCNV Converts the raw data to physical parameters.

WILDEDIT For every block of 100 scans, flags all scans whose pressure, temperature, conductivity and oxygen values differ from the mean by more than 2 standard deviations. Recomputes mean from unflagged data then marks as bad all scans exceeding 20 standard deviations from these new values.

FILTER Low pass filter pressure channel with time constant used for pressure 0.150 seconds.

ALIGNCTD Aligns the oxygen values relative to the pressure values accounting for the time delays in the system. Time offsets of 4.000 secs for oxygen are used.

CELLTM A recursive filter used to remove the thermal mass effects from the conductivity data. Thermal anomaly amplitude and time constants of 0.0300 and 7.0000 were used.

LOOPEDIT Marks as bad, all cycles on the down trace for which the vertical velocity of the CTD unit is less than 0.25 metres/sec.

WINDOW FILTER cosine filter temperature and conductivity, window size 23 scans.

DERIVE Computes salinity, potential temperature, sigma-t, sigma theta and oxygen values.

BINAVG Averages the down cast into 1 dbar pressure bins.

SPLIT Splits the data into DOWN and UP cast.

Calibration data

The CTD calibrations used during this cruise were supplied by Sea Bird Electronics and are as follows:

Pre-cruise calibration:

CALIBRATION DATE: 05-Apr 2016 (all stations)

Conductivity Sensor S/N 044581

g =-9.77563818e+000

h = 1.26403127e+000

i = 4.83945791e-004

j = 2.66846706e-005

CPcor = -9.5700e-008
CTcor = 3.2500e-006

Post-cruise calibration:
CALIBRATION DATE: 09-Aug 2016 (all stations)
Conductivity Sensor S/N 044581
g = -9.78314591e+000
h = 1.26597933e+000
i = 6.67097628e-005
j = 5.43149399e-005

CPcor = -9.5700e-008
CTcor = 3.2500e-006
Average drift between *pre* and *post-cruise* calibrations: +0.0021 PSU/month

Pre-cruise calibration:
CALIBRATION DATE: 19-Mar-16 (all stations)
Temperature Sensor S/N 036088
Temperature ITS-90 = 1/{g + h[*ln*(f0/f)] + i[*ln*2(f0/f)] + j[*ln*3(f0/f)]} - 273.15 (°C)
Following the recommendation of JPOTS: T68 is assumed to be 1.00024 * T90 (-2 to 35°C)
f is the frequency
g = 4.30399160e-003
h = 6.24664940e-004
i = 1.92911249e-005
j = 1.49169748e-006
f0 = 1000.0

Post-cruise calibration:
CALIBRATION DATE: 09-Aug-16 (all stations)
Temperature Sensor 035677
g = 4.30403755e-003
h = 6.24762823e-004
i = 1.93534269e-005
j = 1.50389228e-006
f0 = 1000.0
Average drift between *pre* and *post-cruise* calibrations: -0.00039 Degrees Celsius/year

Pressure Sensor S/N 131735 **(all stations) no drift**
CALIBRATION DATE: 08-Apr-16
C1 = -43120.77
C2 = -0.0172211
C3 = 1.209000e-002
D1 = 3.629600e-002
D2 = 0.000000 e+000
T1 = 30.45887
T2 = -2.99054e-04
T3 = 3.939190e-006
T4 = 2.543630e-009
T5 = 0.000000 e+000
AD590M = 1.28912e-002

AD590B = -8.43097e+000
Slope = 1.00000
Offset = 0.0 (dbars)

Oxygen Sensor 433321
CALIBRATION DATE: 30-Mar-2016 (All Stations)

Soc = 0.4508
Voffset = -0.4758
Tau20 = 1.55
A = -3.3789e-003
B = 1.2319e-004
C = -1.7238e-006
E nominal = 0.036
D1 = 1.92634e-4
D2 = -4.64803e-2
H1 = -3.300000e-2
H2 = 5.00000e+3
H3 = 1.45000e+3

The final coefficients are for sill stations (sta 3444 – 3515)
Soc = 4.68260e-001
Voffset = -3.81500e-001

The final coefficients are for 59.5 N stations (sta 3516 – 3619)
Soc = 4.66910e-001
Voffset = -3.52200e-001

The final coefficients are for Labrador stations (sta 3620 – 3646)
Soc = 4.64460e-001
Voffset = -3.33800e-001

3.1.3 Final Post-Cruise CTD Calibrations

Temperature Calibration Temperature Sensor 036088

-0.00010 sensor drift was applied to the temperature data based on the *pre cruise calibration coefficients* for all stations.

Pressure Calibration Pressure Sensor S/N 131735

Final CTD pressure correction: Since no drift for pressure sensor was defined by SeaBird Electronics pressure was corrected for atmospheric pressure only. With offset in *.con* or *.xmlcon* file set to -0.0026 db, pressure measured by CTD should equal barometric pressure

• Calculate offset (db) = barometer reading – CTD reading

– Conversion of psia to decibars: decibars = (psia - 14.7) * 0.6894759

• Enter calculated offset in *.con* or *.xmlcon* file

• Example:

– CTD reads -2.5 dbars

– Barometer reads 14.65 psia.

Converting to decibars, barometer reads (14.65 - 14.7) * 0.6894759 = -0.034 dbars

– offset (db) = barometer reading – CTD reading = -0.034 - (-2.5) = 2.466

Salinity Calibration Conductivity Sensor 044581

We used *pre-cruise calibration coefficients* with slope correction according to App. Notes No 31 (Revised February 2010).

If **α** is the conductivity computed from the **pre-cruise bath data** (temperature and frequency) using **post-cruise calibration coefficients** and **β** is the true conductivity in the **pre-cruise bath**, then:

$$\textbf{postslope} = \frac{\sum_{i=1}^{n} (\alpha_i)(\beta_i)}{\sum_{i=1}^{n} (\alpha_i)(\alpha_i)}$$

(postslope is typically < 1.0)

Sea-Bird calculates and prints the value for postslope on the conductivity calibration sheet for all calibrations since February 1995 (see *Appendix I: Example Conductivity Calibration Sheet*)

To correct conductivity data taken between pre- and post-cruise calibrations:

islope = 1.0 + (b / n) [(1 / postslope) - 1.0]

where

islope = interpolated slope; this is the value to enter in the configuration (.con or .xmlcon) file
b = number of days between pre-cruise calibration and the cast to be corrected
n = number of days between pre- and post-cruise calibrations
postslope = slope from calibration sheet as calculated above (see *Appendix I: Example Conductivity Calibration Sheet*)

In the configuration (.con or .xmlcon) file, use the **pre-cruise calibration coefficients** and use **islope** for the value of slope.*

Note: In our SEASOFT V2 suite of programs, edit the CTD configuration (.con or .xmlcon) file using the Configure Inputs menu in Seasave V7 (real-time data acquisition software) or the Configure menu in SBE Data Processing (data processing software).

For typical conductivity drift rates (equivalent to -0.003 PSU/month), islope does not need to be recalculated more frequently than at weekly intervals.

We used the following slope corrections because of the large drift of the conductivity sensors:

for sill sections (sta 3444-3515) - 1.00011780
for 59.5 N sections (sta 3516-3560) - 1.00013010

for 59.5 N sections (sta 3561-3619) - 1.00014241
for Labrador stations (sta 3620-3646) - 1.00015824

3.1.4 SBE 43 Dissolved Oxygen Sensor Calibration using Winkler Titrations

We use a method for statistically estimating calibration coefficients for calculating dissolved oxygen in milliliters per liter from SBE 43 output voltage. The technique requires dissolved oxygen concentration in ml/l (determined from Winkler titration of water samples) and SBE 43 oxygen voltage outputs at the times the water samples were collected. Sea-Bird's data processing software, SBE Data Processing, is used to produce a data table suitable for the analysis.

Background

The equation used in Sea-Bird's software for calculating dissolved oxygen in ml/l from SBE 43 output voltage is a form of that given in Owens-Millard (1985):

$$Oxygen\ (ml/l) = \left\{ Soc * \left(V + Voffset + tau(T,P) * \frac{\partial V}{\partial t} \right) \right\} * Oxsol(T,S) * \left(1.0 + A*T + B*T^2 + C*T^3\right) * e^{\left(\frac{E*P}{K}\right)} \qquad eqn\ 1$$

where:

- V = SBE 43 output voltage signal (volts)
- $\partial V/\partial t$ = time derivative of SBE 43 output signal (volts/second), computed over a default window of 2 seconds
- T = CTD temperature (°C)
- S = CTD salinity (psu)
- P = CTD pressure (dbars)
- K = CTD temperature (°K = °C + 273.15)
- *tau(T,P)* = sensor time constant at temperature and pressure
- *Oxsol(T,S)* = oxygen solubility function (ml/L), which converts oxygen partial pressure (sensor measurement) to oxygen concentration (*Garcia and Gordon, 1992*). See Appendix A in *Application Note 64: Background Information, Deployment Recommendations, and Cleaning and Storage* for values at various temperatures and salinities.
- *Soc, Voffset, A, B, C, E*, and *tau20, D1, D2* [terms in calculation of *tau (T,P)*] are calibration coefficients

The SBE 43 is expected to provide an output voltage that is linear with respect to oxygen concentration. Normal calibration drift manifests itself as a loss of sensitivity and is evident as a change of slope (and less so in offset) in the linear relationship between oxygen concentration and voltage output. The coefficients *A, B, C,* and *E* correct for small secondary responses to temperature and pressure. Because these coefficients change very slowly over time, the values given on the SBE 43 calibration certificate will be used in this analysis, and we will concern ourselves with estimating changes in the slope (Soc) and offset (Voffset).

Setting $\frac{\partial V}{\partial t}$ to zero, we rearrange equation 1 into a linear form and perform a linear regression to obtain a new *Soc* and *Voffset*.

Let:

$$\phi = Oxsol(T,S) * \left(1.0 + A*T + B*T^2 + C*T^3\right) * e^{\left(\frac{E*P}{K}\right)} \qquad eqn\ 2$$

The oxygen equation then reduces to the form in equation 3:

$$Oxygen(ml/l) = Soc * (V + Voffset) * \phi \qquad eqn\ 3$$

This may be expressed in a linear form in equation 4.

$$\frac{Oxygen(ml/l)}{\phi} = Soc * (V + Voffset) = M * V + B \qquad eqn\ 4$$

Where:
Soc = M
Voffset = B / M

A linear regression is calculated using Winkler oxygen concentration divided by ϕ as the dependent variable and SBE 43 output voltage as the independent variable.

Winkler oxygen divided by φ versus SBE 43 output voltage for this cruise is shown in

Fig. 14 and includes a linear regression line calculated from the data.

The final coefficients are for sill stations (sta 3444 – 3515)
Soc = 4.68260e-001
Voffset = -3.81500e-001
933 oxygen samples were used to build this linear fit for sill sections.

The final coefficients are for 59.5 N stations (sta 3516 – 3619)
Soc = 4.66910e-001
Voffset = -3.52200e-001
1806 oxygen samples were used to build this linear fit for 59.5 N.

The final coefficients are for Labrador stations (sta 3620 – 3646)
Soc = 4.64460e-001
Voffset = -3.33800e-001
461 oxygen samples were used to build this linear fit for the Labrador stations.

Procedure

The linear regression that yields a new *Soc* and *Voffset* may be accomplished with spreadsheet software, a hand-held calculator with statistical capability, or (with perseverance) a calculator, graph paper, and pencil. As a first step, extract pressure, temperature, salinity, oxygen saturation, and SBE 43 voltage from the parts of your CTD data collected when the water sampler closures occurred.

Run SBE Data Processing, and select Data Conversion in the Run menu. Select the appropriate configuration (*.con*) and data (*.dat* or *.hex*) files on the *File Setup* tab. Click the *Data Setup* tab and set *Convert data from* to *Upcast and downcast* and *Create file types* to *Create bottle (.ros) file only*.

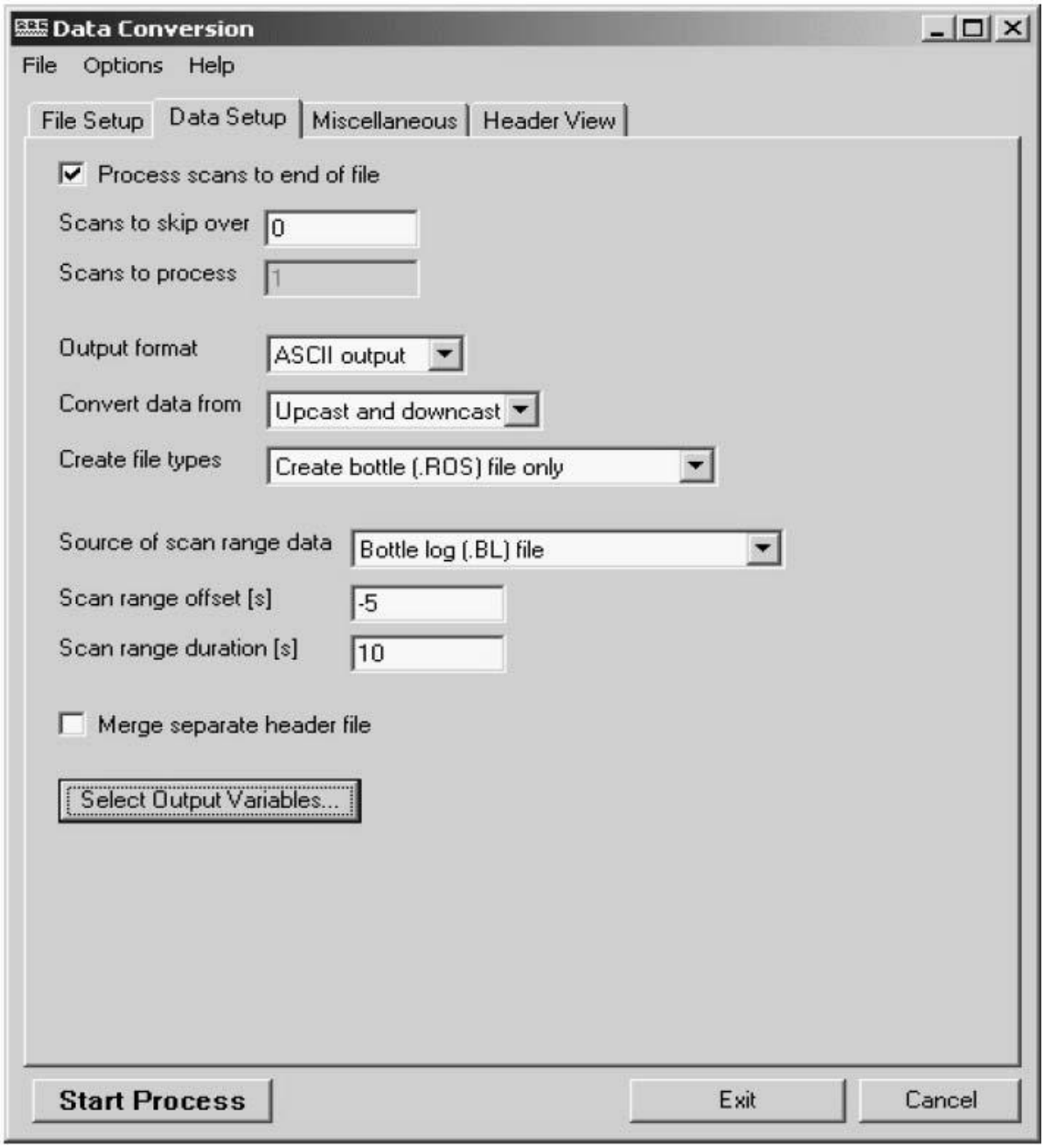

To extract CTD data concurrent to the water sampler closures, Data Conversion must know when the closures occurred. Select an appropriate *Source of scan range data*, depending on your instrument type and how the sampler was commanded to close bottles:

- SBE 9*plus* with SBE 11*plus* or 17*plus* - The data stream is marked with a *bottle confirm* bit each time a closure occurred.
- Using SEASAVE to operate the water sampler - A *.bl* file, with scan ranges corresponding to closures, is created during the cast.
- SBE 19, 19*plus*, 19*plus* V2, or 25 with Auto Fire Module (AFM) and SBE 32 Carousel Water Sampler, or operated autonomously with SBE 55 ECO Water Sampler - The *.afm* file contains scan ranges.

Like all sensors, the SBE 43 has a finite response time to a change in dissolved oxygen concentration. This response time is usually on the order of 6 seconds. For this reason, good sampling procedure dictates that the instrument package should be stopped in the water column long enough for the SBE 43 and all other sensors to completely equilibrate before closing the water sampler. An equilibration time of 5 to 6 response times, or 30 to 36 seconds, is adequate.

In the example above, Data Conversion will begin extracting data 5 seconds before each water sampler closure (*Scan range offset = -5 s*) and will extract a total of 10 seconds of data (*Scan range duration = 10 s*). Note that 10 seconds is longer than the SBE 43 response time. Because we are extracting data for 5 seconds after the water sampler closure, the instrument package must remain stopped for at least this long.

To estimate *Soc* and *Voffset*, you need pressure, temperature, salinity, oxygen saturation (ml/l), and SBE 43 Oxygen Voltage to go with each Winkler titration data value. Click *Select Output Variables* and add each of the required parameters; the dialog box is shown below.

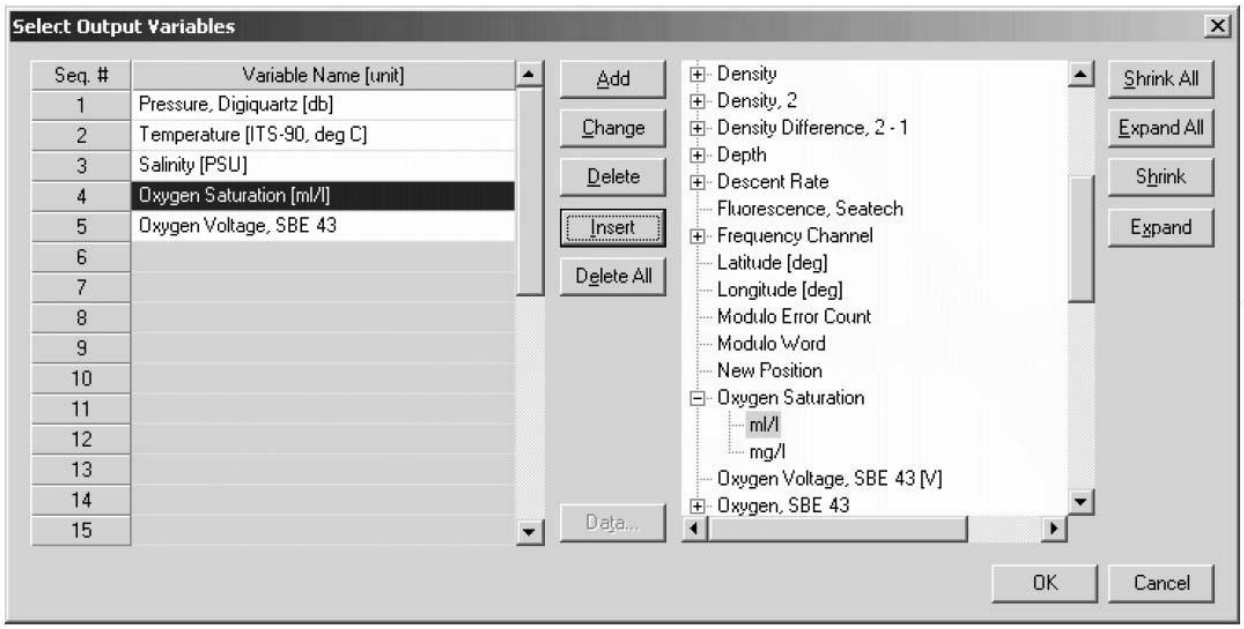

After selecting all the variables, click *OK* to return to the Data Conversion Data Setup tab. Then click *Start Process* to create the *.ros* file.

For this example, the *.ros* file contains 10 seconds of data centered on the moment the bottle closure occurred for every bottle closure. To make a useful table, select Rosette Summary from SBE Data Processing's Run menu. Rosette Summary calculates averages and standard deviations for the variables selected in Data Conversion. Select the appropriate *.con* and *.ros* files on the *File Setup* tab. Click the *Data Setup* tab and then click the *Select Averaged Variables* button; the dialog box is shown below.

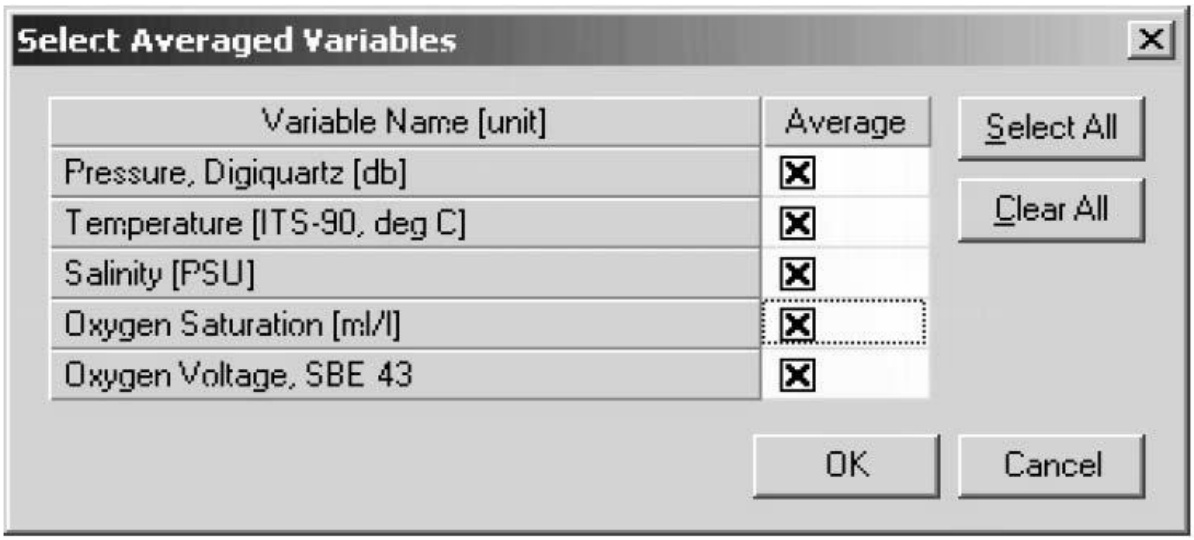

After selecting all the variables, click *OK* to return to the Rosette Summary Data Setup tab. Then click *Start Process* to create a data table file with the *.btl* extension.

Create a table with average pressure, temperature, salinity, oxygen saturation, and SBE 43 output voltage for each water sampler closure depth, by importing the *.btl* file into a spreadsheet. Then, enter by hand the Winkler titration dissolved oxygen values from your titration log, matching water sampler closures to pressures.

Calculate $\phi = Oxsol(T,S) * \left(1.0 + A*T + B*T^2 + C*T^3\right) * e^{\left(\frac{E*P}{K}\right)}$,

using *A, B, C,* and *E* from the SBE 43 calibration sheet.
Then, calculate $Winkler\ O_2 / \phi$.

Perform a linear regression, with:

- $Winkler\ O_2 / \phi$ (shown as Winkler/phi in the table) as the *Y* data
- SBE 43 output voltages as the *X* data

If a spreadsheet or statistical calculator is not available, the regression equations are:

$$M = \frac{n * \sum\left(V * \frac{Winkler\,O_2}{\phi}\right) - \sum V * \sum\left(\frac{Winkler\,O_2}{\phi}\right)}{n * \sum V^2 - \left(\sum V\right)^2}$$

$$B = \frac{\sum\left(\frac{Winkler\,O_2}{\phi}\right) - M * \sum V}{n}$$

Where:
n = number of data pairs
M = Slope
B = Offset

And:
$Soc = M$
$Voffset = B/M$

Reference

Owens, W. B., and R. C. Millard Jr., 1985: A new algorithm for CTD oxygen calibration. J. Phys. Oceanogr., 15, 621-631.

(NOTE: calibration expressed as ml/l)

3.2 Oxygen Bottle Samples

Oxygen samples were drawn first from every bottle. Duplicate samples were taken on each cast, usually from the first two bottles. Samples were drawn into clear, wide necked calibrated glass bottles and fixed on deck with reagents dispensed using Aquastep bottle top dispensers. A test station used to check on the oxygen bottle calibrations and as an opportunity to train a number of people to take the samples. The samples were shaken on deck and again in the laboratory 1/2 hour after collection, when

the bottles were checked for the tightness of the stoppers and presence of bubbles. The samples were then stored under water until analysis.

Bottle temperatures were taken, following sampling for oxygen, using a hand held electronic thermometer probe. The temperatures were used to calculate any temperature-dependent changes in the sample bottle volumes.

Samples were analyzed in the constant temperature laboratory, starting three hours after sample collection, following the Winkler whole bottle titration with an amperometric method of endpoint detection, as described by Culberson (1991). The equipment used was supplied by Metrohm and included the Titrino unit and control pad, exchange unit with 10 ml burette to dispense the thiosulphate in increments of 2 μl , with an electrode for amperometric end point detection.

The difference for the duplicate pairs sampled on each station was in a range 0.00-0.02 ml/l .

The thiosulphate normality was checked on each run and recalculated every time the reservoir was topped up against potassium iodate. The exact weight of this standard, the calibrated 5 ml exchange unit driven by a Metrohm Dosimat and the 1L glass volumetric flask used to dispense and prepare the standard.

The introduction of oxygen with the reagents and impurities in the manganese chloride were corrected for by blank measurements made on each run, as described in the WOCE Manual of Operations and Methods (Culberson, 1991).

Collected data shows that dissolved oxygen concentrations varied from 4.91 to 8.71 ml/l. In order to control the accuracy of the oxygen measurements at each cast were taken parallel samples from the 1-2 bottles or duplicate samples.

Reproducibility of measurements

3407 samples were taken during the cruise; in addition 54 duplicates were analyzed. These include both duplicates taken from the same bottle (replicates) and those taken from different bottles fired at the same depth. The data gave a standard deviation of 0.007 ml/l.

3.3 Nutrient Bottle Samples

Samples for nutrient measurements were collected following oxygen samples from each Niskin bottle. Water was collected in clean plastic containers that had been rinsed three times by seawater through the latex tube.

Concentrations of silicate and phosphate were determined by photometric methods with spectrophotometer Cary 100 Seam Varian. All samples were analyzed immediately after sampling.

Silicate determined by Korolev's method based on colorimeter of blue silicomolybdic complex (methodology described in Modern methods..., 1992). The ascorbic acid used as a restorative. The absorbance was read at 810 nm. Relative error of this method on concentration of dissolved silicate at 4.5 μM is ±4%, on concentration at 45 μM - ± 2,5%. Measured concentrations were in a range from 0.20 to 20.71 μM.

Phosphates determined according to the method Murphy and Raily (Modern methods..., 1992). Phosphate, dissolved in sea water, react with ammonium molibdate in a presence of sulfuric acid and tartrate potassium-antimony. The generated complex aggregate of phosphomolybdic heteropolyacid and trivalent antimony restorative by the ascorbic acid, and then determined the absorbance at 885 nm (we use the cavity 10cm). Relative error of this method ± 1%.

In order to ensure accuracy and increase precision of determination 3-4 duplicate samples were analyzed at each run. The mean difference for the duplicate pairs sampled on each station was in an error limit of the methods.

References:

Culberson, C.H. 1991.15 pp in the WOCE Operations Manual (WHP Operations and Methods) WHPO 91/1, Woods Hole.

Modern methods of hydrochemical research of the ocean, 1992. IO RAS, Moscow (in Russian).

3.4 Lowered Acoustic Doppler Current Profiler (LADCP)

The TRDI WHS 300 kHz ADCPs consists of a pressure case rated to 6000 meters with 4 transducers at one end in a convex arrangement and the beams diverging at 20 degrees from the vertical. At the opposite end to the transducers is a connector that enables downloading of data and connects it to other pressure cases containing another ADCP and the power supply pack. This arrangement allowed the ADCPs and the battery pack to be mounted vertically as up and down-looking on the CTD frame. Connection amongst all units was established using star cable with three male and two female terminations. Two male cable ends were always attached to the frame, this enabled comms leads to be readily connected pre and post deployment.

Communications: The 20-m communication leads (which also allow external power to be supplied to the ADCP) were sufficiently long to route it through to the port side of the deck lab where it was connected to a dedicated PC and external power supply. The latter was set at 48+ volts and was left on

whilst the ADCP was on deck. 5 minutes prior to deployment the external power supply was shut off, the instrument checked and the configuration file sent to the ADCP as described in the manual instructions. The free end of the fly leads was greased and the end cap refitted, this was then taped to the frame for security.

Post deployment: When the CTD/LADCP was brought inboard, the fly-lead connectors were dried and the comms leads were connected to them. This stopped undue bending of the cables and kept them clear of the water bottles, aiding sampling. External power was applied again and the cast data downloaded as per the manual with a baud rate of 57600. The processing is accomplished using software developed by Visbeck after transferring the data to the PC.

Battery power was supplied to the ADCP in the form of 42 volts from 28 x 1.5 volt alkaline cells. Four of these packs were available for the cruise, as the ADCP will function at a minimum of 32 volts this was deemed an adequate stock for the duration.

Data quality: The data quality from the ADCP was good throughout. Due to the bad weather instrument titles sometimes exceeded 12° and this data was rejected during processing.

The LADCPs seem to function well and generates useful information on currents. The battery supply has its limitations though and thought should be given to alternatives to the present set-up.

3.4.1 LADCP Processing for Current Profiles

A brief account of the LADCP current data processing, file nomenclature and directory structure is provided in the following lines. Little emphasis is put into a detailed description of the main programming tools used, since these are part of a standard software package developed by Gerd Krahmann (version 10.13).

Outline of LADCP current calculation method

The Broad Band LADCP used during AI51 cruise was designed to measure the instantaneous relative velocities of scatterers in the water column by taking advantage of the Doppler frequency shift, phase changes and correlation between coded pulses transmitted and received by the LADCP's four transducers. Conversion of this raw data stream to a profile of absolute currents involved an elaborate calculation method.

Firstly, Doppler shifts needed to be scaled to velocity units by taking into account the depth-dependent sound velocity (estimated from CTD T and S measurements). Directions could be inferred from trigonometric calculations based on the geometry of the transducer set, the orientation of the package (measured with a flux gate compass) and the local magnetic declination. The depth of the instrument was calculated from the integration of the measured vertical velocity and later adjusted to match the depth given by the CTD's pressure sensor.

The velocities corresponding to each single ensemble (or, in effect, to each transducer ping) were gridded in bins of depth set 10 meters. Statistical rejection of spiky measurements within each of these bins followed.

In order to reject the unwanted motion of the instrument (but also the barotropic component of the current), shear profiles were calculated for each ensemble. A complicated editing scheme preceded this shear calculation. A final shear profile (baroclinic current) was derived by real- depth gridding of the shear profiles calculated for individual ensembles. It was hoped that any relative velocities introduced by the high-frequency motion of the CTD package would be smoothed out by this repeated averaging.

The barotropic component of the flow was finally calculated from bottom-tracking measurements (bottom-track mode) or, in most occasions, in an integral sense from differential GPS positions of the ship (water-track mode).

The definitive velocity profile was hence obtained as the sum of the baroclinic and barotropic components.

During AI51 cruise, no specific error calculation was performed. Profiles of shear standard deviation were included in the cast log sheet folder. Internal wave signals were obvious throughout the cruise.

Relevant PC files

The raw data were downloaded from the LADCP into a devoted PC after each cast and stored as a binary file called vNNNNm_01.000 for Master and vNNNNs_01.000 for Slave the c:\ladcp\AI51\dNNN directory, where NNNN stands for the CTD cast number, e.g. raw data from cast 3330 were stored in the files d:\AI51\data\ladcp\v3330m_01.000 and v3330s_01..000.

The configuration files (named Mconf.txt and Sconf.txt) containing the operating instructions (setting of track mode, bin depth, etc.) given to the LADCP previously to deployment was stored in the same directory.

Text files of the form NNNNm.log and NNNNs.log are the log of the 'bbtalk' session (testing the state and functioning of the instrument) previous to deployment. The details of the sessions for every single cast in the cruise are to be found in the cast log sheets.

A whole variety of files were created and manipulated during the different processing stages, and no mention will be made of the majority of them for reasons of clarity. The processing procedure may be summarised in two steps:

1- create CTD pressure, temperature and salinity data file as well as navigation collected every second in order to obtain the best possible estimates of depth and sound velocity. This is done using 'SBE Data Processing software and ConvLADCP Fortran program.

2- use the Gerd Krahmann's standard matlab package (v.10.13) with P. Lherminier's improvements (LPO, IFREMER) to process LADCP and CTD data

References

M. Visbeck 2002 Deep Velocity Profiling using Lowered Acoustic Doppler Current Profiler: Bottom Track and Inverse Solutions J. Atmos. Oceanic Technol. 10, 764-773.

3.5 Geological studies in the North Atlantic

The goal of this study was to describe the modern sediment system of the North Atlantic and to collect cores for a high-resolution reconstruction of climate change.

The research team had several objectives: an atmospheric aerosol study; collection of water samples to estimate the concentration and composition of suspended matter, including total and organic carbon, and phytoplankton pigments; collection of bottom sediment samples; microbiological and biogeochemical studies; and recovery and deployment of mooring stations (MS) (**Fig. 17, table 2**).

Atmospheric aerosols. A TSI AeroTrak APC-9303-01 airborne particle counter, (United States) was used to obtain the granulometric spectrum of aerosol particles in the surface layer. The atmospheric suspended particulate matter in surface layer was sampled using nylon nets.

Suspended sediment matter. The water was sampled for suspended sediment studies at the surface along the ship's route and in the ocean interior at oceanographic stations. To estimate the total concentration of the suspended matter, seawater was filtered under a vacuum of –0.4 atm through preliminary weighted nuclear filters 47 mm in diameter (pore diameter of 0.45 μm). To find the concentration of suspended organic carbon and chlorophyll, filtration was done through preliminarily calcinated Whatman GF/F glass fiber filters with a diameter of 47 mm (effective pore size of approximately 0.7 μm) under a vacuum of –0.2 atm in order to remove organic substances. The filters for the total content of the suspended particulate matter were dried in situ, and the glass fiber filters for the calculation of chlorophyll content were frozen and transported in a container with silicagel to Moscow. The content of suspended organic carbon was calculated on an AN-7529 device at the Institute of Oceanology, Russian Academy of Sciences. The concentrations of phytoplankton pigments (chlorophyll a and pheophytin a) were determined by the fluorometric method using a Turner Trilogy fluorimeter, which was preliminarily gauged at the Chair of Biophysics of the Department of Biology, Moscow State University. The contents of Si, Al, and P were estimated by the photometric method.

Bottom sediments. Large samples of bottom sediments were extracted with an Okean-0.25 Grab Sampler (GS), and sediment cores were recovered with a Multicorer 71.500 KC Denmark (MC) and a Gravity Corer (GC). Five cores from the GC, 19 minicores with above-bottom water from the MC and 27 minicores from the GS were carried out in total. Mineral composition of the sediments was examined with the help of microscope POLAM L-213M, foraminifera composition was examined with the help of binocular Bresser Advance ICD. Iceberg-rafted debris (IRD) was studied too. Ship's Innomar SES-2000 deep-36 parametric sub-bottom profiler was used for seismoacoustic profiling on the stations.

Microbiological studies. At key stations of the studied transect, a set of measurements was carried out to assess the activity of microbial carbon and serum transformation, including the intensity of microbial carbon dioxide assimilation and methanogenesis and sulfidogenesis efficiency. Some samples were collected to define the isotopic composition of organic and mineral carbon in the suspended matter and bottom sediment. An express analysis was performed to assess the oxidation–reduction potential of sediment and the alkaline reserve of pore water.

Vertical fluxes of suspended matter were studied with sediment traps set in the MS. Three MS from 2015 expedition were recovered. Four new MS, where 6 large sediment traps Lotos-3 with 12 sample bottles and 40 integrated small sediment traps MSL-110 were installed. Three Teledyne RDI DVS-750, two Nortek Aquadopp and one DVS-6000 current meters were used to assess the horizontal flow component (**Fig. 18–20**).

Preliminary results

Prevailing wind directions were northwest, and northeast during the entire transit along the transect. The granulometric spectrum of surface layer aerosols varies depending on the wind state. The highest concentration of the aerosols in the underwater layer (42000 particles per L) was found in the North and Baltic seas, the low concentrations (2000 particles per L) were found in the atmosphere over the Labrador Sea.

Suspended matter concentrations were found to be in a range from 0.07 to 1.4 mg/L. The highest concentrations were observed rather close to the coast (the North Sea and Greenland), but also in areas affected by the Irminger and North Atlantic currents. As for the vertical profiles, the highest concentrations were marked out in the upper ocean mixed layer (to a depth of 50 m), and for most of cases, at the surface (0 m). At nearly all stations, an increase in suspended matter concentration was found in the near-bottom layer. The highest concentrations (40–500 mg/L) were found in the above-bottom water from the MC samples.

The upper sediment layer consisted mainly of carbon silt-pelite sediments, with sandy dimension foraminipheric debris and material of ice rafting. The pattern of active bioturbation was noted at every station.

The oxidation–reduction potential was positive all along the collected sediment core. At the same time, the Eh value decreased by 25–40 mV from the upper to the deeper part of the core, which suggests that microbial oxidation of organic matter was taking place with oxygen consumption. Apparently, the activity of microbial processes attenuates deeper into the sediment. A weak increase in the alkaline reserve of pore water is noted deeper into the sediment.

The material from the sediment traps shows the increasing of the vertical particulate fluxes in the bottom layer in September 2015. Also the high values of the fluxes were found in August, December 2015 and February and June 2016. Minimum of the fluxes was found on the st. 3778 (the Irminger Sea), maximum – on the st. 3359 (Gardar drift, the zone of influence of Island-Scotland current).

. CRUISE LOGISTICS

Mobilization

Mobilization for the cruise took place on the way from Gdansk (Poland) to the first station of the cruise. It took four days. The scientific team arrived at the ship on June 1th.

ACKNOWLEDGEMENTS

The principal scientists would like to thank the Master, officers, crew and scientists of the RV Akademik Ioffe for making this such an enjoyable, as well as successful cruise.

TABLES

FIGURES

Fig. l Station locations (red diamonds for sill stations, circles for 59.5 N stations and triangles for Labrador Sea stations). The shelf area with depth less than 200 m is shaded

Fig.2 Vertical distribution of samples along (a) sill section (b) the 59.5 section.

Fig. 3. Schematic diagram of the large-scale circulation in the northern North Atlantic compiled from [Schmitz and McCartney, 1993; Schott and Brandt, 2007; Sutherland and Pickart, 2008; Lherminier et al., 2010]. Abbreviations for the main topographic features, currents and water masses are explained in the legend. The nominal locations of the 59.5°N hydrographic section (1997 – present) and sections across the straits between Greenland, Iceland, Faeroe and Shetland Islands (2011 – present) are shown with the solid green lines.

Fig. 4. Oxygen concentrations (ml/l) in the water column (lower panel) as observed in March–October 1997 in four hydrographic sections (upper panel) ending nearby the southern tip of Greenland. A separate oxygen maximum in the LSW layer (1000–2000 m) in the Irminger Sea at 59.5°N strongly implies local convective renewal of LSW before 1997. Adapted from [Falina et al., 2007].

Fig. 5. Warming and salinification in the northern North Atlantic between the mid-1990s and mid-2000s, as observed at 59.5°N. The figure shows the 2006–1997 temperature (°C, left) and salinity (right) differences on isobaric surfaces in the Irminger Sea and Iceland Basin. Adapted from [Sarafanov et al., 2007].

Fig. 6. Coherence of the decadal salinity changes (1950s – 2000s) of the intermediate (LSW) and deep (ISOW) waters in the northern North Atlantic and their link to the North Atlantic Oscillation (NAO) index. **(a)** Schematic representation of the LSW and ISOW pathways and locations of the Icelandic Low (L) and Azores High (H) centers constituting the NAO dipole pattern. The red dotted line indicates the 59.5°N transatlantic section. **(b)** Salinity time series for LSW in the Labrador Sea [Yashayaev, 2007] and ISOW in the Iceland basin [Boessenkool et al., 2007; Sarafanov et al., 2007] overlaid by the third order polynomial fits. **(c)** Time series of the winter NAO index, after [Hurrell, 1995], overlaid by 7-year running mean and third order polynomial fit. **(d)** Mechanism of the NAO effect on the decadal changes in temperature (T) and salinity (S) of the northern North Atlantic intermediate and deep waters. Positive / negative links shown with the dark / light grey arrows mean that changes in ‘causative’ and ‘consequential’ characteristics have the same / opposite sign(s). The overall effect of the NAO on T and S of the in the water column is negative: persistent NAO decline leads to warming and salinification of the water masses and vice versa, as shown in (b) and (c). Adapted from [Sarafanov, 2009].

Fig. 7. Schematic representation of the upper-ocean circulation and convection intensity in the northern North Atlantic under high (left) and low (right) NAO conditions. Blue (magenta) solid arrows indicate the upper-ocean flows with higher fraction of colder fresher subpolar (warmer saltier subtropical) waters. The main pathways of the Nordic overflow-derived deep waters are shown with the dotted curves. "C" and "E" symbols are used to denote, respectively, the deep convection sites and the domain, where the Atlantic waters are entrained into ISOW. Larger (smaller) circles indicate stronger (weaker) convection. SPG and STG – the subpolar and subtropical gyres, respectively. Adapted from [Sarafanov, 2009].

Fig. 8. The Deep Western Boundary Current (DWBC) transport variability and its link to the convection intensity in the Labrador Sea. **(a)** Locations of the hydrographic sections (1991–2007) and schematic of the deep water circulation in the Irminger Sea. **(b)** The DWBC transport anomalies at Cape Farewell in 1991–2007, 1 Sv = 10^6 m^3 s^{-1}. The 1994–1997 and 2000–2007 mean anomalies and the 1994–2007 linear trend are shown. **(c)** Anomalies of the DWBC transport at Cape Farewell and the Labrador Sea Water (LSW) thickness in the Labrador Sea in the 1950s–2000s. **(d)** Correlation coefficient (R^2) for the two times series shown in **(c)** at the 0–5-year lag, the LSW thickness leads. The correlation maximum is achieved at the 1–3-year lag. The DWBC transport anomalies in the southern Irminger Sea are foregone by the convection intensity anomalies in the Labrador Sea. Adapted from [Sarafanov et al., 2009].

Fig. 9. Schematic diagram of the Meridional Overturning Circulation (MOC) at the northern periphery of the Atlantic Ocean, northeast of Cape Farewell. The dotted lines refer to the σ_0 isopycnals 27.55 and 27.80. The arrows denote the integral meridional and diapycnal volume fluxes. Where the signs are specified, the positive (negative) transports are northward (southward). The NAC and EGIC transports in the upper layer ($\sigma_0 < 27.55$) at 59.5°N are the throughputs accounting for the recirculations. EGIC – the East Greenland / Irminger Current – refers to the upper part of the Western Boundary Current. Other abbreviations are explained in the legend to **Fig. 3**. Adapted from [Sarafanov et al., 2012].

Fig. 10. Salinity observed in the northwestern Irminger Sea at 64.3°N in February 1998. The σ_0 isopycnals 27.55, 27.70, 27.80 and 27.88 are plotted as the thick black lines; the station locations are marked with the ticks on the top axis. The plot shows fresh dense waters descending (cascading) down the continental slope of Greenland down to the LSW layer ($27.70 < \sigma_0 < 27.80$) and the layer of the Nordic Seas overflow-derived deep waters ($\sigma_0 > 27.80$). Adapted from [Falina et al., 2012].

	CLIVAR		UTC		POSITION						
3444	1	ROS	060716	0754	BE	59 11.2 N	000 37.6 E	GPS	190	5	24	CTD,LADCP,O2,SiO3,PO4,CO2
3444	1	ROS	060716	0814	BO	59 11.2 N	000 37.6 E	GPS	190	5	24	CTD,LADCP,O2,SiO3,PO4,CO2
3444	1	ROS	060716	0830	EN	59 11.2 N	000 37.7 E	GPS	190	5	24	CTD,LADCP,O2,SiO3,PO4,CO2
3445	1	ROS	060816	0014	BE	60 25.0 N	001 54.9 W	GPS	115	4	12	CTD,LADCP,O2,SiO3,PO4,CO2
3445	1	ROS	060816	0035	BO	60 25.0 N	001 54.9 W	GPS	115	4	12	CTD,LADCP,O2,SiO3,PO4,CO2
3445	1	ROS	060816	0045	EN	60 24.9 N	001 54.9 W	GPS	115	4	12	CTD,LADCP,O2,SiO3,PO4,CO2
3446	1	ROS	060816	0214	BE	60 30.8 N	002 15.5 W	GPS	142	4	7	CTD,LADCP,O2,SiO3,PO4,CO2
3446	1	ROS	060816	0235	BO	60 31.0 N	002 16.0 W	GPS	142	4	7	CTD,LADCP,O2,SiO3,PO4,CO2
3446	1	ROS	060816	0246	EN	60 31.0 N	002 16.1 W	GPS	142	4	7	CTD,LADCP,O2,SiO3,PO4,CO2
3447	1	ROS	060816	0413	BE	60 37.8 N	002 35.5 W	GPS	135	4	7	CTD,LADCP,O2,SiO3,PO4,CO2
3447	1	ROS	060816	0434	BO	60 38.0 N	002 36.1 W	GPS	135	4	7	CTD,LADCP,O2,SiO3,PO4,CO2
3447	1	ROS	060816	0445	EN	60 38.0 N	002 36.1 W	GPS	135	4	7	CTD,LADCP,O2,SiO3,PO4,CO2
3448	1	ROS	060816	0609	BE	60 44.8 N	002 54.5 W	GPS	355	4	13	CTD,LADCP,O2,SiO3,PO4,CO2
3448	1	ROS	060816	0626	BO	60 45.0 N	002 55.1 W	GPS	355	4	13	CTD,LADCP,O2,SiO3,PO4,CO2
3448	1	ROS	060816	0646	EN	60 44.9 N	002 55.1 W	GPS	355	4	13	CTD,LADCP,O2,SiO3,PO4,CO2
3449	1	ROS	060816	0819	BE	60 51.7 N	003 17.4 W	GPS	681	3	22	CTD,LADCP,O2,SiO3,PO4,CO2
3449	1	ROS	060816	0842	BO	60 51.9 N	003 17.8 W	GPS	681	3	22	CTD,LADCP,O2,SiO3,PO4,CO2
3449	1	ROS	060816	0910	EN	60 51.9 N	003 17.5 W	GPS	681	3	22	CTD,LADCP,O2,SiO3,PO4,CO2
3450	1	ROS	060816	1056	BE	60 58.8 N	003 37.6 W	GPS	1105	4	17	CTD,LADCP,O2,SiO3,PO4,CO2
3450	1	ROS	060816	1125	BO	60 59.2 N	003 38.0 W	GPS	1105	4	17	CTD,LADCP,O2,SiO3,PO4,CO2
3450	1	ROS	060816	1159	EN	60 59.3 N	003 38.2 W	GPS	1105	4	17	CTD,LADCP,O2,SiO3,PO4,CO2
3451	1	ROS	060816	1538	BE	61 04.0 N	003 51.9 W	GPS	1149	3	22	CTD,LADCP,O2,SiO3,PO4,CO2
3451	1	ROS	060816	1601	BO	61 04.0 N	003 52.1 W	GPS	1149	3	22	CTD,LADCP,O2,SiO3,PO4,CO2
3451	1	ROS	060816	1634	EN	61 04.0 N	003 52.6 W	GPS	1149	3	22	CTD,LADCP,O2,SiO3,PO4,CO2
3452	1	ROS	060816	1736	BE	61 08.0 N	004 04.0 W	GPS	1120	3	22	CTD,LADCP,O2,SiO3,PO4,CO2
3452	1	ROS	060816	1800	BO	61 08.1 N	004 04.0 W	GPS	1120	3	22	CTD,LADCP,O2,SiO3,PO4,CO2
3452	1	ROS	060816	1837	EN	61 08.1 N	004 04.1 W	GPS	1120	3	22	CTD,LADCP,O2,SiO3,PO4,CO2
3453	1	ROS	060816	1928	BE	61 12.1 N	004 17.4 W	GPS	1081	5	21	CTD,LADCP,O2,SiO3,PO4,CO2
3453	1	ROS	060816	1958	BO	61 12.0 N	004 18.0 W	GPS	1081	5	21	CTD,LADCP,O2,SiO3,PO4,CO2
3453	1	ROS	060816	2036	EN	61 12.0 N	004 18.0 W	GPS	1081	5	21	CTD,LADCP,O2,SiO3,PO4,CO2
3454	1	ROS	060816	2118	BE	61 15.8 N	004 28.0 W	GPS	1057	4	18	CTD,LADCP,O2,SiO3,PO4,CO2
3454	1	ROS	060816	2144	BO	61 16.0 N	004 27.9 W	GPS	1057	4	18	CTD,LADCP,O2,SiO3,PO4,CO2
3454	1	ROS	060816	2220	EN	61 16.1 N	004 27.9 W	GPS	1057	4	18	CTD,LADCP,O2,SiO3,PO4,CO2

3455	1	ROS	060816	2321	BE	61 19.7 N	004 43.0 W	GPS	739	4	19	CTD,LADCP,O2,SiO3,PO4,CO2
3455	1	ROS	060816	2341	BO	61 19.9 N	004 42.8 W	GPS	739	4	19	CTD,LADCP,O2,SiO3,PO4,CO2
3455	1	ROS	060916	0014	EN	61 19.8 N	004 42.8 W	GPS	739	4	19	CTD,LADCP,O2,SiO3,PO4,CO2
3456	1	ROS	060916	0123	BE	61 24.8 N	005 00.5 W	GPS	227	2	10	CTD,LADCP,O2,SiO3,PO4,CO2
3456	1	ROS	060916	0138	BO	61 25.0 N	005 00.9 W	GPS	227	2	10	CTD,LADCP,O2,SiO3,PO4,CO2
3456	1	ROS	060916	0155	EN	61 24.9 N	005 00.9 W	GPS	227	2	10	CTD,LADCP,O2,SiO3,PO4,CO2
3457	1	ROS	060916	0307	BE	61 30.8 N	005 18.5 W	GPS	290	4	12	CTD,LADCP,O2,SiO3,PO4,CO2
3457	1	ROS	060916	0322	BO	61 31.0 N	005 19.0 W	GPS	290	4	12	CTD,LADCP,O2,SiO3,PO4,CO2
3457	1	ROS	060916	0341	EN	61 31.0 N	005 19.1 W	GPS	290	4	12	CTD,LADCP,O2,SiO3,PO4,CO2
3458	1	ROS	060916	0450	BE	61 36.8 N	005 35.5 W	GPS	320	3	12	CTD,LADCP,O2,SiO3,PO4,CO2
3458	1	ROS	060916	0504	BO	61 36.9 N	005 36.0 W	GPS	320	3	12	CTD,LADCP,O2,SiO3,PO4,CO2
3458	1	ROS	060916	0524	EN	61 36.9 N	005 36.2 W	GPS	320	3	12	CTD,LADCP,O2,SiO3,PO4,CO2
3459	1	ROS	060916	0636	BE	61 42.4 N	005 57.3 W	GPS	296	5	11	CTD,LADCP,O2,SiO3,PO4,CO2
3459	1	ROS	060916	0651	BO	61 42.5 N	005 57.7 W	GPS	296	5	11	CTD,LADCP,O2,SiO3,PO4,CO2
3459	1	ROS	060916	0707	EN	61 42.4 N	005 58.0 W	GPS	296	5	11	CTD,LADCP,O2,SiO3,PO4,CO2
3460	1	ROS	060916	0829	BE	61 49.8 N	006 21.8 W	GPS	79	4	5	CTD,LADCP,O2,SiO3,PO4,CO2
3460	1	ROS	060916	0850	BO	61 50.0 N	006 22.0 W	GPS	79	4	5	CTD,LADCP,O2,SiO3,PO4,CO2
3460	1	ROS	060916	0857	EN	61 50.1 N	006 22.0 W	GPS	79	4	5	CTD,LADCP,O2,SiO3,PO4,CO2
3461	1	ROS	060916	1603	BE	62 20.1 N	007 14.6 W	GPS	93	5	19	CTD,LADCP,O2,SiO3,PO4,CO2
3461	1	ROS	060916	1623	BO	62 19.9 N	007 15.0 W	GPS	93	5	19	CTD,LADCP,O2,SiO3,PO4,CO2
3461	1	ROS	060916	1631	EN	62 19.9 N	007 15.1 W	GPS	93	5	19	CTD,LADCP,O2,SiO3,PO4,CO2
3462	1	ROS	060916	1748	BE	62 25.8 N	007 38.5 W	GPS	107	4	6	CTD,LADCP,O2,SiO3,PO4,CO2
3462	1	ROS	060916	1813	BO	62 25.8 N	007 39.6 W	GPS	107	4	6	CTD,LADCP,O2,SiO3,PO4,CO2
3462	1	ROS	060916	1821	EN	62 25.7 N	007 39.7 W	GPS	107	4	6	CTD,LADCP,O2,SiO3,PO4,CO2
3463	1	ROS	060916	1942	BE	62 34.8 N	008 01.7 W	GPS	413	4	13	CTD,LADCP,O2,SiO3,PO4,CO2
3463	1	ROS	060916	1958	BO	62 35.0 N	008 02.0 W	GPS	413	4	13	CTD,LADCP,O2,SiO3,PO4,CO2
3463	1	ROS	060916	2017	EN	62 35.0 N	008 02.0 W	GPS	413	4	13	CTD,LADCP,O2,SiO3,PO4,CO2
3464	1	ROS	060916	2144	BE	62 43.7 N	008 27.1 W	GPS	486	5	22	CTD,LADCP,O2,SiO3,PO4,CO2
3464	1	ROS	060916	2202	BO	62 44.0 N	008 27.2 W	GPS	486	5	22	CTD,LADCP,O2,SiO3,PO4,CO2
3464	1	ROS	060916	2225	EN	62 44.2 N	008 27.5 W	GPS	486	5	22	CTD,LADCP,O2,SiO3,PO4,CO2
3465	1	ROS	061016	0010	BE	62 50.7 N	008 50.0 W	GPS	463	3	14	CTD,LADCP,O2,SiO3,PO4,CO2
3465	1	ROS	061016	0027	BO	62 51.1 N	008 49.9 W	GPS	463	3	14	CTD,LADCP,O2,SiO3,PO4,CO2
3465	1	ROS	061016	0049	EN	62 51.2 N	008 49.5 W	GPS	463	3	14	CTD,LADCP,O2,SiO3,PO4,CO2

3466	1	ROS	061016	0207	BE	62 57.8 N	009 08.5 W	GPS	450	4	15	CTD,LADCP,O2,SiO3,PO4,CO2
3466	1	ROS	061016	0226	BO	62 58.0 N	009 08.8 W	GPS	450	4	15	CTD,LADCP,O2,SiO3,PO4,CO2
3466	1	ROS	061016	0248	EN	62 58.1 N	009 08.5 W	GPS	450	4	15	CTD,LADCP,O2,SiO3,PO4,CO2
3467	1	ROS	061016	0431	BE	63 05.8 N	009 37.4 W	GPS	493	3	16	CTD,LADCP,O2,SiO3,PO4,CO2
3467	1	ROS	061016	0449	BO	63 05.9 N	009 38.2 W	GPS	493	3	16	CTD,LADCP,O2,SiO3,PO4,CO2
3467	1	ROS	061016	0514	EN	63 05.9 N	009 38.4 W	GPS	493	3	16	CTD,LADCP,O2,SiO3,PO4,CO2
3468	1	ROS	061016	0630	BE	63 13.8 N	009 57.6 W	GPS	484	4	15	CTD,LADCP,O2,SiO3,PO4,CO2
3468	1	ROS	061016	0648	BO	63 13.9 N	009 58.1 W	GPS	484	4	15	CTD,LADCP,O2,SiO3,PO4,CO2
3468	1	ROS	061016	0709	EN	63 13.9 N	009 58.2 W	GPS	484	4	15	CTD,LADCP,O2,SiO3,PO4,CO2
3469	1	ROS	061016	0838	BE	63 19.9 N	010 24.9 W	GPS	329	4	11	CTD,LADCP,O2,SiO3,PO4,CO2
3469	1	ROS	061016	0850	BO	63 20.0 N	010 25.0 W	GPS	329	4	11	CTD,LADCP,O2,SiO3,PO4,CO2
3469	1	ROS	061016	0905	EN	63 20.0 N	010 25.1 W	GPS	329	4	11	CTD,LADCP,O2,SiO3,PO4,CO2
3470	1	ROS	061016	1045	BE	63 29.0 N	010 49.0 W	GPS	445	3	22	CTD,LADCP,O2,SiO3,PO4,CO2
3470	1	ROS	061016	1056	BO	63 29.0 N	010 48.9 W	GPS	445	3	22	CTD,LADCP,O2,SiO3,PO4,CO2
3470	1	ROS	061016	1115	EN	63 29.2 N	010 48.8 W	GPS	445	3	22	CTD,LADCP,O2,SiO3,PO4,CO2
3471	1	ROS	061016	1252	BE	63 35.9 N	011 14.4 W	GPS	303	3	12	CTD,LADCP,O2,SiO3,PO4,CO2
3471	1	ROS	061016	1306	BO	63 36.0 N	011 14.5 W	GPS	303	3	12	CTD,LADCP,O2,SiO3,PO4,CO2
3471	1	ROS	061016	1322	EN	63 36.0 N	011 14.2 W	GPS	303	3	12	CTD,LADCP,O2,SiO3,PO4,CO2
3472	1	ROS	061016	1504	BE	63 43.9 N	011 39.7 W	GPS	348	3	14	CTD,LADCP,O2,SiO3,PO4,CO2
3472	1	ROS	061016	1519	BO	63 43.9 N	011 40.0 W	GPS	348	3	14	CTD,LADCP,O2,SiO3,PO4,CO2
3472	1	ROS	061016	1535	EN	63 43.8 N	011 39.9 W	GPS	348	3	14	CTD,LADCP,O2,SiO3,PO4,CO2
3473	1	ROS	061016	1655	BE	63 49.9 N	011 59.6 W	GPS	389	4	17	CTD,LADCP,O2,SiO3,PO4,CO2
3473	1	ROS	061016	1710	BO	63 49.9 N	011 59.9 W	GPS	389	4	17	CTD,LADCP,O2,SiO3,PO4,CO2
3473	1	ROS	061016	1731	EN	63 49.9 N	011 59.9 W	GPS	389	4	17	CTD,LADCP,O2,SiO3,PO4,CO2
3474	1	ROS	061016	1854	BE	63 56.9 N	012 20.0 W	GPS	457	2	15	CTD,LADCP,O2,SiO3,PO4,CO2
3474	1	ROS	061016	1906	BO	63 56.9 N	012 19.9 W	GPS	457	2	15	CTD,LADCP,O2,SiO3,PO4,CO2
3474	1	ROS	061016	1927	EN	63 56.8 N	012 19.8 W	GPS	457	2	15	CTD,LADCP,O2,SiO3,PO4,CO2
3475	1	ROS	061016	2027	BE	64 01.0 N	012 37.6 W	GPS	570	2	18	CTD,LADCP,O2,SiO3,PO4,CO2
3475	1	ROS	061016	2046	BO	64 01.0 N	012 38.3 W	GPS	570	2	18	CTD,LADCP,O2,SiO3,PO4,CO2
3475	1	ROS	061016	2113	EN	64 01.0 N	012 38.4 W	GPS	570	2	18	CTD,LADCP,O2,SiO3,PO4,CO2
3476	1	ROS	061016	2203	BE	64 05.1 N	012 51.4 W	GPS	578	3	18	CTD,LADCP,O2,SiO3,PO4,CO2
3476	1	ROS	061016	2221	BO	64 05.1 N	012 51.6 W	GPS	578	3	18	CTD,LADCP,O2,SiO3,PO4,CO2
3476	1	ROS	061016	2248	EN	64 05.1 N	012 51.3 W	GPS	578	3	18	CTD,LADCP,O2,SiO3,PO4,CO2

3477	1	ROS	061016	2335	BE	64 08.1 N	013 02.4 W	GPS	169	3	8	CTD,LADCP,O2,SiO3,PO4,CO2
3477	1	ROS	061016	2346	BO	64 08.0 N	013 02.5 W	GPS	169	3	8	CTD,LADCP,O2,SiO3,PO4,CO2
3477	1	ROS	061016	2358	EN	64 08.1 N	013 02.1 W	GPS	169	3	8	CTD,LADCP,O2,SiO3,PO4,CO2
3478	1	ROS	061116	0104	BE	64 13.8 N	013 20.5 W	GPS	176	3	8	CTD,LADCP,O2,SiO3,PO4,CO2
3478	1	ROS	061116	0116	BO	64 14.1 N	013 20.9 W	GPS	176	3	8	CTD,LADCP,O2,SiO3,PO4,CO2
3478	1	ROS	061116	0128	EN	64 14.3 N	013 20.7 W	GPS	176	3	8	CTD,LADCP,O2,SiO3,PO4,CO2
3479	1	ROS	061116	0222	BE	64 16.8 N	013 35.3 W	GPS	170	4	8	CTD,LADCP,O2,SiO3,PO4,CO2
3479	1	ROS	061116	0234	BO	64 17.0 N	013 35.9 W	GPS	170	4	8	CTD,LADCP,O2,SiO3,PO4,CO2
3479	1	ROS	061116	0245	EN	64 17.1 N	013 35.7 W	GPS	170	4	8	CTD,LADCP,O2,SiO3,PO4,CO2
3480	1	ROS	061116	0421	BE	64 24.4 N	014 02.6 W	GPS	108	5	5	CTD,LADCP,O2,SiO3,PO4,CO2
3480	1	ROS	061116	0433	BO	64 24.6 N	014 03.0 W	GPS	108	5	5	CTD,LADCP,O2,SiO3,PO4,CO2
3480	1	ROS	061116	0441	EN	64 24.6 N	014 02.9 W	GPS	108	5	5	CTD,LADCP,O2,SiO3,PO4,CO2
3481	1	ROS	061116	0614	BE	64 17.1 N	013 36.5 W	GPS	169	4	8	CTD,LADCP,O2,SiO3,PO4,CO2
3481	1	ROS	061116	0627	BO	64 17.0 N	013 35.9 W	GPS	169	4	8	CTD,LADCP,O2,SiO3,PO4,CO2
3481	1	ROS	061116	0648	EN	64 16.9 N	013 35.9 W	GPS	169	4	8	CTD,LADCP,O2,SiO3,PO4,CO2
3482	1	ROS	061116	0741	BE	64 14.0 N	013 20.9 W	GPS	176	3	10	CTD,LADCP,O2,SiO3,PO4,CO2
3482	1	ROS	061116	0757	BO	64 13.8 N	013 20.9 W	GPS	176	3	10	CTD,LADCP,O2,SiO3,PO4,CO2
3482	1	ROS	061116	0810	EN	64 13.8 N	013 20.9 W	GPS	176	3	10	CTD,LADCP,O2,SiO3,PO4,CO2
3483	1	ROS	061116	0918	BE	64 08.0 N	013 03.2 W	GPS	163	5	13	CTD,LADCP,O2,SiO3,PO4,CO2
3483	1	ROS	061116	0935	BO	64 08.0 N	013 03.4 W	GPS	163	5	13	CTD,LADCP,O2,SiO3,PO4,CO2
3483	1	ROS	061116	0945	EN	64 07.9 N	013 03.5 W	GPS	163	5	13	CTD,LADCP,O2,SiO3,PO4,CO2
3484	1	ROS	061116	1029	BE	64 05.1 N	012 52.3 W	GPS	578	4	16	CTD,LADCP,O2,SiO3,PO4,CO2
3484	1	ROS	061116	1046	BO	64 05.0 N	012 52.0 W	GPS	578	4	16	CTD,LADCP,O2,SiO3,PO4,CO2
3484	1	ROS	061116	1110	EN	64 05.1 N	012 52.0 W	GPS	578	4	16	CTD,LADCP,O2,SiO3,PO4,CO2
3485	1	ROS	061116	1202	BE	64 01.0 N	012 38.1 W	GPS	567	4	22	CTD,LADCP,O2,SiO3,PO4,CO2
3485	1	ROS	061116	1218	BO	64 01.1 N	012 37.8 W	GPS	567	4	22	CTD,LADCP,O2,SiO3,PO4,CO2
3485	1	ROS	061116	1241	EN	64 01.4 N	012 37.2 W	GPS	567	4	22	CTD,LADCP,O2,SiO3,PO4,CO2
3486	1	ROS	061116	1405	BE	63 57.0 N	012 20.2 W	GPS	453	4	16	CTD,LADCP,O2,SiO3,PO4,CO2
3486	1	ROS	061116	1420	BO	63 57.0 N	012 19.4 W	GPS	453	4	16	CTD,LADCP,O2,SiO3,PO4,CO2
3486	1	ROS	061116	1441	EN	63 57.1 N	012 18.8 W	GPS	453	4	16	CTD,LADCP,O2,SiO3,PO4,CO2
3487	1	ROS	061116	1557	BE	63 50.0 N	012 00.2 W	GPS	390	4	12	CTD,LADCP,O2,SiO3,PO4,CO2
3487	1	ROS	061116	1611	BO	63 50.0 N	012 00.1 W	GPS	390	4	12	CTD,LADCP,O2,SiO3,PO4,CO2
3487	1	ROS	061116	1627	EN	63 50.0 N	012 00.3 W	GPS	390	4	12	CTD,LADCP,O2,SiO3,PO4,CO2

3488	1	ROS	061116	1753	BE	63 44.1 N	011 40.3 W	GPS	349	1	14	CTD,LADCP,O2,SiO3,PO4,CO2
3488	1	ROS	061116	1807	BO	63 44.0 N	011 40.3 W	GPS	349	1	14	CTD,LADCP,O2,SiO3,PO4,CO2
3488	1	ROS	061116	1827	EN	63 44.1 N	011 40.8 W	GPS	349	1	14	CTD,LADCP,O2,SiO3,PO4,CO2
3489	1	ROS	061116	2006	BE	63 36.1 N	011 15.5 W	GPS	306	3	12	CTD,LADCP,O2,SiO3,PO4,CO2
3489	1	ROS	061116	2020	BO	63 35.8 N	011 15.1 W	GPS	306	3	12	CTD,LADCP,O2,SiO3,PO4,CO2
3489	1	ROS	061116	2036	EN	63 35.7 N	011 15.2 W	GPS	306	3	12	CTD,LADCP,O2,SiO3,PO4,CO2
3490	1	ROS	061116	2201	BE	63 29.2 N	010 49.5 W	GPS	444	4	14	CTD,LADCP,O2,SiO3,PO4,CO2
3490	1	ROS	061116	2217	BO	63 29.1 N	010 48.9 W	GPS	444	4	14	CTD,LADCP,O2,SiO3,PO4,CO2
3490	1	ROS	061116	2236	EN	63 29.3 N	010 48.7 W	GPS	444	4	14	CTD,LADCP,O2,SiO3,PO4,CO2
3491	1	ROS	061216	0016	BE	63 20.1 N	010 25.4 W	GPS	332	3	13	CTD,LADCP,O2,SiO3,PO4,CO2
3491	1	ROS	061216	0031	BO	63 20.0 N	010 24.8 W	GPS	332	3	13	CTD,LADCP,O2,SiO3,PO4,CO2
3491	1	ROS	061216	0049	EN	63 20.1 N	010 24.6 W	GPS	332	3	13	CTD,LADCP,O2,SiO3,PO4,CO2
3492	1	ROS	061216	0216	BE	63 14.1 N	009 58.5 W	GPS	487	5	15	CTD,LADCP,O2,SiO3,PO4,CO2
3492	1	ROS	061216	0233	BO	63 14.1 N	009 57.5 W	GPS	487	5	15	CTD,LADCP,O2,SiO3,PO4,CO2
3492	1	ROS	061216	0255	EN	63 14.3 N	009 56.9 W	GPS	487	5	15	CTD,LADCP,O2,SiO3,PO4,CO2
3493	1	ROS	061216	0415	BE	63 06.1 N	009 38.5 W	GPS	495	3	16	CTD,LADCP,O2,SiO3,PO4,CO2
3493	1	ROS	061216	0432	BO	63 06.0 N	009 38.0 W	GPS	495	3	16	CTD,LADCP,O2,SiO3,PO4,CO2
3493	1	ROS	061216	0453	EN	63 06.0 N	009 37.9 W	GPS	495	3	16	CTD,LADCP,O2,SiO3,PO4,CO2
3494	1	ROS	061216	0633	BE	62 58.1 N	009 09.5 W	GPS	449	4	15	CTD,LADCP,O2,SiO3,PO4,CO2
3494	1	ROS	061216	0650	BO	62 58.0 N	009 08.8 W	GPS	449	4	15	CTD,LADCP,O2,SiO3,PO4,CO2
3494	1	ROS	061216	0710	EN	62 57.9 N	009 08.7 W	GPS	449	4	15	CTD,LADCP,O2,SiO3,PO4,CO2
3495	1	ROS	061216	0824	BE	62 51.0 N	008 50.2 W	GPS	464	6	14	CTD,LADCP,O2,SiO3,PO4,CO2
3495	1	ROS	061216	0838	BO	62 51.0 N	008 50.0 W	GPS	464	6	14	CTD,LADCP,O2,SiO3,PO4,CO2
3495	1	ROS	061216	0857	EN	62 50.9 N	008 50.0 W	GPS	464	6	14	CTD,LADCP,O2,SiO3,PO4,CO2
3496	1	ROS	061216	1025	BE	62 44.0 N	008 27.2 W	GPS	482	4	17	CTD,LADCP,O2,SiO3,PO4,CO2
3496	1	ROS	061216	1040	BO	62 44.0 N	008 27.1 W	GPS	482	4	17	CTD,LADCP,O2,SiO3,PO4,CO2
3496	1	ROS	061216	1102	EN	62 44.0 N	008 27.2 W	GPS	482	4	17	CTD,LADCP,O2,SiO3,PO4,CO2
3497	1	ROS	061216	1246	BE	62 35.0 N	008 02.1 W	GPS	410	4	13	CTD,LADCP,O2,SiO3,PO4,CO2
3497	1	ROS	061216	1302	BO	62 35.1 N	008 01.6 W	GPS	410	4	13	CTD,LADCP,O2,SiO3,PO4,CO2
3497	1	ROS	061216	1317	EN	62 35.2 N	008 01.4 W	GPS	410	4	13	CTD,LADCP,O2,SiO3,PO4,CO2
3498	1	ROS	061216	1455	BE	62 26.0 N	007 39.0 W	GPS	105	4	6	CTD,LADCP,O2,SiO3,PO4,CO2
3498	1	ROS	061216	1509	BO	62 26.0 N	007 38.8 W	GPS	105	4	6	CTD,LADCP,O2,SiO3,PO4,CO2
3498	1	ROS	061216	1517	EN	62 26.1 N	007 38.7 W	GPS	105	4	6	CTD,LADCP,O2,SiO3,PO4,CO2

3499	1	ROS	061216	1637	BE	62 20.1 N	007 15.6 W	GPS	93	5	6	CTD,LADCP,O2,SiO3,PO4,CO2
3499	1	ROS	061216	1656	BO	62 20.1 N	007 14.7 W	GPS	93	5	6	CTD,LADCP,O2,SiO3,PO4,CO2
3499	1	ROS	061216	1703	EN	62 20.1 N	007 14.6 W	GPS	93	5	6	CTD,LADCP,O2,SiO3,PO4,CO2
3500	1	ROS	061316	0041	BE	61 50.2 N	006 22.3 W	GPS	78	4	10	CTD,LADCP,O2,SiO3,PO4,CO2
3500	1	ROS	061316	0100	BO	61 50.1 N	006 22.2 W	GPS	78	4	10	CTD,LADCP,O2,SiO3,PO4,CO2
3500	1	ROS	061316	0109	EN	61 50.2 N	006 22.3 W	GPS	78	4	10	CTD,LADCP,O2,SiO3,PO4,CO2
3501	1	ROS	061316	0247	BE	61 42.7 N	005 58.1 W	GPS	302	3	12	CTD,LADCP,O2,SiO3,PO4,CO2
3501	1	ROS	061316	0302	BO	61 42.6 N	005 57.5 W	GPS	302	3	12	CTD,LADCP,O2,SiO3,PO4,CO2
3501	1	ROS	061316	0317	EN	61 42.7 N	005 57.5 W	GPS	302	3	12	CTD,LADCP,O2,SiO3,PO4,CO2
3502	1	ROS	061316	0439	BE	61 37.1 N	005 36.4 W	GPS	318	4	12	CTD,LADCP,O2,SiO3,PO4,CO2
3502	1	ROS	061316	0453	BO	61 37.0 N	005 36.0 W	GPS	318	4	12	CTD,LADCP,O2,SiO3,PO4,CO2
3502	1	ROS	061316	0509	EN	61 37.0 N	005 35.9 W	GPS	318	4	12	CTD,LADCP,O2,SiO3,PO4,CO2
3503	1	ROS	061316	0615	BE	61 31.1 N	005 19.4 W	GPS	289	4	12	CTD,LADCP,O2,SiO3,PO4,CO2
3503	1	ROS	061316	0628	BO	61 31.0 N	005 19.0 W	GPS	289	4	12	CTD,LADCP,O2,SiO3,PO4,CO2
3503	1	ROS	061316	0643	EN	61 30.9 N	005 19.0 W	GPS	289	4	12	CTD,LADCP,O2,SiO3,PO4,CO2
3504	1	ROS	061316	0756	BE	61 24.9 N	005 01.1 W	GPS	225	3	10	CTD,LADCP,O2,SiO3,PO4,CO2
3504	1	ROS	061316	0805	BO	61 24.9 N	005 01.1 W	GPS	225	3	10	CTD,LADCP,O2,SiO3,PO4,CO2
3504	1	ROS	061316	0816	EN	61 24.9 N	005 01.3 W	GPS	225	3	10	CTD,LADCP,O2,SiO3,PO4,CO2
3505	1	ROS	061316	0927	BE	61 20.1 N	004 43.3 W	GPS	721	2	22	CTD,LADCP,O2,SiO3,PO4,CO2
3505	1	ROS	061316	0947	BO	61 19.8 N	004 43.5 W	GPS	721	2	22	CTD,LADCP,O2,SiO3,PO4,CO2
3505	1	ROS	061316	1014	EN	61 19.7 N	004 43.8 W	GPS	721	2	22	CTD,LADCP,O2,SiO3,PO4,CO2
3506	1	ROS	061316	1118	BE	61 16.0 N	004 28.2 W	GPS	1067	10	19	CTD,LADCP,O2,SiO3,PO4,CO2
3506	1	ROS	061316	1142	BO	61 15.9 N	004 28.1 W	GPS	1067	10	19	CTD,LADCP,O2,SiO3,PO4,CO2
3506	1	ROS	061316	1214	EN	61 16.0 N	004 28.3 W	GPS	1067	10	19	CTD,LADCP,O2,SiO3,PO4,CO2
3507	1	ROS	061316	1302	BE	61 12.1 N	004 18.4 W	GPS	1082	4	19	CTD,LADCP,O2,SiO3,PO4,CO2
3507	1	ROS	061316	1329	BO	61 12.1 N	004 18.1 W	GPS	1082	4	19	CTD,LADCP,O2,SiO3,PO4,CO2
3507	1	ROS	061316	1403	EN	61 12.3 N	004 18.1 W	GPS	1082	4	19	CTD,LADCP,O2,SiO3,PO4,CO2
3508	1	ROS	061316	1508	BE	61 08.0 N	004 04.2 W	GPS	1120	4	19	CTD,LADCP,O2,SiO3,PO4,CO2
3508	1	ROS	061316	1533	BO	61 08.1 N	004 04.2 W	GPS	1120	4	19	CTD,LADCP,O2,SiO3,PO4,CO2
3508	1	ROS	061316	1605	EN	61 08.2 N	004 04.4 W	GPS	1120	4	19	CTD,LADCP,O2,SiO3,PO4,CO2
3509	1	ROS	061316	1703	BE	61 04.1 N	003 52.4 W	GPS	1150	5	20	CTD,LADCP,O2,SiO3,PO4,CO2
3509	1	ROS	061316	1730	BO	61 04.0 N	003 52.2 W	GPS	1150	5	20	CTD,LADCP,O2,SiO3,PO4,CO2
3509	1	ROS	061316	1807	EN	61 03.9 N	003 52.5 W	GPS	1150	5	20	CTD,LADCP,O2,SiO3,PO4,CO2

3510	1	ROS	061316	1952	BE	60 59.1 N	003 38.3 W	GPS	1105	5	20	CTD,LADCP,O2,SiO3,PO4,CO2
3510	1	ROS	061316	2018	BO	60 59.1 N	003 37.9 W	GPS	1105	5	20	CTD,LADCP,O2,SiO3,PO4,CO2
3510	1	ROS	061316	2056	EN	60 59.3 N	003 38.3 W	GPS	1105	5	20	CTD,LADCP,O2,SiO3,PO4,CO2
3511	1	ROS	061316	2227	BE	60 52.1 N	003 18.4 W	GPS	687	5	18	CTD,LADCP,O2,SiO3,PO4,CO2
3511	1	ROS	061316	2246	BO	60 52.2 N	003 17.9 W	GPS	687	5	18	CTD,LADCP,O2,SiO3,PO4,CO2
3511	1	ROS	061316	2313	EN	60 52.3 N	003 18.1 W	GPS	687	5	18	CTD,LADCP,O2,SiO3,PO4,CO2
3512	1	ROS	061416	0049	BE	60 45.1 N	002 55.4 W	GPS	356	5	13	CTD,LADCP,O2,SiO3,PO4,CO2
3512	1	ROS	061416	0103	BO	60 45.0 N	002 54.8 W	GPS	356	5	13	CTD,LADCP,O2,SiO3,PO4,CO2
3512	1	ROS	061416	0120	EN	60 45.0 N	002 54.7 W	GPS	356	5	13	CTD,LADCP,O2,SiO3,PO4,CO2
3513	1	ROS	061416	0240	BE	60 38.2 N	002 36.4 W	GPS	134	5	7	CTD,LADCP,O2,SiO3,PO4,CO2
3513	1	ROS	061416	0300	BO	60 38.0 N	002 35.9 W	GPS	134	5	7	CTD,LADCP,O2,SiO3,PO4,CO2
3513	1	ROS	061416	0310	EN	60 38.0 N	002 35.9 W	GPS	134	5	7	CTD,LADCP,O2,SiO3,PO4,CO2
3514	1	ROS	061416	0433	BE	60 31.1 N	002 16.4 W	GPS	143	4	8	CTD,LADCP,O2,SiO3,PO4,CO2
3514	1	ROS	061416	0453	BO	60 31.0 N	002 16.0 W	GPS	143	4	8	CTD,LADCP,O2,SiO3,PO4,CO2
3514	1	ROS	061416	0503	EN	60 31.0 N	002 16.0 W	GPS	143	4	8	CTD,LADCP,O2,SiO3,PO4,CO2
3515	1	ROS	061416	0622	BE	60 25.1 N	001 55.4 W	GPS	115	5	6	CTD,LADCP,O2,SiO3,PO4,CO2
3515	1	ROS	061416	0641	BO	60 24.9 N	001 55.0 W	GPS	115	5	6	CTD,LADCP,O2,SiO3,PO4,CO2
3515	1	ROS	061416	0649	EN	60 24.9 N	001 55.0 W	GPS	115	5	6	CTD,LADCP,O2,SiO3,PO4,CO2
3516	1	ROS	061416	1509	BE	59 30.0 N	003 49.8 W	GPS	159	4	14	CTD,LADCP,O2,SiO3,PO4,CO2
3516	1	ROS	061416	1528	BO	59 30.0 N	003 49.9 W	GPS	159	4	14	CTD,LADCP,O2,SiO3,PO4,CO2
3516	1	ROS	061416	1538	EN	59 30.0 N	003 49.8 W	GPS	159	4	14	CTD,LADCP,O2,SiO3,PO4,CO2
3517	1	ROS	061416	1833	BE	59 29.9 N	004 35.7 W	GPS	91	4	6	CTD,LADCP,O2,SiO3,PO4,CO2
3517	1	ROS	061416	1850	BO	59 30.0 N	004 36.0 W	GPS	91	4	6	CTD,LADCP,O2,SiO3,PO4,CO2
3517	1	ROS	061416	1857	EN	59 30.0 N	004 36.1 W	GPS	91	4	6	CTD,LADCP,O2,SiO3,PO4,CO2
3518	1	ROS	061416	2114	BE	59 29.8 N	005 17.5 W	GPS	108	4	6	CTD,LADCP,O2,SiO3,PO4,CO2
3518	1	ROS	061416	2133	BO	59 30.0 N	005 18.2 W	GPS	108	4	6	CTD,LADCP,O2,SiO3,PO4,CO2
3518	1	ROS	061416	2140	EN	59 30.0 N	005 18.2 W	GPS	108	4	6	CTD,LADCP,O2,SiO3,PO4,CO2
3519	1	ROS	061416	2357	BE	59 29.7 N	005 59.6 W	GPS	139	5	7	CTD,LADCP,O2,SiO3,PO4,CO2
3519	1	ROS	061516	0016	BO	59 29.9 N	006 00.1 W	GPS	139	5	7	CTD,LADCP,O2,SiO3,PO4,CO2
3519	1	ROS	061516	0027	EN	59 29.9 N	006 00.2 W	GPS	139	5	7	CTD,LADCP,O2,SiO3,PO4,CO2
3520	1	ROS	061516	0245	BE	59 29.8 N	006 39.4 W	GPS	578	4	16	CTD,LADCP,O2,SiO3,PO4,CO2
3520	1	ROS	061516	0305	BO	59 30.1 N	006 40.0 W	GPS	578	4	16	CTD,LADCP,O2,SiO3,PO4,CO2
3520	1	ROS	061516	0333	EN	59 30.2 N	006 40.1 W	GPS	578	4	16	CTD,LADCP,O2,SiO3,PO4,CO2

3521	1	ROS	061516	0548	BE	59 29.8 N	007 19.6 W	GPS	1065	4	22	CTD,LADCP,O2,SiO3,PO4,CO2
3521	1	ROS	061516	0615	BO	59 30.0 N	007 19.9 W	GPS	1065	4	22	CTD,LADCP,O2,SiO3,PO4,CO2
3521	1	ROS	061516	0649	EN	59 30.0 N	007 20.0 W	GPS	1065	4	22	CTD,LADCP,O2,SiO3,PO4,CO2
3522	1	ROS	061516	1127	BE	59 29.9 N	007 59.8 W	GPS	1126	4	20	CTD,LADCP,O2,SiO3,PO4,CO2
3522	1	ROS	061516	1152	BO	59 30.1 N	008 00.1 W	GPS	1126	4	20	CTD,LADCP,O2,SiO3,PO4,CO2
3522	1	ROS	061516	1231	EN	59 30.2 N	008 00.3 W	GPS	1126	4	20	CTD,LADCP,O2,SiO3,PO4,CO2
3523	1	ROS	061516	1450	BE	59 29.8 N	008 39.8 W	GPS	1379	1	21	CTD,LADCP,O2,SiO3,PO4,CO2
3523	1	ROS	061516	1519	BO	59 29.9 N	008 39.9 W	GPS	1379	1	21	CTD,LADCP,O2,SiO3,PO4,CO2
3523	1	ROS	061516	1558	EN	59 29.9 N	008 39.9 W	GPS	1379	1	21	CTD,LADCP,O2,SiO3,PO4,CO2
3524	1	ROS	061516	1818	BE	59 29.8 N	009 19.9 W	GPS	1492	9	22	CTD,LADCP,O2,SiO3,PO4,CO2
3524	1	ROS	061516	1851	BO	59 29.9 N	009 20.0 W	GPS	1492	9	22	CTD,LADCP,O2,SiO3,PO4,CO2
3524	1	ROS	061516	1936	EN	59 29.9 N	009 20.0 W	GPS	1492	9	22	CTD,LADCP,O2,SiO3,PO4,CO2
3525	1	ROS	061516	2329	BE	59 29.8 N	009 59.7 W	GPS	1032	3	18	CTD,LADCP,O2,SiO3,PO4,CO2
3525	1	ROS	061516	2354	BO	59 30.0 N	010 00.0 W	GPS	1032	3	18	CTD,LADCP,O2,SiO3,PO4,CO2
3525	1	ROS	061616	0032	EN	59 29.9 N	009 59.8 W	GPS	1032	3	18	CTD,LADCP,O2,SiO3,PO4,CO2
3526	1	ROS	061616	0252	BE	59 29.8 N	010 39.6 W	GPS	1526	4	20	CTD,LADCP,O2,SiO3,PO4,CO2
3526	1	ROS	061616	0326	BO	59 29.9 N	010 39.9 W	GPS	1526	4	20	CTD,LADCP,O2,SiO3,PO4,CO2
3526	1	ROS	061616	0419	EN	59 29.9 N	010 39.9 W	GPS	1526	4	20	CTD,LADCP,O2,SiO3,PO4,CO2
3527	1	ROS	061616	0640	BE	59 29.9 N	011 19.5 W	GPS	1612	5	22	CTD,LADCP,O2,SiO3,PO4,CO2
3527	1	ROS	061616	0718	BO	59 29.9 N	011 20.0 W	GPS	1612	5	22	CTD,LADCP,O2,SiO3,PO4,CO2
3527	1	ROS	061616	0800	EN	59 29.9 N	011 20.0 W	GPS	1612	5	22	CTD,LADCP,O2,SiO3,PO4,CO2
3528	1	ROS	061616	1235	BE	59 29.8 N	011 39.5 W	GPS	1561	5	22	CTD,LADCP,O2,SiO3,PO4,CO2
3528	1	ROS	061616	1311	BO	59 30.0 N	011 39.7 W	GPS	1561	5	22	CTD,LADCP,O2,SiO3,PO4,CO2
3528	1	ROS	061616	1401	EN	59 30.0 N	011 39.5 W	GPS	1561	5	22	CTD,LADCP,O2,SiO3,PO4,CO2
3529	1	ROS	061616	1521	BE	59 29.9 N	011 59.8 W	GPS	1504	10	22	CTD,LADCP,O2,SiO3,PO4,CO2
3529	1	ROS	061616	1551	BO	59 29.9 N	011 59.8 W	GPS	1504	10	22	CTD,LADCP,O2,SiO3,PO4,CO2
3529	1	ROS	061616	1633	EN	59 29.9 N	011 59.8 W	GPS	1504	10	22	CTD,LADCP,O2,SiO3,PO4,CO2
3530	1	ROS	061616	1855	BE	59 29.8 N	012 39.8 W	GPS	1363	8	22	CTD,LADCP,O2,SiO3,PO4,CO2
3530	1	ROS	061616	1924	BO	59 30.0 N	012 39.9 W	GPS	1363	8	22	CTD,LADCP,O2,SiO3,PO4,CO2
3530	1	ROS	061616	2015	EN	59 30.0 N	012 39.9 W	GPS	1363	8	22	CTD,LADCP,O2,SiO3,PO4,CO2
3531	1	ROS	061616	2232	BE	59 29.8 N	013 19.6 W	GPS	1289	3	21	CTD,LADCP,O2,SiO3,PO4,CO2
3531	1	ROS	061616	2302	BO	59 30.0 N	013 19.9 W	GPS	1289	3	21	CTD,LADCP,O2,SiO3,PO4,CO2
3531	1	ROS	061616	2346	EN	59 30.0 N	013 19.9 W	GPS	1289	3	21	CTD,LADCP,O2,SiO3,PO4,CO2

3532	1	ROS	061716	0404	BE	59 29.8 N	013 59.5 W	GPS	1000	5	19	CTD,LADCP,O2,SiO3,PO4,CO2
3532	1	ROS	061716	0430	BO	59 30.0 N	013 59.8 W	GPS	1000	5	19	CTD,LADCP,O2,SiO3,PO4,CO2
3532	1	ROS	061716	0506	EN	59 30.1 N	013 59.8 W	GPS	1000	5	19	CTD,LADCP,O2,SiO3,PO4,CO2
3533	1	ROS	061716	0727	BE	59 29.8 N	014 39.6 W	GPS	1001	3	20	CTD,LADCP,O2,SiO3,PO4,CO2
3533	1	ROS	061716	0752	BO	59 30.0 N	014 39.7 W	GPS	1001	3	20	CTD,LADCP,O2,SiO3,PO4,CO2
3533	1	ROS	061716	0828	EN	59 30.0 N	014 39.4 W	GPS	1001	3	20	CTD,LADCP,O2,SiO3,PO4,CO2
3534	1	ROS	061716	1048	BE	59 30.0 N	015 19.6 W	GPS	1544	9	22	CTD,LADCP,O2,SiO3,PO4,CO2
3534	1	ROS	061716	1125	BO	59 30.1 N	015 19.9 W	GPS	1544	9	22	CTD,LADCP,O2,SiO3,PO4,CO2
3534	1	ROS	061716	1201	EN	59 30.1 N	015 19.9 W	GPS	1544	9	22	CTD,LADCP,O2,SiO3,PO4,CO2
3535	1	ROS	061716	1614	BE	59 29.8 N	015 59.7 W	GPS	1575	10	22	CTD,LADCP,O2,SiO3,PO4,CO2
3535	1	ROS	061716	1648	BO	59 30.0 N	015 59.5 W	GPS	1575	10	22	CTD,LADCP,O2,SiO3,PO4,CO2
3535	1	ROS	061716	1726	EN	59 30.2 N	015 59.3 W	GPS	1575	10	22	CTD,LADCP,O2,SiO3,PO4,CO2
3536	1	ROS	061716	2001	BE	59 30.1 N	016 39.6 W	GPS	1089	4	22	CTD,LADCP,O2,SiO3,PO4,CO2
3536	1	ROS	061716	2030	BO	59 30.0 N	016 39.5 W	GPS	1089	4	22	CTD,LADCP,O2,SiO3,PO4,CO2
3536	1	ROS	061716	2109	EN	59 30.1 N	016 38.8 W	GPS	1089	4	22	CTD,LADCP,O2,SiO3,PO4,CO2
3537	1	ROS	061716	2233	BE	59 30.2 N	016 59.6 W	GPS	1240	6	22	CTD,LADCP,O2,SiO3,PO4,CO2
3537	1	ROS	061716	2302	BO	59 30.0 N	016 59.3 W	GPS	1240	6	22	CTD,LADCP,O2,SiO3,PO4,CO2
3537	1	ROS	061716	2346	EN	59 30.2 N	016 58.5 W	GPS	1240	6	22	CTD,LADCP,O2,SiO3,PO4,CO2
3538	1	ROS	061816	0111	BE	59 30.0 N	017 19.9 W	GPS	1772	4	22	CTD,LADCP,O2,SiO3,PO4,CO2
3538	1	ROS	061816	0146	BO	59 30.0 N	017 19.8 W	GPS	1772	4	22	CTD,LADCP,O2,SiO3,PO4,CO2
3538	1	ROS	061816	0238	EN	59 30.1 N	017 19.4 W	GPS	1772	4	22	CTD,LADCP,O2,SiO3,PO4,CO2
3539	1	ROS	061816	0357	BE	59 30.1 N	017 39.5 W	GPS	548	-999	-999	CTD,LADCP,O2,SiO3,PO4,CO2
3539	1	ROS	061816	0416	BO	59 30.0 N	017 39.9 W	GPS	548	-999	-999	CTD,LADCP,O2,SiO3,PO4,CO2
3539	1	ROS	061816	0417	EN	59 30.0 N	017 39.9 W	GPS	548	-999	-999	CTD,LADCP,O2,SiO3,PO4,CO2
3539_a	1	ROS	061816	0422	BE	59 30.0 N	017 39.9 W	GPS	2038	4	22	CTD,LADCP,O2,SiO3,PO4,CO2
3539_a	1	ROS	061816	0448	BO	59 30.0 N	017 39.8 W	GPS	2038	4	22	CTD,LADCP,O2,SiO3,PO4,CO2
3539_a	1	ROS	061816	0543	EN	59 30.2 N	017 39.5 W	GPS	2038	4	22	CTD,LADCP,O2,SiO3,PO4,CO2
3540	1	ROS	061816	1250	BE	59 30.0 N	017 59.9 W	GPS	2220	3	22	CTD,LADCP,O2,SiO3,PO4,CO2
3540	1	ROS	061816	1336	BO	59 30.0 N	017 59.9 W	GPS	2220	3	22	CTD,LADCP,O2,SiO3,PO4,CO2
3540	1	ROS	061816	1430	EN	59 30.0 N	018 00.0 W	GPS	2220	3	22	CTD,LADCP,O2,SiO3,PO4,CO2
3540g	1	ROS	061816	0830	BE	59 30.7 N	018 00.1 W	GPS	2228	5	-	
3540g	1	ROS	061816	0913	BO	59 30.9 N	018 00.1 W	GPS	2228	5	-	
3540g	1	ROS	061816	0913	EN	59 30.9 N	018 00.1 W	GPS	2228	5	-	

3540g1	1	ROS	061816	0915	BE	59 30.9 N	018 00.1 W	GPS	2228	4	22	Suspended sediment matter
3540g1	1	ROS	061816	0915	BO	59 30.9 N	018 00.1 W	GPS	2228	4	22	Suspended sediment matter
3540g1	1	ROS	061816	1002	EN	59 31.1 N	018 00.0 W	GPS	2228	4	22	Suspended sediment matter
3541	1	ROS	061816	1738	BE	59 30.0 N	018 19.6 W	GPS	2642	5	22	CTD,LADCP,O2,SiO3,PO4,CO2
3541	1	ROS	061816	1831	BO	59 30.0 N	018 20.0 W	GPS	2642	5	22	CTD,LADCP,O2,SiO3,PO4,CO2
3541	1	ROS	061816	1935	EN	59 30.2 N	018 20.0 W	GPS	2642	5	22	CTD,LADCP,O2,SiO3,PO4,CO2
3542	1	ROS	061816	2042	BE	59 30.0 N	018 39.7 W	GPS	2778	10	22	CTD,LADCP,O2,SiO3,PO4,CO2
3542	1	ROS	061816	2136	BO	59 30.0 N	018 40.0 W	GPS	2778	10	22	CTD,LADCP,O2,SiO3,PO4,CO2
3542	1	ROS	061816	2245	EN	59 30.0 N	018 40.1 W	GPS	2778	10	22	CTD,LADCP,O2,SiO3,PO4,CO2
3543	1	ROS	061916	0033	BE	59 30.1 N	019 19.6 W	GPS	2701	4	22	CTD,LADCP,O2,SiO3,PO4,CO2
3543	1	ROS	061916	0125	BO	59 30.3 N	019 19.7 W	GPS	2701	4	22	CTD,LADCP,O2,SiO3,PO4,CO2
3543	1	ROS	061916	0235	EN	59 30.7 N	019 19.5 W	GPS	2701	4	22	CTD,LADCP,O2,SiO3,PO4,CO2
3544	1	ROS	061916	0424	BE	59 30.0 N	019 59.4 W	GPS	2766	4	22	CTD,LADCP,O2,SiO3,PO4,CO2
3544	1	ROS	061916	0521	BO	59 29.4 N	020 00.0 W	GPS	2766	4	22	CTD,LADCP,O2,SiO3,PO4,CO2
3544	1	ROS	061916	0630	EN	59 29.1 N	020 00.1 W	GPS	2766	4	22	CTD,LADCP,O2,SiO3,PO4,CO2
3545	1	ROS	061916	0812	BE	59 29.9 N	020 40.2 W	GPS	2825	4	22	CTD,LADCP,O2,SiO3,PO4,CO2
3545	1	ROS	061916	0907	BO	59 29.8 N	020 40.5 W	GPS	2825	4	22	CTD,LADCP,O2,SiO3,PO4,CO2
3545	1	ROS	061916	1015	EN	59 29.8 N	020 41.4 W	GPS	2825	4	22	CTD,LADCP,O2,SiO3,PO4,CO2
3546	1	ROS	061916	1334	BE	59 29.8 N	021 19.5 W	GPS	2903	10	22	CTD,LADCP,O2,SiO3,PO4,CO2
3546	1	ROS	061916	1431	BO	59 30.5 N	021 20.2 W	GPS	2903	10	22	CTD,LADCP,O2,SiO3,PO4,CO2
3546	1	ROS	061916	1537	EN	59 31.2 N	021 21.1 W	GPS	2903	10	22	CTD,LADCP,O2,SiO3,PO4,CO2
3547	1	ROS	061916	1627	BE	59 29.8 N	021 39.5 W	GPS	2876	7	22	CTD,LADCP,O2,SiO3,PO4,CO2
3547	1	ROS	061916	1724	BO	59 30.0 N	021 40.2 W	GPS	2876	7	22	CTD,LADCP,O2,SiO3,PO4,CO2
3547	1	ROS	061916	1833	EN	59 30.0 N	021 40.2 W	GPS	2876	7	22	CTD,LADCP,O2,SiO3,PO4,CO2
3548	1	ROS	061916	1929	BE	59 29.8 N	021 59.3 W	GPS	2790	6	22	CTD,LADCP,O2,SiO3,PO4,CO2
3548	1	ROS	061916	2026	BO	59 29.9 N	021 59.6 W	GPS	2790	6	22	CTD,LADCP,O2,SiO3,PO4,CO2
3548	1	ROS	061916	2130	EN	59 29.6 N	021 59.2 W	GPS	2790	6	22	CTD,LADCP,O2,SiO3,PO4,CO2
3549	1	ROS	061916	2342	BE	59 29.9 N	022 19.6 W	GPS	2656	9	22	CTD,LADCP,O2,SiO3,PO4,CO2
3549	1	ROS	062016	0034	BO	59 29.7 N	022 19.6 W	GPS	2656	9	22	CTD,LADCP,O2,SiO3,PO4,CO2
3549	1	ROS	062016	0135	EN	59 29.5 N	022 19.5 W	GPS	2656	9	22	CTD,LADCP,O2,SiO3,PO4,CO2
3550	1	ROS	062016	0246	BE	59 29.9 N	022 39.4 W	GPS	2492	1	22	CTD,LADCP,O2,SiO3,PO4,CO2
3550	1	ROS	062016	0337	BO	59 29.6 N	022 39.8 W	GPS	2492	1	22	CTD,LADCP,O2,SiO3,PO4,CO2
3550	1	ROS	062016	0435	EN	59 29.1 N	022 39.6 W	GPS	2492	1	22	CTD,LADCP,O2,SiO3,PO4,CO2

3551	1	ROS	062016	0556	BE	59 29.9 N	022 59.4 W	GPS	2391	2	22	CTD,LADCP,O2,SiO3,PO4,CO2
3551	1	ROS	062016	0653	BO	59 30.1 N	022 59.8 W	GPS	2391	2	22	CTD,LADCP,O2,SiO3,PO4,CO2
3551	1	ROS	062016	0755	EN	59 30.1 N	022 59.5 W	GPS	2391	2	22	CTD,LADCP,O2,SiO3,PO4,CO2
3552	1	ROS	062016	0910	BE	59 29.9 N	023 19.4 W	GPS	2419	5	22	CTD,LADCP,O2,SiO3,PO4,CO2
3552	1	ROS	062016	0959	BO	59 29.8 N	023 19.6 W	GPS	2419	5	22	CTD,LADCP,O2,SiO3,PO4,CO2
3552	1	ROS	062016	1100	EN	59 29.6 N	023 19.5 W	GPS	2419	5	22	CTD,LADCP,O2,SiO3,PO4,CO2
3553	1	ROS	062016	1344	BE	59 29.9 N	023 39.6 W	GPS	2482	6	22	CTD,LADCP,O2,SiO3,PO4,CO2
3553	1	ROS	062016	1435	BO	59 29.7 N	023 39.9 W	GPS	2482	6	22	CTD,LADCP,O2,SiO3,PO4,CO2
3553	1	ROS	062016	1531	EN	59 29.3 N	023 39.8 W	GPS	2482	6	22	CTD,LADCP,O2,SiO3,PO4,CO2
3554	1	ROS	062016	1716	BE	59 29.9 N	023 59.4 W	GPS	2523	5	22	CTD,LADCP,O2,SiO3,PO4,CO2
3554	1	ROS	062016	1809	BO	59 29.9 N	024 00.0 W	GPS	2523	5	22	CTD,LADCP,O2,SiO3,PO4,CO2
3554	1	ROS	062016	1913	EN	59 30.0 N	023 59.9 W	GPS	2523	5	22	CTD,LADCP,O2,SiO3,PO4,CO2
3555	1	ROS	062016	2104	BE	59 30.0 N	024 19.6 W	GPS	2616	3	22	CTD,LADCP,O2,SiO3,PO4,CO2
3555	1	ROS	062016	2155	BO	59 29.9 N	024 20.0 W	GPS	2616	3	22	CTD,LADCP,O2,SiO3,PO4,CO2
3555	1	ROS	062016	2256	EN	59 30.0 N	024 20.0 W	GPS	2616	3	22	CTD,LADCP,O2,SiO3,PO4,CO2
3556	1	ROS	062116	1025	BE	59 29.8 N	024 42.5 W	GPS	2533	5	22	CTD,LADCP,O2,SiO3,PO4,CO2
3556	1	ROS	062116	1114	BO	59 29.8 N	024 42.6 W	GPS	2533	5	22	CTD,LADCP,O2,SiO3,PO4,CO2
3556	1	ROS	062116	1213	EN	59 29.9 N	024 42.6 W	GPS	2533	5	22	CTD,LADCP,O2,SiO3,PO4,CO2
3556g	1	ROS	062116	0601	BE	59 29.8 N	024 42.0 W	GPS	2552	7	22	Suspended sediment matter
3556g	1	ROS	062116	0648	BO	59 29.8 N	024 42.0 W	GPS	2552	7	22	Suspended sediment matter
3556g	1	ROS	062116	0738	EN	59 29.8 N	024 42.1 W	GPS	2552	7	22	Suspended sediment matter
3557	1	ROS	062116	1328	BE	59 30.0 N	024 59.8 W	GPS	2507	11	22	CTD,LADCP,O2,SiO3,PO4,CO2
3557	1	ROS	062116	1414	BO	59 29.8 N	025 00.0 W	GPS	2507	11	22	CTD,LADCP,O2,SiO3,PO4,CO2
3557	1	ROS	062116	1511	EN	59 29.8 N	025 00.0 W	GPS	2507	11	22	CTD,LADCP,O2,SiO3,PO4,CO2
3558	1	ROS	062116	1624	BE	59 29.9 N	025 19.5 W	GPS	2488	5	22	CTD,LADCP,O2,SiO3,PO4,CO2
3558	1	ROS	062116	1714	BO	59 29.9 N	025 20.0 W	GPS	2488	5	22	CTD,LADCP,O2,SiO3,PO4,CO2
3558	1	ROS	062116	1813	EN	59 29.9 N	025 20.0 W	GPS	2488	5	22	CTD,LADCP,O2,SiO3,PO4,CO2
3559	1	ROS	062116	1925	BE	59 29.9 N	025 39.5 W	GPS	2506	3	22	CTD,LADCP,O2,SiO3,PO4,CO2
3559	1	ROS	062116	2017	BO	59 29.7 N	025 40.0 W	GPS	2506	3	22	CTD,LADCP,O2,SiO3,PO4,CO2
3559	1	ROS	062116	2118	EN	59 29.3 N	025 40.4 W	GPS	2506	3	22	CTD,LADCP,O2,SiO3,PO4,CO2
3560	1	ROS	062116	2231	BE	59 29.9 N	025 59.5 W	GPS	2387	5	22	CTD,LADCP,O2,SiO3,PO4,CO2
3560	1	ROS	062116	2322	BO	59 30.2 N	025 59.5 W	GPS	2387	5	22	CTD,LADCP,O2,SiO3,PO4,CO2
3560	1	ROS	062216	0022	EN	59 30.3 N	025 59.6 W	GPS	2387	5	22	CTD,LADCP,O2,SiO3,PO4,CO2

3561	1	ROS	062216	0136	BE	59 29.9 N	026 19.4 W	GPS	2305	4	22	CTD,LADCP,O2,SiO3,PO4,CO2
3561	1	ROS	062216	0226	BO	59 30.1 N	026 19.5 W	GPS	2305	4	22	CTD,LADCP,O2,SiO3,PO4,CO2
3561	1	ROS	062216	0328	EN	59 30.2 N	026 19.0 W	GPS	2305	4	22	CTD,LADCP,O2,SiO3,PO4,CO2
3562	1	ROS	062216	0446	BE	59 29.9 N	026 39.4 W	GPS	2239	4	22	CTD,LADCP,O2,SiO3,PO4,CO2
3562	1	ROS	062216	0534	BO	59 29.9 N	026 39.8 W	GPS	2239	4	22	CTD,LADCP,O2,SiO3,PO4,CO2
3562	1	ROS	062216	0633	EN	59 29.9 N	026 39.6 W	GPS	2239	4	22	CTD,LADCP,O2,SiO3,PO4,CO2
3562g	1	ROS	062216	1016	BE	59 29.9 N	026 39.6 W	GPS	2277	5	22	Suspended sediment matter
3562g	1	ROS	062216	1102	BO	59 29.9 N	026 39.6 W	GPS	2277	5	22	Suspended sediment matter
3562g	1	ROS	062216	1146	EN	59 29.9 N	026 39.7 W	GPS	2277	5	22	Suspended sediment matter
3563	1	ROS	062216	1414	BE	59 29.8 N	026 59.7 W	GPS	1993	10	22	CTD,LADCP,O2,SiO3,PO4,CO2
3563	1	ROS	062216	1456	BO	59 29.8 N	027 00.0 W	GPS	1993	10	22	CTD,LADCP,O2,SiO3,PO4,CO2
3563	1	ROS	062216	1544	EN	59 29.6 N	027 00.1 W	GPS	1993	10	22	CTD,LADCP,O2,SiO3,PO4,CO2
3564	1	ROS	062216	1651	BE	59 29.8 N	027 19.5 W	GPS	1907	5	22	CTD,LADCP,O2,SiO3,PO4,CO2
3564	1	ROS	062216	1731	BO	59 29.9 N	027 20.0 W	GPS	1907	5	22	CTD,LADCP,O2,SiO3,PO4,CO2
3564	1	ROS	062216	1819	EN	59 29.9 N	027 20.0 W	GPS	1907	5	22	CTD,LADCP,O2,SiO3,PO4,CO2
3565	1	ROS	062216	1924	BE	59 29.9 N	027 39.5 W	GPS	2029	9	22	CTD,LADCP,O2,SiO3,PO4,CO2
3565	1	ROS	062216	2007	BO	59 29.9 N	027 40.2 W	GPS	2029	9	22	CTD,LADCP,O2,SiO3,PO4,CO2
3565	1	ROS	062216	2101	EN	59 29.9 N	027 40.3 W	GPS	2029	9	22	CTD,LADCP,O2,SiO3,PO4,CO2
3566	1	ROS	062216	2203	BE	59 29.9 N	027 59.6 W	GPS	1999	3	22	CTD,LADCP,O2,SiO3,PO4,CO2
3566	1	ROS	062216	2245	BO	59 30.0 N	028 00.2 W	GPS	1999	3	22	CTD,LADCP,O2,SiO3,PO4,CO2
3566	1	ROS	062216	2337	EN	59 30.0 N	028 00.4 W	GPS	1999	3	22	CTD,LADCP,O2,SiO3,PO4,CO2
3567	1	ROS	062316	0047	BE	59 30.0 N	028 19.9 W	GPS	1993	25	22	CTD,LADCP,O2,SiO3,PO4,CO2
3567	1	ROS	062316	0128	BO	59 30.0 N	028 19.9 W	GPS	1993	25	22	CTD,LADCP,O2,SiO3,PO4,CO2
3567	1	ROS	062316	0224	EN	59 30.0 N	028 19.9 W	GPS	1993	25	22	CTD,LADCP,O2,SiO3,PO4,CO2
3568	1	ROS	062316	0332	BE	59 29.9 N	028 39.4 W	GPS	1718	10	22	CTD,LADCP,O2,SiO3,PO4,CO2
3568	1	ROS	062316	0409	BO	59 30.0 N	028 40.0 W	GPS	1718	10	22	CTD,LADCP,O2,SiO3,PO4,CO2
3568	1	ROS	062316	0456	EN	59 30.0 N	028 40.0 W	GPS	1718	10	22	CTD,LADCP,O2,SiO3,PO4,CO2
3569	1	ROS	062316	0756	BE	59 30.0 N	028 59.9 W	GPS	1498	1	22	CTD,LADCP,O2,SiO3,PO4,CO2
3569	1	ROS	062316	0828	BO	59 30.0 N	029 00.2 W	GPS	1498	1	22	CTD,LADCP,O2,SiO3,PO4,CO2
3569	1	ROS	062316	0907	EN	59 29.9 N	029 00.3 W	GPS	1498	1	22	CTD,LADCP,O2,SiO3,PO4,CO2
3570	1	ROS	062316	1013	BE	59 30.1 N	029 19.9 W	GPS	1413	10	22	CTD,LADCP,O2,SiO3,PO4,CO2
3570	1	ROS	062316	1045	BO	59 30.1 N	029 19.6 W	GPS	1413	10	22	CTD,LADCP,O2,SiO3,PO4,CO2
3570	1	ROS	062316	1123	EN	59 30.2 N	029 19.4 W	GPS	1413	10	22	CTD,LADCP,O2,SiO3,PO4,CO2

3571	1	ROS	062316	1239	BE	59 30.0 N	029 39.8 W	GPS	1430	8	22	CTD,LADCP,O2,SiO3,PO4,CO2
3571	1	ROS	062316	1309	BO	59 29.8 N	029 39.3 W	GPS	1430	8	22	CTD,LADCP,O2,SiO3,PO4,CO2
3571	1	ROS	062316	1347	EN	59 29.5 N	029 38.8 W	GPS	1430	8	22	CTD,LADCP,O2,SiO3,PO4,CO2
3572	1	ROS	062316	1503	BE	59 30.0 N	029 59.7 W	GPS	1433	8	22	CTD,LADCP,O2,SiO3,PO4,CO2
3572	1	ROS	062316	1534	BO	59 29.9 N	029 59.7 W	GPS	1433	8	22	CTD,LADCP,O2,SiO3,PO4,CO2
3572	1	ROS	062316	1614	EN	59 29.8 N	029 59.2 W	GPS	1433	8	22	CTD,LADCP,O2,SiO3,PO4,CO2
3573	1	ROS	062316	1725	BE	59 30.1 N	030 19.7 W	GPS	1307	5	22	CTD,LADCP,O2,SiO3,PO4,CO2
3573	1	ROS	062316	1754	BO	59 30.1 N	030 19.7 W	GPS	1307	5	22	CTD,LADCP,O2,SiO3,PO4,CO2
3573	1	ROS	062316	1830	EN	59 30.3 N	030 19.6 W	GPS	1307	5	22	CTD,LADCP,O2,SiO3,PO4,CO2
3574	1	ROS	062316	1939	BE	59 30.1 N	030 39.5 W	GPS	1532	5	22	CTD,LADCP,O2,SiO3,PO4,CO2
3574	1	ROS	062316	2013	BO	59 30.1 N	030 39.8 W	GPS	1532	5	22	CTD,LADCP,O2,SiO3,PO4,CO2
3574	1	ROS	062316	2057	EN	59 30.3 N	030 39.6 W	GPS	1532	5	22	CTD,LADCP,O2,SiO3,PO4,CO2
3575	1	ROS	062416	0003	BE	59 30.1 N	030 59.5 W	GPS	1528	5	22	CTD,LADCP,O2,SiO3,PO4,CO2
3575	1	ROS	062416	0038	BO	59 30.0 N	030 59.7 W	GPS	1528	5	22	CTD,LADCP,O2,SiO3,PO4,CO2
3575	1	ROS	062416	0122	EN	59 29.9 N	030 59.7 W	GPS	1528	5	22	CTD,LADCP,O2,SiO3,PO4,CO2
3576	1	ROS	062416	0236	BE	59 30.0 N	031 19.8 W	GPS	1749	1	22	CTD,LADCP,O2,SiO3,PO4,CO2
3576	1	ROS	062416	0311	BO	59 29.9 N	031 19.9 W	GPS	1749	1	22	CTD,LADCP,O2,SiO3,PO4,CO2
3576	1	ROS	062416	0359	EN	59 29.9 N	031 19.9 W	GPS	1749	1	22	CTD,LADCP,O2,SiO3,PO4,CO2
3577	1	ROS	062416	0513	BE	59 30.0 N	031 39.9 W	GPS	1902	5	22	CTD,LADCP,O2,SiO3,PO4,CO2
3577	1	ROS	062416	0548	BO	59 29.9 N	031 39.9 W	GPS	1902	5	22	CTD,LADCP,O2,SiO3,PO4,CO2
3577	1	ROS	062416	0638	EN	59 30.0 N	031 39.9 W	GPS	1902	5	22	CTD,LADCP,O2,SiO3,PO4,CO2
3578	1	ROS	062416	0748	BE	59 30.1 N	031 59.7 W	GPS	1922	5	22	CTD,LADCP,O2,SiO3,PO4,CO2
3578	1	ROS	062416	0828	BO	59 30.0 N	032 00.0 W	GPS	1922	5	22	CTD,LADCP,O2,SiO3,PO4,CO2
3578	1	ROS	062416	0913	EN	59 30.0 N	031 59.9 W	GPS	1922	5	22	CTD,LADCP,O2,SiO3,PO4,CO2
3579	1	ROS	062416	1047	BE	59 30.0 N	032 25.1 W	GPS	2126	4	22	CTD,LADCP,O2,SiO3,PO4,CO2
3579	1	ROS	062416	1130	BO	59 30.1 N	032 24.9 W	GPS	2126	4	22	CTD,LADCP,O2,SiO3,PO4,CO2
3579	1	ROS	062416	1220	EN	59 30.3 N	032 24.3 W	GPS	2126	4	22	CTD,LADCP,O2,SiO3,PO4,CO2
3580	1	ROS	062416	1739	BE	59 30.0 N	032 50.0 W	GPS	2204	5	22	CTD,LADCP,O2,SiO3,PO4,CO2
3580	1	ROS	062416	1825	BO	59 30.0 N	032 50.3 W	GPS	2204	5	22	CTD,LADCP,O2,SiO3,PO4,CO2
3580	1	ROS	062416	1916	EN	59 30.0 N	032 49.8 W	GPS	2204	5	22	CTD,LADCP,O2,SiO3,PO4,CO2
3580g	1	ROS	062416	1504	BE	59 30.0 N	032 49.4 W	GPS	2271	4	22	Suspended sediment matter
3580g	1	ROS	062416	1548	BO	59 30.0 N	032 49.2 W	GPS	2271	4	22	Suspended sediment matter
3580g	1	ROS	062416	1632	EN	59 30.0 N	032 49.1 W	GPS	2271	4	22	Suspended sediment matter

3581	1	ROS	062416	2237	BE	59 30.0 N	033 19.9 W	GPS	2220	9	22	CTD,LADCP,O2,SiO3,PO4,CO2
3581	1	ROS	062416	2319	BO	59 30.0 N	033 19.8 W	GPS	2220	9	22	CTD,LADCP,O2,SiO3,PO4,CO2
3581	1	ROS	062516	0019	EN	59 30.0 N	033 19.8 W	GPS	2220	9	22	CTD,LADCP,O2,SiO3,PO4,CO2
3582	1	ROS	062516	0137	BE	59 30.0 N	033 39.9 W	GPS	2773	10	22	CTD,LADCP,O2,SiO3,PO4,CO2
3582	1	ROS	062516	0232	BO	59 29.9 N	033 39.9 W	GPS	2773	10	22	CTD,LADCP,O2,SiO3,PO4,CO2
3582	1	ROS	062516	0340	EN	59 30.0 N	033 40.0 W	GPS	2773	10	22	CTD,LADCP,O2,SiO3,PO4,CO2
3583	1	ROS	062516	0458	BE	59 30.0 N	033 59.9 W	GPS	2420	5	22	CTD,LADCP,O2,SiO3,PO4,CO2
3583	1	ROS	062516	0546	BO	59 29.9 N	033 59.7 W	GPS	2420	5	22	CTD,LADCP,O2,SiO3,PO4,CO2
3583	1	ROS	062516	0648	EN	59 29.7 N	033 59.7 W	GPS	2420	5	22	CTD,LADCP,O2,SiO3,PO4,CO2
3584	1	ROS	062516	0804	BE	59 30.1 N	034 19.5 W	GPS	2701	5	22	CTD,LADCP,O2,SiO3,PO4,CO2
3584	1	ROS	062516	0858	BO	59 29.6 N	034 19.7 W	GPS	2701	5	22	CTD,LADCP,O2,SiO3,PO4,CO2
3584	1	ROS	062516	0959	EN	59 29.1 N	034 19.3 W	GPS	2701	5	22	CTD,LADCP,O2,SiO3,PO4,CO2
3585	1	ROS	062516	1123	BE	59 30.1 N	034 39.6 W	GPS	2791	2	22	CTD,LADCP,O2,SiO3,PO4,CO2
3585	1	ROS	062516	1217	BO	59 30.1 N	034 39.8 W	GPS	2791	2	22	CTD,LADCP,O2,SiO3,PO4,CO2
3585	1	ROS	062516	1318	EN	59 30.2 N	034 39.2 W	GPS	2791	2	22	CTD,LADCP,O2,SiO3,PO4,CO2
3586	1	ROS	062516	1449	BE	59 30.0 N	034 59.6 W	GPS	3063	4	22	CTD,LADCP,O2,SiO3,PO4,CO2
3586	1	ROS	062516	1549	BO	59 30.1 N	034 59.6 W	GPS	3063	4	22	CTD,LADCP,O2,SiO3,PO4,CO2
3586	1	ROS	062516	1656	EN	59 30.1 N	034 59.0 W	GPS	3063	4	22	CTD,LADCP,O2,SiO3,PO4,CO2
3587	1	ROS	062516	1942	BE	59 30.0 N	035 19.8 W	GPS	1871	2	22	CTD,LADCP,O2,SiO3,PO4,CO2
3587	1	ROS	062516	2018	BO	59 30.1 N	035 19.8 W	GPS	1871	2	22	CTD,LADCP,O2,SiO3,PO4,CO2
3587	1	ROS	062516	2115	EN	59 30.1 N	035 19.8 W	GPS	1871	2	22	CTD,LADCP,O2,SiO3,PO4,CO2
3588	1	ROS	062616	0011	BE	59 30.0 N	035 59.8 W	GPS	3091	4	22	CTD,LADCP,O2,SiO3,PO4,CO2
3588	1	ROS	062616	0109	BO	59 29.7 N	035 59.5 W	GPS	3091	4	22	CTD,LADCP,O2,SiO3,PO4,CO2
3588	1	ROS	062616	0222	EN	59 29.4 N	035 58.9 W	GPS	3091	4	22	CTD,LADCP,O2,SiO3,PO4,CO2
3589	1	ROS	062616	0707	BE	59 29.8 N	036 40.4 W	GPS	3099	6	22	CTD,LADCP,O2,SiO3,PO4,CO2
3589	1	ROS	062616	0810	BO	59 29.8 N	036 40.1 W	GPS	3099	6	22	CTD,LADCP,O2,SiO3,PO4,CO2
3589	1	ROS	062616	0918	EN	59 29.6 N	036 39.7 W	GPS	3099	6	22	CTD,LADCP,O2,SiO3,PO4,CO2
3590	1	ROS	062716	0609	BE	59 30.0 N	038 40.0 W	GPS	2996	1	22	CTD,LADCP,O2,SiO3,PO4,CO2
3590	1	ROS	062716	0705	BO	59 30.0 N	038 39.9 W	GPS	2996	1	22	CTD,LADCP,O2,SiO3,PO4,CO2
3590	1	ROS	062716	0813	EN	59 29.9 N	038 39.8 W	GPS	2996	1	22	CTD,LADCP,O2,SiO3,PO4,CO2
3591	1	ROS	062716	0957	BE	59 30.3 N	037 59.8 W	GPS	3126	5	22	CTD,LADCP,O2,SiO3,PO4,CO2
3591	1	ROS	062716	1114	BO	59 29.7 N	037 59.4 W	GPS	3126	5	22	CTD,LADCP,O2,SiO3,PO4,CO2
3591	1	ROS	062716	1221	EN	59 29.7 N	037 59.4 W	GPS	3126	5	22	CTD,LADCP,O2,SiO3,PO4,CO2

3592	1	ROS	062716	1729	BE	59 29.8 N	037 19.7 W	GPS	3208	7	22	CTD,LADCP,O2,SiO3,PO4,CO2
3592	1	ROS	062716	1829	BO	59 29.9 N	037 19.5 W	GPS	3208	7	22	CTD,LADCP,O2,SiO3,PO4,CO2
3592	1	ROS	062716	1939	EN	59 29.8 N	037 19.4 W	GPS	3208	7	22	CTD,LADCP,O2,SiO3,PO4,CO2
3592g	1	ROS	062716	1401	BE	59 29.7 N	037 20.3 W	GPS	3156	4	22	Suspended sediment matter
3592g	1	ROS	062716	1506	BO	59 29.8 N	037 19.7 W	GPS	3156	4	22	Suspended sediment matter
3592g	1	ROS	062716	1605	EN	59 29.6 N	037 19.5 W	GPS	3156	4	22	Suspended sediment matter
3593	1	ROS	062816	0529	BE	59 29.9 N	039 19.9 W	GPS	2923	4	22	CTD,LADCP,O2,SiO3,PO4,CO2
3593	1	ROS	062816	0626	BO	59 30.1 N	039 19.9 W	GPS	2923	4	22	CTD,LADCP,O2,SiO3,PO4,CO2
3593	1	ROS	062816	0732	EN	59 30.1 N	039 19.9 W	GPS	2923	4	22	CTD,LADCP,O2,SiO3,PO4,CO2
3593a	1	ROS	062816	1050	BE	59 30.1 N	039 20.0 W	GPS	598	999	22	CTD,LADCP,O2,SiO3,PO4,CO2
3593a	1	ROS	062816	1102	BO	59 30.1 N	039 20.1 W	GPS	598	999	22	CTD,LADCP,O2,SiO3,PO4,CO2
3593a	1	ROS	062816	1112	EN	59 30.1 N	039 20.1 W	GPS	598	999	22	CTD,LADCP,O2,SiO3,PO4,CO2
3594	1	ROS	062816	1333	BE	59 29.9 N	039 59.8 W	GPS	2864	4	22	CTD,LADCP,O2,SiO3,PO4,CO2
3594	1	ROS	062816	1429	BO	59 29.8 N	040 00.4 W	GPS	2864	4	22	CTD,LADCP,O2,SiO3,PO4,CO2
3594	1	ROS	062816	1533	EN	59 29.6 N	040 00.7 W	GPS	2864	4	22	CTD,LADCP,O2,SiO3,PO4,CO2
3595	1	ROS	062816	1644	BE	59 29.9 N	040 19.7 W	GPS	2669	4	22	CTD,LADCP,O2,SiO3,PO4,CO2
3595	1	ROS	062816	1736	BO	59 29.9 N	040 20.1 W	GPS	2669	4	22	CTD,LADCP,O2,SiO3,PO4,CO2
3595	1	ROS	062816	1837	EN	59 29.9 N	040 20.1 W	GPS	2669	4	22	CTD,LADCP,O2,SiO3,PO4,CO2
3596	1	ROS	062816	1956	BE	59 30.0 N	040 40.1 W	GPS	2579	4	22	CTD,LADCP,O2,SiO3,PO4,CO2
3596	1	ROS	062816	2046	BO	59 30.1 N	040 39.9 W	GPS	2579	4	22	CTD,LADCP,O2,SiO3,PO4,CO2
3596	1	ROS	062816	2153	EN	59 30.2 N	040 39.7 W	GPS	2579	4	22	CTD,LADCP,O2,SiO3,PO4,CO2
3597	1	ROS	062816	2322	BE	59 33.9 N	041 00.0 W	GPS	2400	6	22	CTD,LADCP,O2,SiO3,PO4,CO2
3597	1	ROS	062916	0011	BO	59 33.9 N	041 00.1 W	GPS	2400	6	22	CTD,LADCP,O2,SiO3,PO4,CO2
3597	1	ROS	062916	0110	EN	59 33.8 N	041 00.4 W	GPS	2400	6	22	CTD,LADCP,O2,SiO3,PO4,CO2
3597g	1	ROS	062916	0214	BE	59 33.7 N	041 00.4 W	GPS	2396	6	22	Suspended sediment matter
3597g	1	ROS	062916	0258	BO	59 33.6 N	041 00.6 W	GPS	2396	6	22	Suspended sediment matter
3597g	1	ROS	062916	0348	EN	59 33.5 N	041 00.8 W	GPS	2396	6	22	Suspended sediment matter
3598	1	ROS	062916	0505	BE	59 38.4 N	041 15.9 W	GPS	2171	5	22	CTD,LADCP,O2,SiO3,PO4,CO2
3598	1	ROS	062916	0550	BO	59 38.4 N	041 16.0 W	GPS	2171	5	22	CTD,LADCP,O2,SiO3,PO4,CO2
3598	1	ROS	062916	0646	EN	59 38.4 N	041 16.2 W	GPS	2171	5	22	CTD,LADCP,O2,SiO3,PO4,CO2
3599	1	ROS	062916	0750	BE	59 42.4 N	041 31.9 W	GPS	1993	5	22	CTD,LADCP,O2,SiO3,PO4,CO2
3599	1	ROS	062916	0829	BO	59 42.4 N	041 32.1 W	GPS	1993	5	22	CTD,LADCP,O2,SiO3,PO4,CO2
3599	1	ROS	062916	0932	EN	59 42.2 N	041 32.1 W	GPS	1993	5	22	CTD,LADCP,O2,SiO3,PO4,CO2

3600	1	ROS	062916	1146	BE	59 46.6 N	041 46.8 W	GPS	1833	5	18	CTD,LADCP,O2,SiO3,PO4,CO2
3600	1	ROS	062916	1238	BO	59 46.1 N	041 46.6 W	GPS	1833	5	18	CTD,LADCP,O2,SiO3,PO4,CO2
3600	1	ROS	062916	1323	EN	59 45.2 N	041 46.4 W	GPS	1833	5	18	CTD,LADCP,O2,SiO3,PO4,CO2
3601	1	ROS	062916	2318	BE	59 54.5 N	042 29.9 W	GPS	200	4	9	CTD,LADCP,O2,SiO3,PO4,CO2
3601	1	ROS	062916	2336	BO	59 54.5 N	042 29.8 W	GPS	200	4	9	CTD,LADCP,O2,SiO3,PO4,CO2
3601	1	ROS	062916	2347	EN	59 54.4 N	042 29.7 W	GPS	200	4	9	CTD,LADCP,O2,SiO3,PO4,CO2
3602	1	ROS	063016	0018	BE	59 54.8 N	042 33.3 W	GPS	186	4	9	CTD,LADCP,O2,SiO3,PO4,CO2
3602	1	ROS	063016	0042	BO	59 54.6 N	042 33.4 W	GPS	186	4	9	CTD,LADCP,O2,SiO3,PO4,CO2
3602	1	ROS	063016	0052	EN	59 54.4 N	042 33.3 W	GPS	186	4	9	CTD,LADCP,O2,SiO3,PO4,CO2
3603	1	ROS	063016	0125	BE	59 55.2 N	042 37.1 W	GPS	184	4	8	CTD,LADCP,O2,SiO3,PO4,CO2
3603	1	ROS	063016	0143	BO	59 55.1 N	042 37.1 W	GPS	184	4	8	CTD,LADCP,O2,SiO3,PO4,CO2
3603	1	ROS	063016	0153	EN	59 55.1 N	042 37.1 W	GPS	184	4	8	CTD,LADCP,O2,SiO3,PO4,CO2
3604	1	ROS	063016	0227	BE	59 55.5 N	042 40.8 W	GPS	192	4	8	CTD,LADCP,O2,SiO3,PO4,CO2
3604	1	ROS	063016	0243	BO	59 55.5 N	042 40.9 W	GPS	192	4	8	CTD,LADCP,O2,SiO3,PO4,CO2
3604	1	ROS	063016	0255	EN	59 55.4 N	042 41.0 W	GPS	192	4	8	CTD,LADCP,O2,SiO3,PO4,CO2
3605	1	ROS	063016	0324	BE	59 55.7 N	042 44.4 W	GPS	190	5	9	CTD,LADCP,O2,SiO3,PO4,CO2
3605	1	ROS	063016	0339	BO	59 55.7 N	042 44.5 W	GPS	190	5	9	CTD,LADCP,O2,SiO3,PO4,CO2
3605	1	ROS	063016	0351	EN	59 55.6 N	042 44.6 W	GPS	190	5	9	CTD,LADCP,O2,SiO3,PO4,CO2
3606	1	ROS	063016	0420	BE	59 56.2 N	042 47.9 W	GPS	184	3	8	CTD,LADCP,O2,SiO3,PO4,CO2
3606	1	ROS	063016	0435	BO	59 56.2 N	042 48.1 W	GPS	184	3	8	CTD,LADCP,O2,SiO3,PO4,CO2
3606	1	ROS	063016	0445	EN	59 56.2 N	042 48.3 W	GPS	184	3	8	CTD,LADCP,O2,SiO3,PO4,CO2
3607	1	ROS	063016	0514	BE	59 56.2 N	042 51.7 W	GPS	172	5	8	CTD,LADCP,O2,SiO3,PO4,CO2
3607	1	ROS	063016	0531	BO	59 56.1 N	042 51.7 W	GPS	172	5	8	CTD,LADCP,O2,SiO3,PO4,CO2
3607	1	ROS	063016	0542	EN	59 56.0 N	042 51.9 W	GPS	172	5	8	CTD,LADCP,O2,SiO3,PO4,CO2
3608	1	ROS	063016	0607	BE	59 56.8 N	042 55.0 W	GPS	170	5	8	CTD,LADCP,O2,SiO3,PO4,CO2
3608	1	ROS	063016	0624	BO	59 56.6 N	042 55.6 W	GPS	170	5	8	CTD,LADCP,O2,SiO3,PO4,CO2
3608	1	ROS	063016	0635	EN	59 56.5 N	042 55.7 W	GPS	170	5	8	CTD,LADCP,O2,SiO3,PO4,CO2
3609	1	ROS	063016	0702	BE	59 57.3 N	042 59.3 W	GPS	166	4	8	CTD,LADCP,O2,SiO3,PO4,CO2
3609	1	ROS	063016	0712	BO	59 57.2 N	042 59.3 W	GPS	166	4	8	CTD,LADCP,O2,SiO3,PO4,CO2
3609	1	ROS	063016	0728	EN	59 57.1 N	042 59.6 W	GPS	166	4	8	CTD,LADCP,O2,SiO3,PO4,CO2
3610	1	ROS	063016	0757	BE	59 57.4 N	043 00.5 W	GPS	163	5	8	CTD,LADCP,O2,SiO3,PO4,CO2
3610	1	ROS	063016	0814	BO	59 57.4 N	043 00.6 W	GPS	163	5	8	CTD,LADCP,O2,SiO3,PO4,CO2
3610	1	ROS	063016	0823	EN	59 57.4 N	043 00.7 W	GPS	163	5	8	CTD,LADCP,O2,SiO3,PO4,CO2

3611	1	ROS	063016	1045	BE	59 54.4 N	042 26.7 W	GPS	215	4	9	CTD,LADCP,O2,SiO3,PO4,CO2
3611	1	ROS	063016	1103	BO	59 54.2 N	042 26.6 W	GPS	215	4	9	CTD,LADCP,O2,SiO3,PO4,CO2
3611	1	ROS	063016	1113	EN	59 54.1 N	042 26.6 W	GPS	215	4	9	CTD,LADCP,O2,SiO3,PO4,CO2
3612	1	ROS	063016	1141	BE	59 54.2 N	042 22.9 W	GPS	239	6	9	CTD,LADCP,O2,SiO3,PO4,CO2
3612	1	ROS	063016	1157	BO	59 54.0 N	042 22.4 W	GPS	239	6	9	CTD,LADCP,O2,SiO3,PO4,CO2
3612	1	ROS	063016	1208	EN	59 53.9 N	042 22.4 W	GPS	239	6	9	CTD,LADCP,O2,SiO3,PO4,CO2
3613	1	ROS	063016	1238	BE	59 54.0 N	042 19.0 W	GPS	328	3	19	CTD,LADCP,O2,SiO3,PO4,CO2
3613	1	ROS	063016	1251	BO	59 53.8 N	042 19.0 W	GPS	328	3	19	CTD,LADCP,O2,SiO3,PO4,CO2
3613	1	ROS	063016	1305	EN	59 53.7 N	042 18.9 W	GPS	328	3	19	CTD,LADCP,O2,SiO3,PO4,CO2
3614	1	ROS	063016	1343	BE	59 53.8 N	042 15.6 W	GPS	386	5	10	CTD,LADCP,O2,SiO3,PO4,CO2
3614	1	ROS	063016	1359	BO	59 53.3 N	042 15.5 W	GPS	386	5	10	CTD,LADCP,O2,SiO3,PO4,CO2
3614	1	ROS	063016	1412	EN	59 53.1 N	042 15.6 W	GPS	386	5	10	CTD,LADCP,O2,SiO3,PO4,CO2
3615	1	ROS	063016	1444	BE	59 53.0 N	042 12.0 W	GPS	943	5	12	CTD,LADCP,O2,SiO3,PO4,CO2
3615	1	ROS	063016	1505	BO	59 52.6 N	042 12.1 W	GPS	943	5	12	CTD,LADCP,O2,SiO3,PO4,CO2
3615	1	ROS	063016	1529	EN	59 52.3 N	042 12.2 W	GPS	943	5	12	CTD,LADCP,O2,SiO3,PO4,CO2
3616	1	ROS	063016	1558	BE	59 52.3 N	042 09.1 W	GPS	1471	6	17	CTD,LADCP,O2,SiO3,PO4,CO2
3616	1	ROS	063016	1628	BO	59 51.8 N	042 09.1 W	GPS	1471	6	17	CTD,LADCP,O2,SiO3,PO4,CO2
3616	1	ROS	063016	1705	EN	59 51.2 N	042 09.2 W	GPS	1471	6	17	CTD,LADCP,O2,SiO3,PO4,CO2
3617	1	ROS	063016	1730	BE	59 51.5 N	042 06.3 W	GPS	1567	6	15	CTD,LADCP,O2,SiO3,PO4,CO2
3617	1	ROS	063016	1804	BO	59 51.1 N	042 06.5 W	GPS	1567	6	15	CTD,LADCP,O2,SiO3,PO4,CO2
3617	1	ROS	063016	1841	EN	59 50.8 N	042 06.8 W	GPS	1567	6	15	CTD,LADCP,O2,SiO3,PO4,CO2
3618	1	ROS	063016	1907	BE	59 50.8 N	042 03.4 W	GPS	1646	3	19	CTD,LADCP,O2,SiO3,PO4,CO2
3618	1	ROS	063016	1952	BO	59 50.2 N	042 03.7 W	GPS	1646	3	19	CTD,LADCP,O2,SiO3,PO4,CO2
3618	1	ROS	063016	2037	EN	59 49.6 N	042 03.9 W	GPS	1646	3	19	CTD,LADCP,O2,SiO3,PO4,CO2
3619	1	ROS	063016	2141	BE	59 48.6 N	041 55.5 W	GPS	1767	5	21	CTD,LADCP,O2,SiO3,PO4,CO2
3619	1	ROS	063016	2214	BO	59 48.1 N	041 55.4 W	GPS	1767	5	21	CTD,LADCP,O2,SiO3,PO4,CO2
3619	1	ROS	063016	2302	EN	59 47.4 N	041 55.2 W	GPS	1767	5	21	CTD,LADCP,O2,SiO3,PO4,CO2
3620	1	ROS	070116	1655	BE	60 06.0 N	046 29.0 W	GPS	159	4	6	CTD,LADCP,O2,SiO3,PO4,CO2
3620	1	ROS	070116	1711	BO	60 06.1 N	046 29.2 W	GPS	159	4	6	CTD,LADCP,O2,SiO3,PO4,CO2
3620	1	ROS	070116	1717	EN	60 06.1 N	046 29.3 W	GPS	159	4	6	CTD,LADCP,O2,SiO3,PO4,CO2
3621	1	ROS	070116	1736	BE	60 05.7 N	046 31.1 W	GPS	211	4	7	CTD,LADCP,O2,SiO3,PO4,CO2
3621	1	ROS	070116	1745	BO	60 05.8 N	046 31.1 W	GPS	211	4	7	CTD,LADCP,O2,SiO3,PO4,CO2
3621	1	ROS	070116	1754	EN	60 05.9 N	046 31.2 W	GPS	211	4	7	CTD,LADCP,O2,SiO3,PO4,CO2

3622	1	ROS	070116	1829	BE	60 04.6 N	046 34.9 W	GPS	374	7	9	CTD,LADCP,O2,SiO3,PO4,CO2
3622	1	ROS	070116	1842	BO	60 04.7 N	046 35.2 W	GPS	374	7	9	CTD,LADCP,O2,SiO3,PO4,CO2
3622	1	ROS	070116	1855	EN	60 04.8 N	046 35.3 W	GPS	374	7	9	CTD,LADCP,O2,SiO3,PO4,CO2
3623	1	ROS	070116	1917	BE	60 04.3 N	046 36.4 W	GPS	745	5	12	CTD,LADCP,O2,SiO3,PO4,CO2
3623	1	ROS	070116	1933	BO	60 04.4 N	046 36.6 W	GPS	745	5	12	CTD,LADCP,O2,SiO3,PO4,CO2
3623	1	ROS	070116	1954	EN	60 04.5 N	046 36.9 W	GPS	745	5	12	CTD,LADCP,O2,SiO3,PO4,CO2
3624	1	ROS	070116	2018	BE	60 03.8 N	046 38.1 W	GPS	907	5	14	CTD,LADCP,O2,SiO3,PO4,CO2
3624	1	ROS	070116	2038	BO	60 04.0 N	046 38.3 W	GPS	907	5	14	CTD,LADCP,O2,SiO3,PO4,CO2
3624	1	ROS	070116	2107	EN	60 04.1 N	046 38.6 W	GPS	907	5	14	CTD,LADCP,O2,SiO3,PO4,CO2
3625	1	ROS	070116	2142	BE	60 03.0 N	046 41.8 W	GPS	793	4	12	CTD,LADCP,O2,SiO3,PO4,CO2
3625	1	ROS	070116	2200	BO	60 03.2 N	046 42.1 W	GPS	793	4	12	CTD,LADCP,O2,SiO3,PO4,CO2
3625	1	ROS	070116	2223	EN	60 03.3 N	046 42.3 W	GPS	793	4	12	CTD,LADCP,O2,SiO3,PO4,CO2
3626	1	ROS	070116	2310	BE	60 02.0 N	046 46.6 W	GPS	1271	3	17	CTD,LADCP,O2,SiO3,PO4,CO2
3626	1	ROS	070116	2337	BO	60 02.1 N	046 47.0 W	GPS	1271	3	17	CTD,LADCP,O2,SiO3,PO4,CO2
3626	1	ROS	070216	0012	EN	60 02.3 N	046 47.1 W	GPS	1271	3	17	CTD,LADCP,O2,SiO3,PO4,CO2
3627	1	ROS	070216	0107	BE	60 00.5 N	046 51.3 W	GPS	2042	5	21	CTD,LADCP,O2,SiO3,PO4,CO2
3627	1	ROS	070216	0147	BO	60 00.7 N	046 51.2 W	GPS	2042	5	21	CTD,LADCP,O2,SiO3,PO4,CO2
3627	1	ROS	070216	0242	EN	60 00.8 N	046 50.9 W	GPS	2042	5	21	CTD,LADCP,O2,SiO3,PO4,CO2
3628	1	ROS	070216	0325	BE	59 59.2 N	046 56.1 W	GPS	2167	5	21	CTD,LADCP,O2,SiO3,PO4,CO2
3628	1	ROS	070216	0406	BO	59 59.3 N	046 56.3 W	GPS	2167	5	21	CTD,LADCP,O2,SiO3,PO4,CO2
3628	1	ROS	070216	0501	EN	59 59.4 N	046 56.7 W	GPS	2167	5	21	CTD,LADCP,O2,SiO3,PO4,CO2
3629	1	ROS	070216	0541	BE	59 57.9 N	047 01.0 W	GPS	2390	4	21	CTD,LADCP,O2,SiO3,PO4,CO2
3629	1	ROS	070216	0626	BO	59 58.0 N	047 01.6 W	GPS	2390	4	21	CTD,LADCP,O2,SiO3,PO4,CO2
3629	1	ROS	070216	0714	EN	59 58.0 N	047 02.1 W	GPS	2390	4	21	CTD,LADCP,O2,SiO3,PO4,CO2
3630	1	ROS	070216	1029	BE	59 55.7 N	047 10.9 W	GPS	2676	4	21	CTD,LADCP,O2,SiO3,PO4,CO2
3630	1	ROS	070216	1119	BO	59 55.5 N	047 11.6 W	GPS	2676	4	21	CTD,LADCP,O2,SiO3,PO4,CO2
3630	1	ROS	070216	1219	EN	59 55.4 N	047 12.4 W	GPS	2676	4	21	CTD,LADCP,O2,SiO3,PO4,CO2
3631	1	ROS	070216	1342	BE	59 51.2 N	047 30.5 W	GPS	2879	5	21	CTD,LADCP,O2,SiO3,PO4,CO2
3631	1	ROS	070216	1436	BO	59 51.0 N	047 30.7 W	GPS	2879	5	21	CTD,LADCP,O2,SiO3,PO4,CO2
3631	1	ROS	070216	1538	EN	59 51.0 N	047 30.9 W	GPS	2879	5	21	CTD,LADCP,O2,SiO3,PO4,CO2
3632	1	ROS	070216	1732	BE	59 44.9 N	047 57.1 W	GPS	3005	5	21	CTD,LADCP,O2,SiO3,PO4,CO2
3632	1	ROS	070216	1830	BO	59 44.7 N	047 57.7 W	GPS	3005	5	21	CTD,LADCP,O2,SiO3,PO4,CO2
3632	1	ROS	070216	1937	EN	59 44.5 N	047 58.1 W	GPS	3005	5	21	CTD,LADCP,O2,SiO3,PO4,CO2

3633	1	ROS	070216	2254	BE	59 32.9 N	048 44.9 W	GPS	3354	0	21	CTD,LADCP,O2,SiO3,PO4,CO2
3633	1	ROS	070216	2355	BO	59 32.6 N	048 44.7 W	GPS	3354	0	21	CTD,LADCP,O2,SiO3,PO4,CO2
3633	1	ROS	070316	0109	EN	59 32.5 N	048 43.9 W	GPS	3354	0	21	CTD,LADCP,O2,SiO3,PO4,CO2
3634	1	ROS	070316	0453	BE	59 19.9 N	049 38.5 W	GPS	3466	7	21	CTD,LADCP,O2,SiO3,PO4,CO2
3634	1	ROS	070316	0558	BO	59 19.8 N	049 38.3 W	GPS	3466	7	21	CTD,LADCP,O2,SiO3,PO4,CO2
3634	1	ROS	070316	0713	EN	59 19.8 N	049 37.9 W	GPS	3466	7	21	CTD,LADCP,O2,SiO3,PO4,CO2
3635	1	ROS	070316	1038	BE	59 06.9 N	050 31.9 W	GPS	3542	7	21	CTD,LADCP,O2,SiO3,PO4,CO2
3635	1	ROS	070316	1147	BO	59 06.7 N	050 31.7 W	GPS	3542	7	21	CTD,LADCP,O2,SiO3,PO4,CO2
3635	1	ROS	070316	1257	EN	59 06.7 N	050 30.8 W	GPS	3542	7	21	CTD,LADCP,O2,SiO3,PO4,CO2
3636	1	ROS	070316	2012	BE	58 53.5 N	051 27.3 W	GPS	3548	1	21	CTD,LADCP,O2,SiO3,PO4,CO2
3636	1	ROS	070316	2121	BO	58 53.4 N	051 27.7 W	GPS	3548	1	21	CTD,LADCP,O2,SiO3,PO4,CO2
3636	1	ROS	070316	2236	EN	58 53.3 N	051 27.8 W	GPS	3548	1	21	CTD,LADCP,O2,SiO3,PO4,CO2
3637	1	ROS	070416	0217	BE	58 40.0 N	052 22.9 W	GPS	3533	10	21	CTD,LADCP,O2,SiO3,PO4,CO2
3637	1	ROS	070416	0322	BO	58 40.4 N	052 23.0 W	GPS	3533	10	21	CTD,LADCP,O2,SiO3,PO4,CO2
3637	1	ROS	070416	0439	EN	58 41.0 N	052 23.0 W	GPS	3533	10	21	CTD,LADCP,O2,SiO3,PO4,CO2
3638	1	ROS	070416	0819	BE	58 27.2 N	053 16.5 W	GPS	3438	4	21	CTD,LADCP,O2,SiO3,PO4,CO2
3638	1	ROS	070416	0929	BO	58 27.5 N	053 16.5 W	GPS	3438	4	21	CTD,LADCP,O2,SiO3,PO4,CO2
3638	1	ROS	070416	1040	EN	58 27.9 N	053 16.3 W	GPS	3438	4	21	CTD,LADCP,O2,SiO3,PO4,CO2
3639	1	ROS	070416	1414	BE	58 14.1 N	054 09.7 W	GPS	3450	4	22	CTD,LADCP,O2,SiO3,PO4,CO2
3639	1	ROS	070416	1524	BO	58 13.6 N	054 09.9 W	GPS	3450	4	22	CTD,LADCP,O2,SiO3,PO4,CO2
3639	1	ROS	070416	1628	EN	58 13.0 N	054 10.0 W	GPS	3450	4	22	CTD,LADCP,O2,SiO3,PO4,CO2
3640	1	ROS	070516	0510	BE	57 49.9 N	053 10.3 W	GPS	3537	7	21	CTD,LADCP,O2,SiO3,PO4,CO2
3640	1	ROS	070516	0614	BO	57 50.1 N	053 10.9 W	GPS	3537	7	21	CTD,LADCP,O2,SiO3,PO4,CO2
3640	1	ROS	070516	0731	EN	57 50.5 N	053 11.8 W	GPS	3537	7	21	CTD,LADCP,O2,SiO3,PO4,CO2
3641	1	ROS	070516	1416	BE	57 32.9 N	052 10.1 W	GPS	3569	3	21	CTD,LADCP,O2,SiO3,PO4,CO2
3641	1	ROS	070516	1522	BO	57 32.9 N	052 10.3 W	GPS	3569	3	21	CTD,LADCP,O2,SiO3,PO4,CO2
3641	1	ROS	070516	1639	EN	57 33.0 N	052 10.3 W	GPS	3569	3	21	CTD,LADCP,O2,SiO3,PO4,CO2
3642	1	ROS	070516	2308	BE	57 12.4 N	051 09.0 W	GPS	3619	5	21	CTD,LADCP,O2,SiO3,PO4,CO2
3642	1	ROS	070616	0014	BO	57 12.5 N	051 10.0 W	GPS	3619	5	21	CTD,LADCP,O2,SiO3,PO4,CO2
3642	1	ROS	070616	0134	EN	57 12.3 N	051 10.3 W	GPS	3619	5	21	CTD,LADCP,O2,SiO3,PO4,CO2
3643	1	ROS	070616	0649	BE	56 51.9 N	050 07.9 W	GPS	3714	7	21	CTD,LADCP,O2,SiO3,PO4,CO2
3643	1	ROS	070616	0759	BO	56 51.9 N	050 08.1 W	GPS	3714	7	21	CTD,LADCP,O2,SiO3,PO4,CO2
3643	1	ROS	070616	0917	EN	56 51.8 N	050 08.3 W	GPS	3714	7	21	CTD,LADCP,O2,SiO3,PO4,CO2

3644	1	ROS	070616	2014	BE	56 12.8 N	048 07.0 W	GPS	3691	5	21	CTD,LADCP,O2,SiO3,PO4,CO2
3644	1	ROS	070616	2122	BO	56 12.7 N	048 07.0 W	GPS	3691	5	21	CTD,LADCP,O2,SiO3,PO4,CO2
3644	1	ROS	070616	2241	EN	56 12.7 N	048 07.5 W	GPS	3691	5	21	CTD,LADCP,O2,SiO3,PO4,CO2
3645	1	ROS	070716	0806	BE	55 34.0 N	046 12.9 W	GPS	2964	7	21	CTD,LADCP,O2,SiO3,PO4,CO2
3645	1	ROS	070716	0905	BO	55 34.4 N	046 13.6 W	GPS	2964	7	21	CTD,LADCP,O2,SiO3,PO4,CO2
3645	1	ROS	070716	1009	EN	55 34.7 N	046 14.6 W	GPS	2964	7	21	CTD,LADCP,O2,SiO3,PO4,CO2
3646	1	ROS	070716	2122	BE	54 59.9 N	043 44.9 W	GPS	3410	10	21	CTD,LADCP,O2,SiO3,PO4,CO2
3646	1	ROS	070716	2223	BO	55 00.0 N	043 45.1 W	GPS	3410	10	21	CTD,LADCP,O2,SiO3,PO4,CO2
3646	1	ROS	070716	2338	EN	55 00.0 N	043 45.3 W	GPS	3410	10	21	CTD,LADCP,O2,SiO3,PO4,CO2

Table 2

Station	Date	Time	Latitude	Longitude	Depth, m	Sampling
A-1-1	07.06.2016	10:20	59 ° 17.990 N	0 ° 11.688 E		Aerosol nets: beginning
P-1	07.06.2016	10:42	59 ° 23.082 N	0 ° 7.251 W		Water: 0 m
A-1-2	07.06.2016	22:20	60 ° 16.259 N	2 ° 20.974 W		Aerosol nets: finishing
3445	07.06.2016	23:30	60 ° 25.002 N	1 ° 54.994 W	115	Water: 3, 23, 40, 110 m
3449	08.06.2016	7:30	60 ° 51.954 N	3 ° 19.908 W	683	Water: 9, 20, 40, 329, 680 m
3451	08.06.2016	11:30	61 ° 4.027 N	3 ° 52.106 W	1163	Water: 0, 40, 150, 440, 1160 m
		12:34	61 ° 4.061 N	3 ° 51.983 W	1150	GS
		13:04	61 ° 4.076 N	3 ° 51.997 W	1150	GS-2
		14:39	61 ° 4.115 N	3 ° 51.919 W	1150	MC
		14:19	61 ° 4.087 N	3 ° 51.949 W	1150	GC
3461	09.06.2016	15:10	62 ° 20.090 N	7 ° 14,82 W	89	Water: 0, 20, 40, 87 m
3464	09.06.2016	20:50	62 ° 44.033 N	8 ° 27.258 W	484	Water: 0, 15, 40, 100, 410, 480 m
		21:33	62 ° 44.329 N	8 ° 27.606 W		GS
3470	10.06.2016	9:50	63 ° 29.095 N	10 ° 48.930 W	445	Water: 0, 20, 100, 390, 440 m
3483	11.06.2016	8:20	64 ° 8.005 N	13 ° 3.418 W	162	Water: 0,20, 158 m
3485	11.06.2016	11:05	64 ° 1.156 N	12 ° 37.885 W	567	Water: 0, 22, 220, 480, 562 m
		11:59	64 ° 1.515 N	12 ° 37,092 W	567	GS
3500	12.06.2016	23:55	61 ° 50.166 N	6 ° 22.234 W	78	Water: 5, 20, 74 m
3505	13.06.2016	8:30	61 ° 19.934 N	4 ° 43.223 W	721	Water: 0, 20, 65, 450, 689, 717 m
3509	13.06.2016	17:29	61 ° 4.016 N	3 ° 52.697 W	1149	MC
3516	14.06.2016	14:10	59 ° 30.035 N	3 ° 49.902 W	158	Water: 0, 30, 60, 114, 154 m, MC (2 water layers)
		14:40	59 ° 30.006 N	3 ° 49.924 W	158	GS
		14:51	59 ° 30.009 N	3 ° 49.915 W	158	MC
3519	14.06.2016	23:27	59 ° 29.975 N	6 ° 0.248 W	137	GS
3521	15.06.2016	4:55	59 ° 30.019 N	7 ° 19.968 W	1052	Water: 0, 30, 112, 1000, 1047 m, MC (2 water layers)
		6:01	59 ° 30.001 N	7 ° 20.061 W	1051	GS
		6:33	59 ° 29.990 N	7 ° 20.061 W	1051	MC
		7:09	59 ° 30,009 N	7 ° 20.062 W	1051	GC
		7:48	59 ° 29.990 N	7 ° 20.066 W	1051	MC
3524	15.06.2016	18:55	59 ° 29,929 N	9 ° 20.017 W	1468	GS
		19:43	59 ° 29.929 N	9 ° 20.066 W	1468	MC
3527	16.06.2016	5:47	59 ° 29.986 N	11 ° 20.084 W	1611	Water: 0, 28, 54, 1098, 1607 m
		7:27	59 ° 29.953 N	11 ° 20.020 W	1611	MC
		8:19	59 ° 29.955 N	11 ° 20.009 W	1611	GS
		9:00	59 ° 29.946 N	11 ° 20.031 W	1611	GS-2
		9:57	59 ° 29.960 N	11 ° 20.000 W	1611	MC-2
3531	16.06.2016	23:00	59 ° 30.068 N	13 ° 20.036 W	1291	GS
		23:33	59 ° 30.055 N	13 ° 20.034 W	1291	GS-2
	17.06.2016	0:24	59 ° 30.068 N	13 ° 20.042 W	1291	MC
3534		9:52	59 ° 30.137 N	15 ° 19.980 W	1519	Water: 0, 20, 151, 833, 1514 m, MC (2 water layers)
		11:21	59 ° 30.170 N	15 ° 19.982 W	1519	GS

		12:21	59 ° 30.178 N	15 ° 19.976 W	1519	MC
3540	18.06.2016	6:00	59 ° 30.020 N	17 ° 59.972 W	2182	MS-1 (AI-49, 3348): recovery
		7:30	59 ° 30.016 N	17 ° 59.984 W	2229	Water: 0, 20, 250, 443, 868, 1290, 1707, 2170, 2220 m
		9:55	59 ° 30.026 N	18 ° 0.019 W		GS
		15:08	59 ° 30.045 N	17 ° 59.980 W	2229	MS-1: deployment
3545	19.06.2016	10:06	59 ° 29.901 N	20 ° 41.678 W	2825	GS
3548	19.06.2016	21:03	59 ° 29.588 N	21 ° 59.189 W	2740	GS
3552	20.06.2016	10:36	59 ° 29.627 N	23 ° 19.316 W	2392	GS
3556	21.06.2016	3:00	59 ° 30.301 N	24 ° 42.962 W	2517	MS-2 (AI-49, 3359): recovery
		5:05	59 ° 29.867 N	24 ° 42.637 W	2513	Water: 0, 20, 100, 417, 930, 1441, 1952, 2462, 2507 m
		7:09	59 ° 29.861 N	24 ° 42.316 W	2512	GS
		8:49	59 ° 29.817 N	24 ° 42.481 W	2512	MC
3562	22.06.2016	6:03	59 ° 29.930 N	26 ° 39.604 W	2237	GS
		7:27	59 ° 29.877 N	26 ° 39.484 W	2237	MC
		8:42	59 ° 29.933 N	26 ° 39.615 W	2237	GC
		10:15	59 ° 29.982 N	26 ° 39.854 W	2243	Water: 0, 20, 80, 450, 880, 1300, 1750, 2180, 2237 m
		11:55	59 ° 29.791 N	26 ° 39.821 W	2237	MS-2: deployment
3568	23.06.2016	4:19	59 ° 30.054 N	28 ° 39.978 W	1694	GS
		5:24	59 ° 30.067 N	28 ° 40.117 W	1694	MC, Water (2 water layers)
3574	23.06.2016	20:15	59 ° 30.373 N	30 ° 39.633 W	1531	GS
		21:21	59 ° 30.364 N	30 ° 39.643 W	1531	MC
3580	24.06.2016	13:00	59 ° 30.267 N	32 ° 50.563 W	2192	MS-3 (AI-49, 3378): recovery
		14:05	59 ° 30.030 N	32 ° 49.296 W	2270	Water: 0, 30, 100, 520, 930, 1330, 1730, 2140, 2266 m
		16:02	59 ° 30.011 N	32 ° 49.065 W	2270	GS
		19:37	59 ° 30.018 N	32 ° 49.647 W	2203	MS-3: deployment
3586	25.06.2016	16:37	59 ° 30.235 N	34 ° 58.918 W	3064	GSт
3588	25.06.2016	23:20	59 ° 29.718 N	35 ° 59.999 W		Water Phytoplankton: 2907 m
3589	26.06.2016	7:20	59 ° 29.886 N	36 ° 40.121 W		Water Phytoplankton: 3094, 3143 m
3590	27.06.2016	5:00	59 ° 30.005 N	38 ° 39.965 W		Water Phytoplankton: 2895, 3036 m
3591	27.06.2016	10:00	59 ° 29.734 N	37 ° 59.483 W		Water Phytoplankton: 3170, 3080 m
3592	27.06.2016	13:10	59 ° 29.885 N	37 ° 19.733 W	3156	Water: 0, 25, 50, 100, 1700, 2000, 3000, 3150 m. Water Phytoplankton: 3200, 3080, 1590, 1400 m
		15:44	59 ° 29.558 N	37 ° 19.451 W	3156	GS
3593	28.06.2016		59 ° 30.121 N	39 ° 20.110 W		Water Phytoplankton: 2967, 2862 m
		7:08	59 ° 30.168 N	39 ° 19.868 W	2922	GS
		9:02	59 ° 30.135 N	39 ° 19.918 W	2922	MC
						MC: Water (2 water layers)
3594	28.06.2016		59 ° 29.836 N	40 ° 0.466 W		Water Phytoplankton: 2905, 2832 m
3595	28.06.2016		59 ° 29.977 N	40 ° 20.140 W		Water Phytoplankton: 2706, 2602 m
3596	28.06.2016		59 ° 30.136 N	40 ° 39.997 W		Water Phytoplankton: 2615,

						2448 m
3597	29.06.2016	0:39	59 ° 33.760 N	41 ° 0.463 W	2399	GS
		1:15	59 ° 33.656 N	41 ° 0.689 W	2395	Water: 0, 20, 50, 100, 1200, 1400, 2200, 2388 m. Water Phytoplankton: 2429, 2387 m
3598	28.06.2016		59 ° 38.462 N	41 ° 16.243 W		Water Phytoplankton: 2198, 2100 m
3599	28.06.2016		59 ° 42.410 N	41 ° 32.117 W		Water Phytoplankton: 2016, 1961 m
3600	28.06.2016		59 ° 46.127 N	41 ° 46.606 W		Water Phytoplankton: 1850, 1797 m
3613	30.06.2016	11:43	59 ° 53.896 N	42 ° 19.033 W	328	Water: 0, 8, 40, 60, 238, 323 m
		12:09	59 ° 53.771 N	42 ° 18.899 W	328	GS
3618	30.06.2016		59 ° 50.249 N	42 ° 3.736 W		Water Phytoplankton: 1663 m
3619	30.06.2016		59 ° 48.169 N	41 ° 55.450 W		Water Phytoplankton: 1701, 1367 m
3629	02.07.2016	3:41	59 ° 58.009 N	47 ° 1.590 W	2390	Water: 0, 20, 90, 200, 1196, 1628, 2343, 2385 m
		5:45	59 ° 57.984 N	47 ° 2.119 W	2389	GS
		7:04	59 ° 57.923 N	47 ° 2.152 W	2389	MC
3635	03.07.2016	8:45	59 ° 6.779 N	50 ° 31.723 W	3476	Water: 0, 18, 52, 137, 960, 2000, 3378, 3472 m
		11:37	59 ° 6.693 N	50 ° 30.649 W	3477	GS
		13:24	59 ° 6.693 N	50 ° 30.672 W	3477	MC
3639	04.07.2016	12:25	58 ° 13.610 N	54 ° 9.936 W	3392	Water: 0, 29, 450, 1175, 1900, 2625, 3337, 3386 m
		15:11	58 ° 13.081 N	54 ° 10.115 W	3393	GS
		16:56	58 ° 13.083 N	54 ° 10.118 W	3393	MC
		18:45	58 ° 13.073 N	54 ° 10.130 W	3393	GC
		21:39	58 ° 13.217 N	54 ° 10.453 W	3393	MS-4: deployment
3643	06.07.2016	8:06	56 ° 51.815 N	50 ° 8.417 W	3711	GS
3646	07.07.2016	22:40	55 ° 0.124 N	43 ° 45.393 W	3346	GC
	08.07.2016	0:11	55 ° 0.124 N	43 ° 45.411 W	3346	GS
		1:54	55 ° 0.098 N	43 ° 45.474 W	3346	MC, Water (2 water layers)

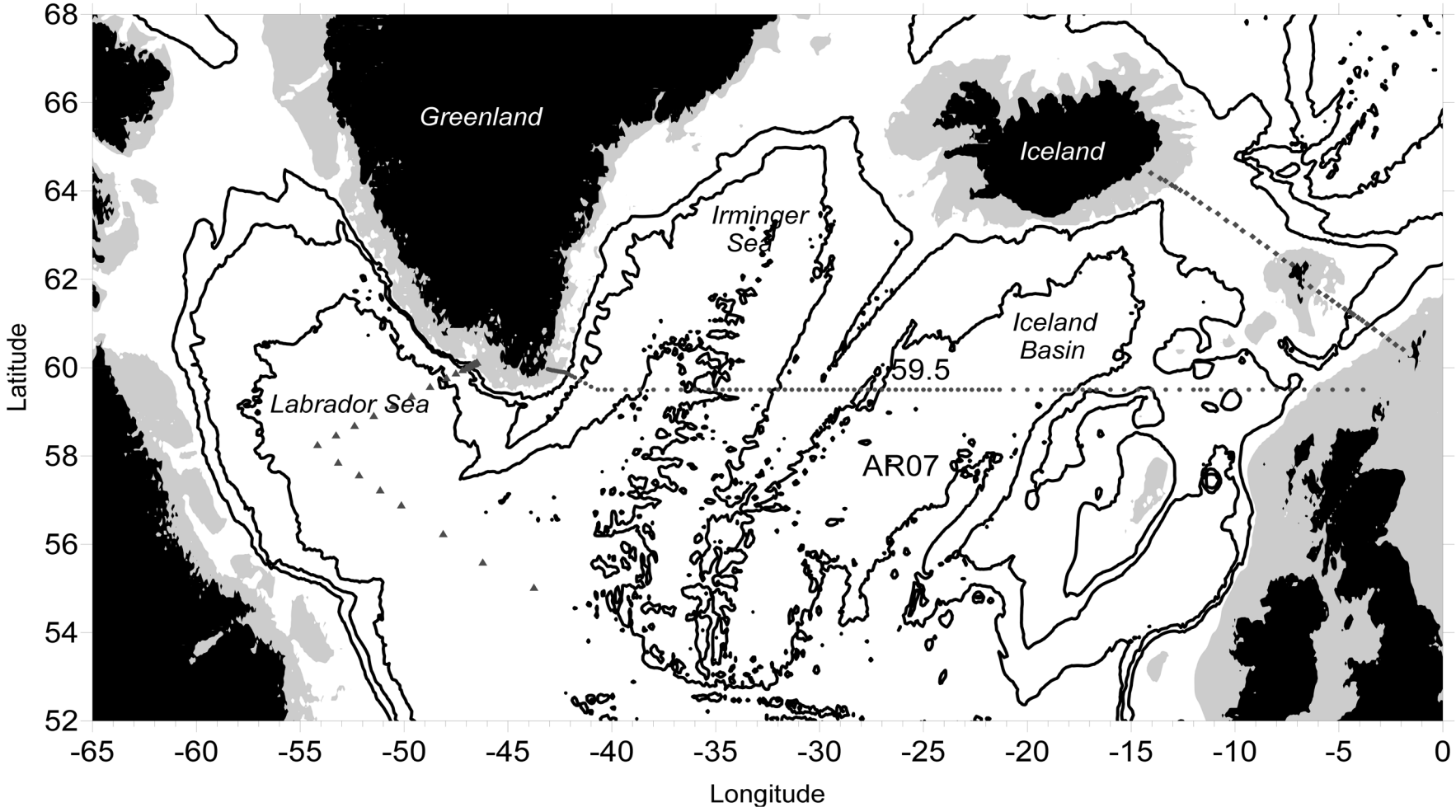

Fig. 1 Station locations (red diamonds for sill stations, circles for 59.5 N stations and triangles for Labrador Sea stations). The shelf area with depth less than 200 m is shaded.

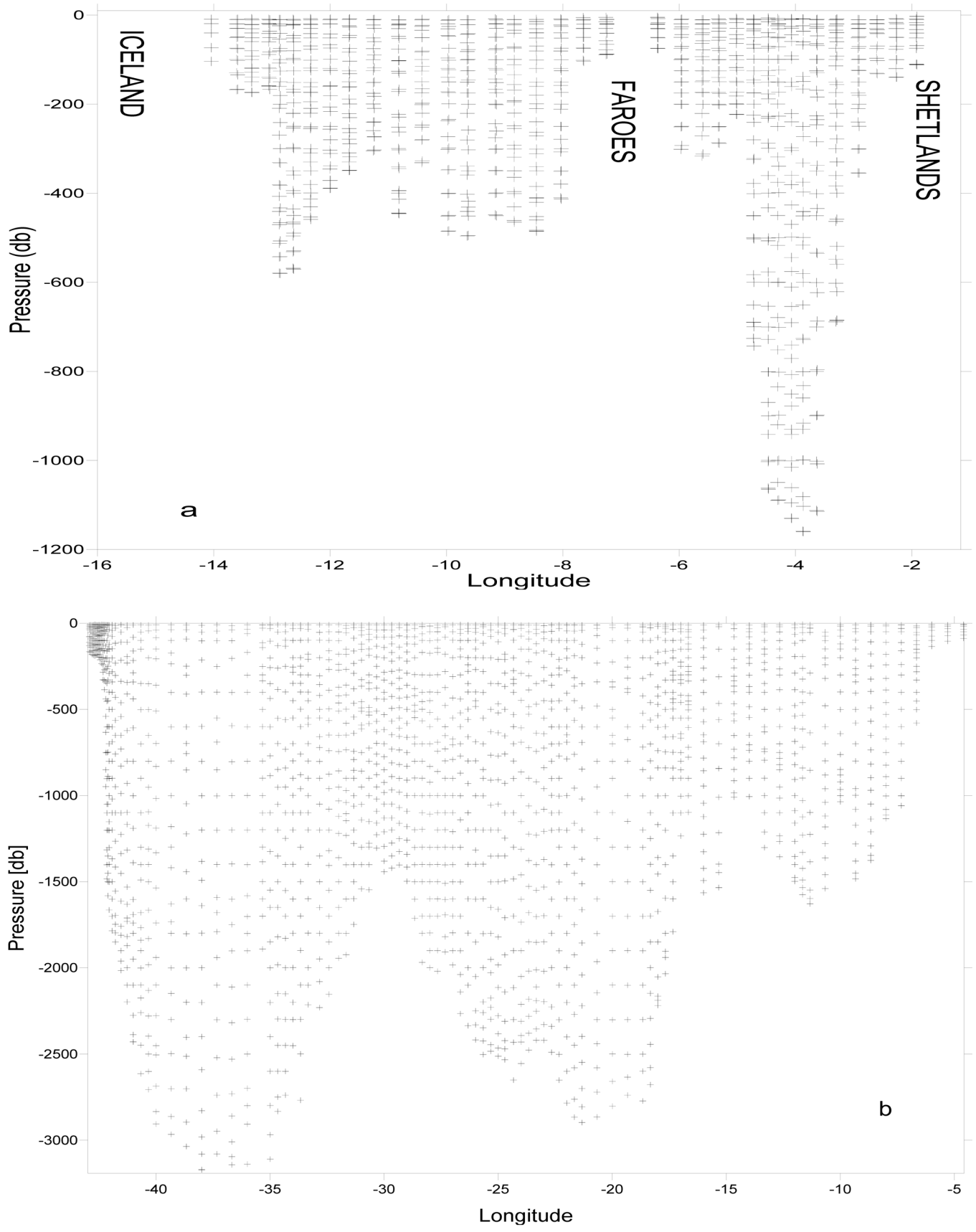

Figure 2. Vertical distribution of samples along (a) sill section (b) the 59.5 section.

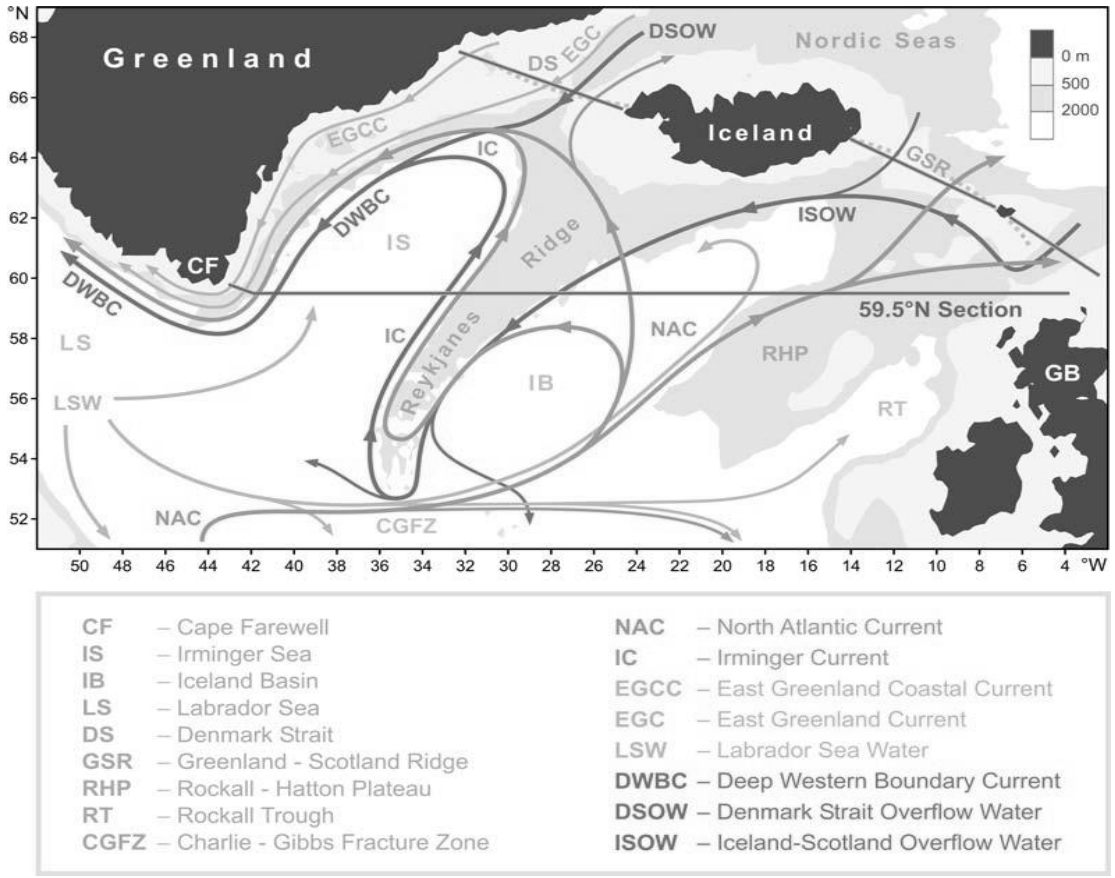

Figure 3. Schematic diagram of the large-scale circulation in the northern North Atlantic compiled from [Schmitz and McCartney, 1993; Schott and Brandt, 2007; Sutherland and Pickart, 2008; Lherminier et al., 2010]. Abbreviations for the main topographic features, currents and water masses are explained in the legend. The nominal locations of the 59.5°N hydrographic section (1997 – present) and sections across the straits between Greenland, Iceland, Faeroe and Shetland Islands (2011 – present) are shown with the solid green lines.

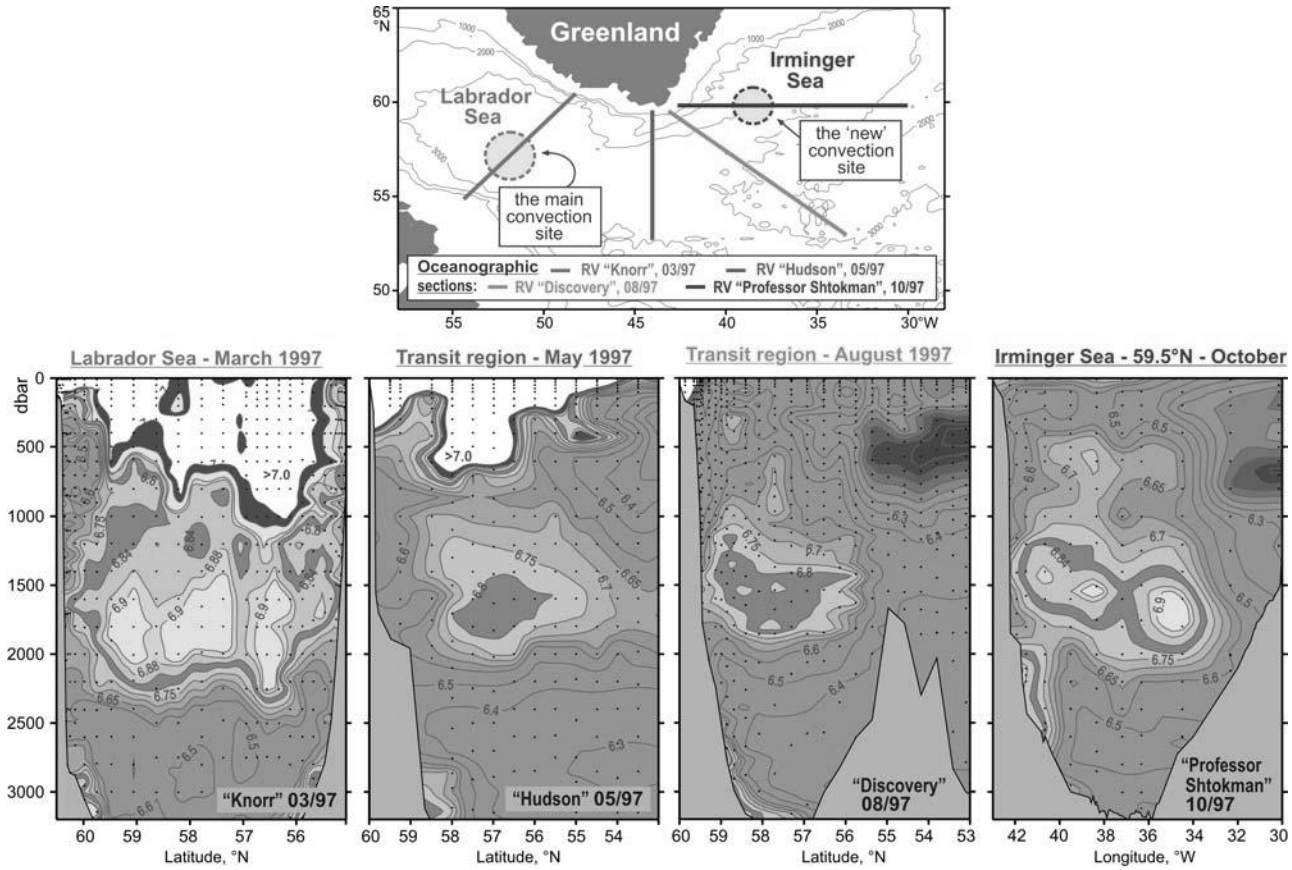

Figure 4. Oxygen concentrations (ml/l) in the water column (lower panel) as observed in March–October 1997 in four hydrographic sections (upper panel) ending nearby the southern tip of Greenland. A separate oxygen maximum in the LSW layer (1000–2000 m) in the Irminger Sea at 59.5°N strongly implies local convective renewal of LSW before 1997. Adapted from [Falina et al., 2007].

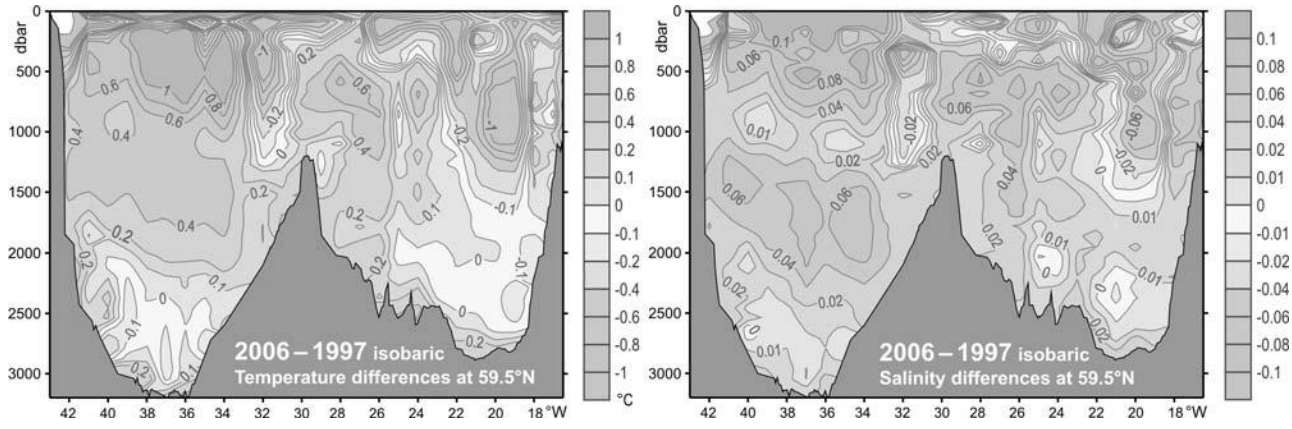

Figure 5. Warming and salinification in the northern North Atlantic between the mid-1990s and mid-2000s, as observed at 59.5°N. The figure shows the 2006–1997 temperature (°C, left) and salinity (right) differences on isobaric surfaces in the Irminger Sea and Iceland Basin. Adapted from [Sarafanov et al., 2007].

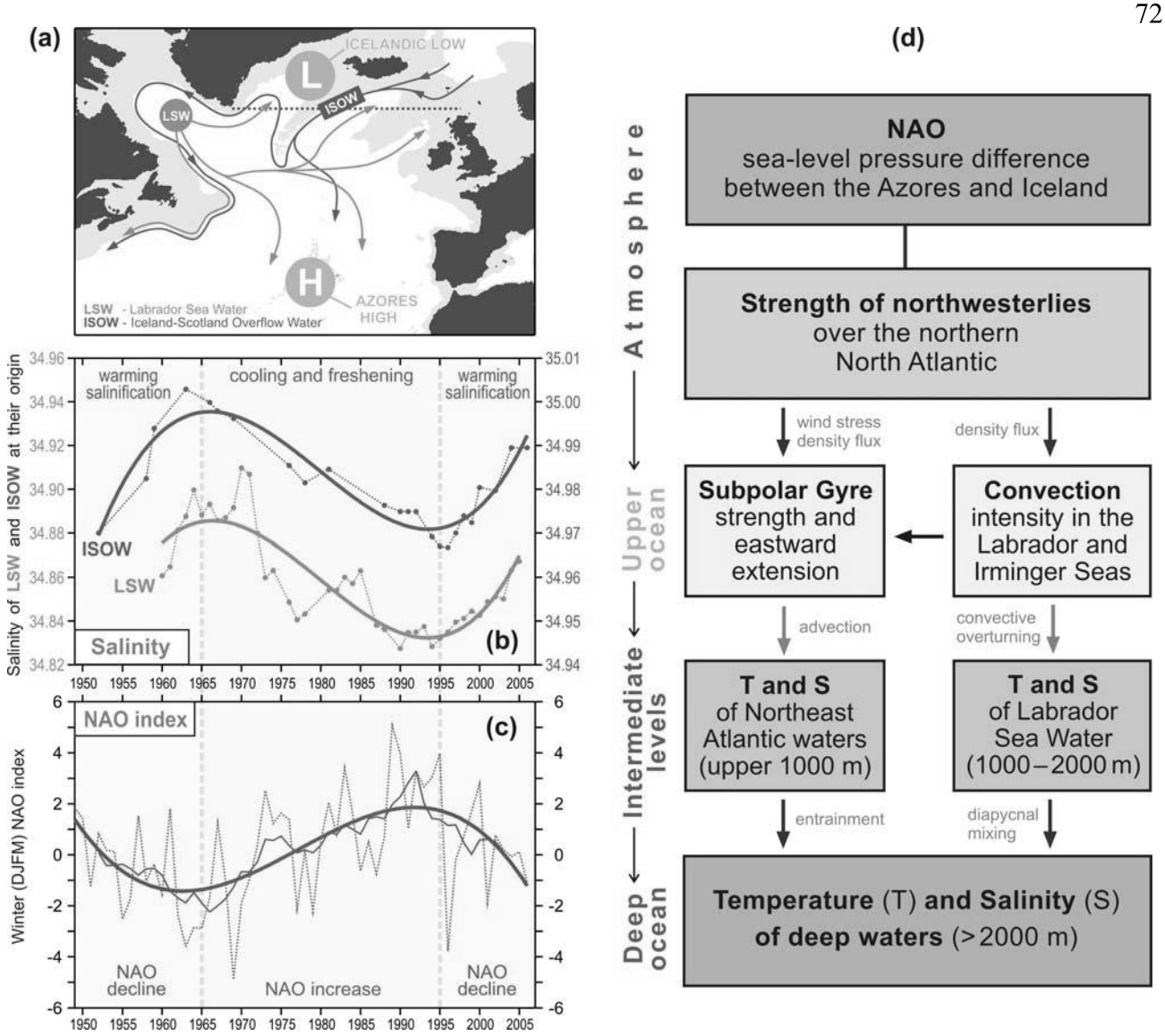

Figure 6. Coherence of the decadal salinity changes (1950s – 2000s) of the intermediate (LSW) and deep (ISOW) waters in the northern North Atlantic and their link to the North Atlantic Oscillation (NAO) index. **(a)** Schematic representation of the LSW and ISOW pathways and locations of the Icelandic Low (L) and Azores High (H) centers constituting the NAO dipole pattern. The red dotted line indicates the 59.5°N transatlantic section. **(b)** Salinity time series for LSW in the Labrador Sea [Yashayaev, 2007] and ISOW in the Iceland basin [Boessenkool et al., 2007; Sarafanov et al., 2007] overlaid by the third order polynomial fits. **(c)** Time series of the winter NAO index, after [Hurrell, 1995], overlaid by 7-year running mean and third order polynomial fit. **(d)** Mechanism of the NAO effect on the decadal changes in temperature (T) and salinity (S) of the northern North Atlantic intermediate and deep waters. Positive / negative links shown with the dark / light grey arrows mean that changes in 'causative' and 'consequential' characteristics have the same / opposite sign(s). The overall effect of the NAO on T and S of the in the water column is negative: persistent NAO decline leads to warming and salinification of the water masses and vice versa, as shown in (b) and (c). Adapted from [Sarafanov, 2009].

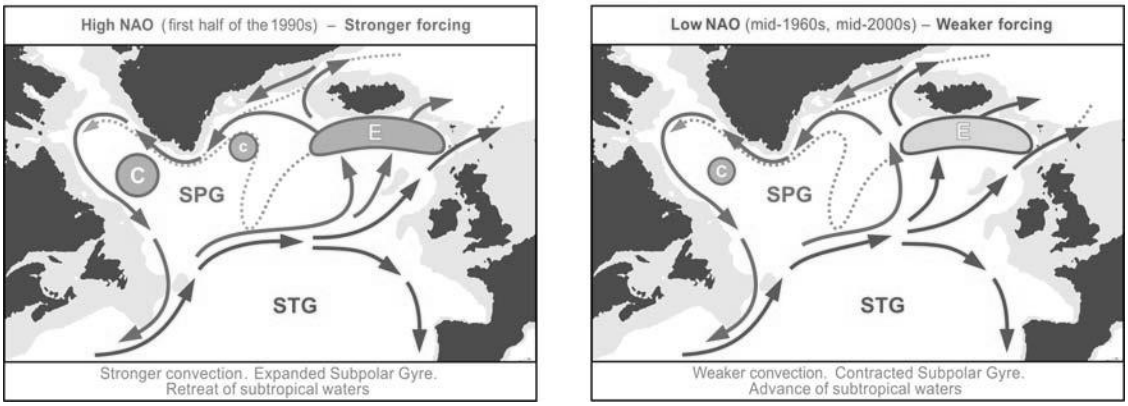

Figure 7. Schematic representation of the upper-ocean circulation and convection intensity in the northern North Atlantic under high (left) and low (right) NAO conditions. Blue (magenta) solid arrows indicate the upper-ocean flows with higher fraction of colder fresher subpolar (warmer saltier subtropical) waters. The main pathways of the Nordic overflow-derived deep waters are shown with the dotted curves. “C” and “E” symbols are used to denote, respectively, the deep convection sites and the domain, where the Atlantic waters are entrained into ISOW. Larger (smaller) circles indicate stronger (weaker) convection. SPG and STG – the subpolar and subtropical gyres, respectively. Adapted from [Sarafanov, 2009].

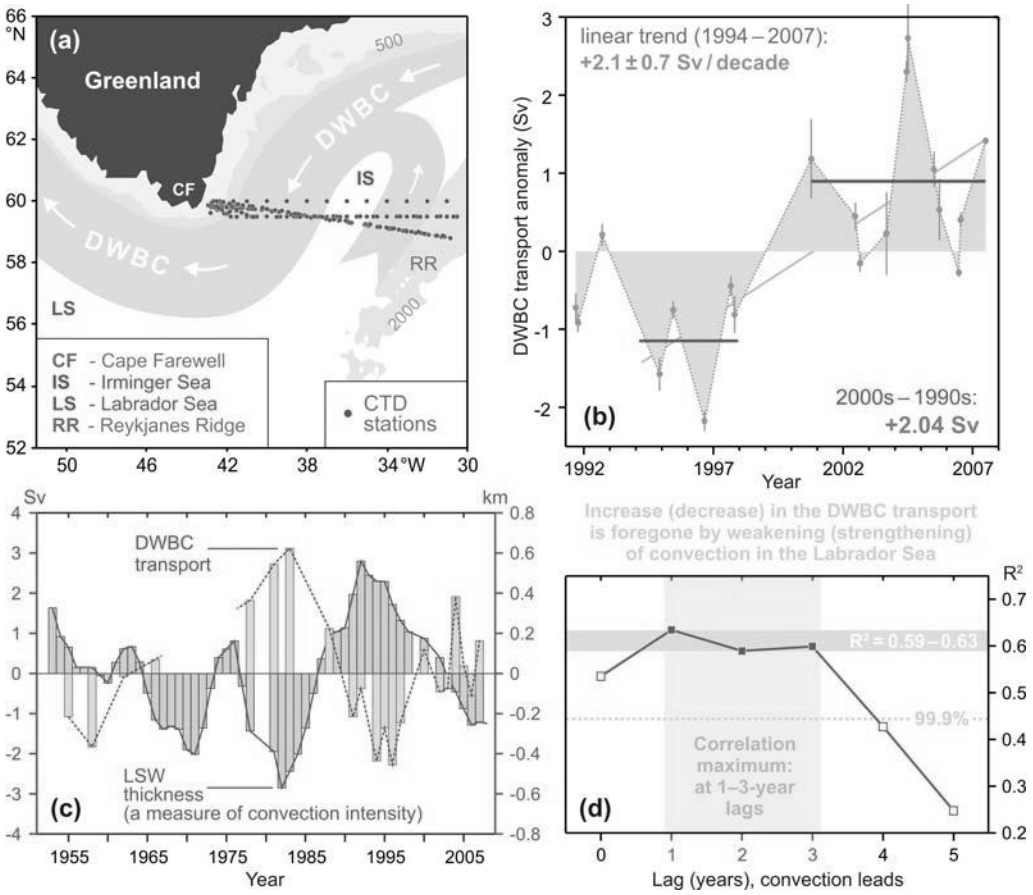

Figure 8. The Deep Western Boundary Current (DWBC) transport variability and its link to the convection intensity in the Labrador Sea. **(a)** Locations of the hydrographic sections (1991–2007) and schematic of the deep water circulation in the Irminger Sea. **(b)** The DWBC transport anomalies at Cape Farewell in 1991–2007, 1 Sv = 10^6 m^3 s^{-1}. The 1994–1997 and 2000–2007 mean anomalies and the 1994–2007 linear trend are shown. **(c)** Anomalies of the DWBC transport at Cape Farewell and the Labrador Sea Water (LSW) thickness in the Labrador Sea in the 1950s–2000s. **(d)** Correlation coefficient (R^2) for the two times series shown in **(c)** at the 0–5-year lag, the LSW thickness leads. The correlation maximum is achieved at the 1–3-year lag. The DWBC transport anomalies in the southern Irminger Sea are foregone by the convection intensity anomalies in the Labrador Sea. Adapted from [Sarafanov et al., 2009].

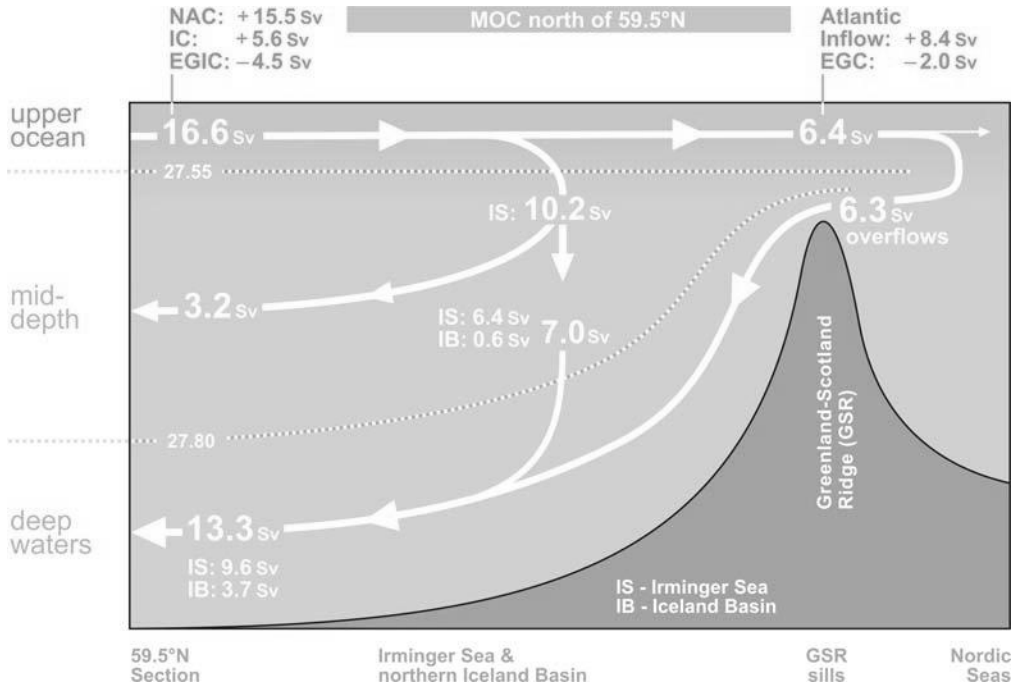

Figure 9. Schematic diagram of the Meridional Overturning Circulation (MOC) at the northern periphery of the Atlantic Ocean, northeast of Cape Farewell. The dotted lines refer to the σ_0 isopycnals 27.55 and 27.80. The arrows denote the integral meridional and diapycnal volume fluxes. Where the signs are specified, the positive (negative) transports are northward (southward). The NAC and EGIC transports in the upper layer ($\sigma_0 < 27.55$) at 59.5°N are the throughputs accounting for the recirculations. EGIC – the East Greenland / Irminger Current – refers to the upper part of the Western Boundary Current. Other abbreviations are explained in the legend to **Figure 3**. Adapted from [Sarafanov et al., 2012].

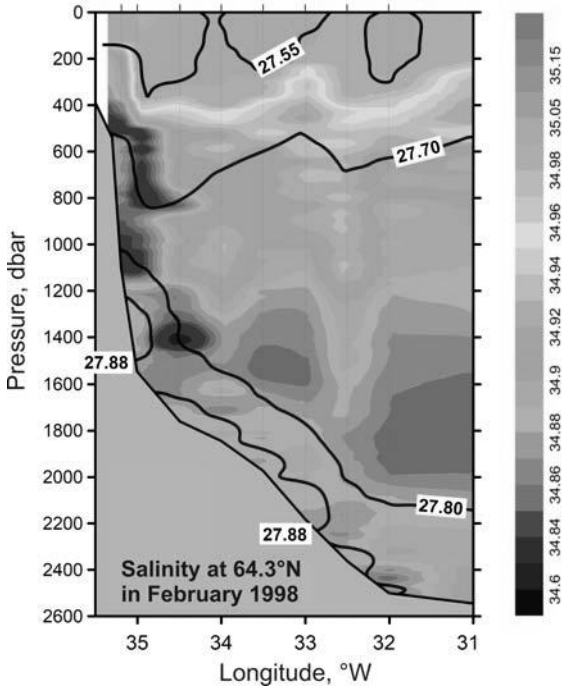

Figure 10. Salinity observed in the northwestern Irminger Sea at 64.3°N in February 1998. The σ_0 isopycnals 27.55, 27.70, 27.80 and 27.88 are plotted as the thick black lines; the station locations are marked with the ticks on the top axis. The plot shows fresh dense waters descending (cascading) down the continental slope of Greenland down to the LSW layer ($27.70 < \sigma_0 < 27.80$) and the layer of the Nordic Seas overflow-derived deep waters ($\sigma_0 > 27.80$). Adapted from [Falina et al., 2012].

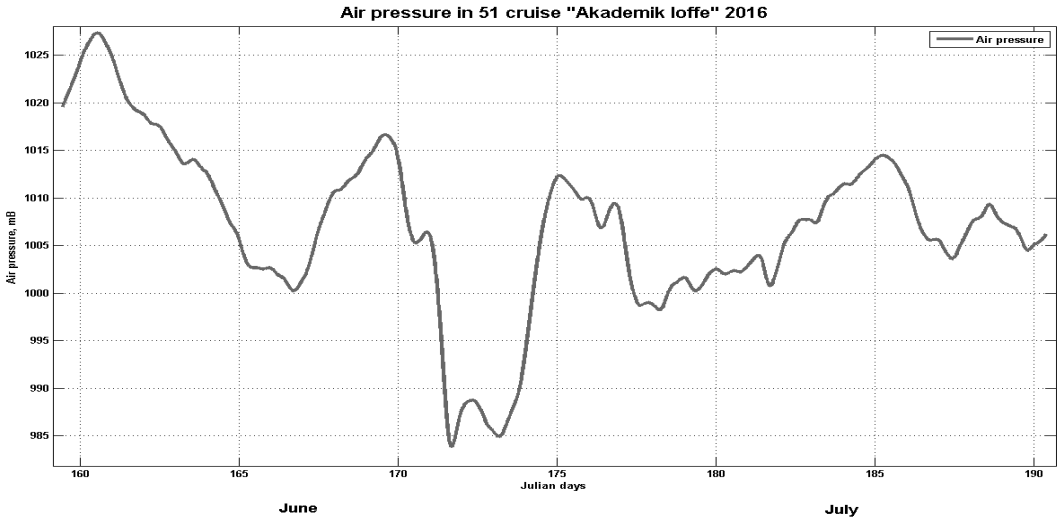

Figure 11. One-hour averaged atmospheric pressure (mb) measured during 51 cruise of Akademik Ioffe.

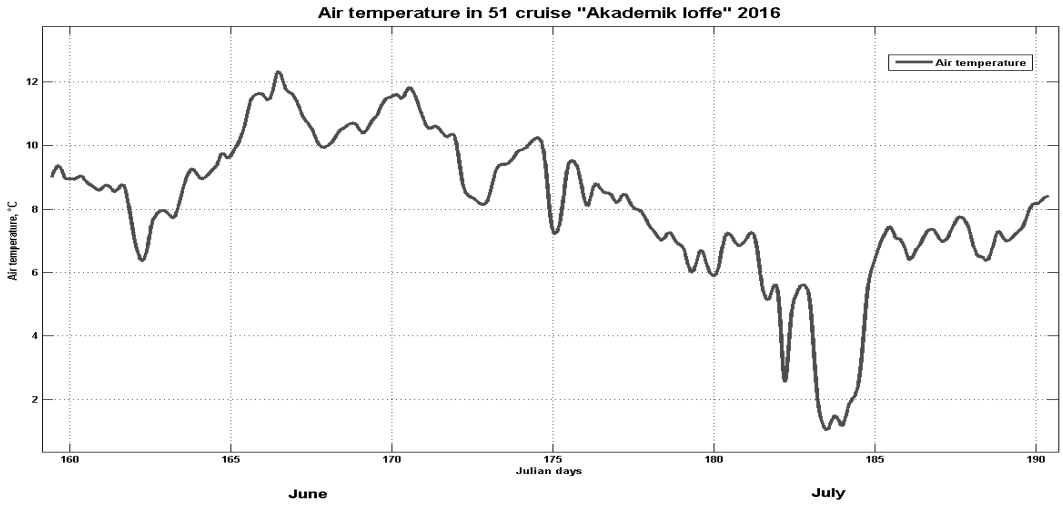

Figure 12. One-hour air temperature (°C) measured during 51cruise of Akademik Ioffe.

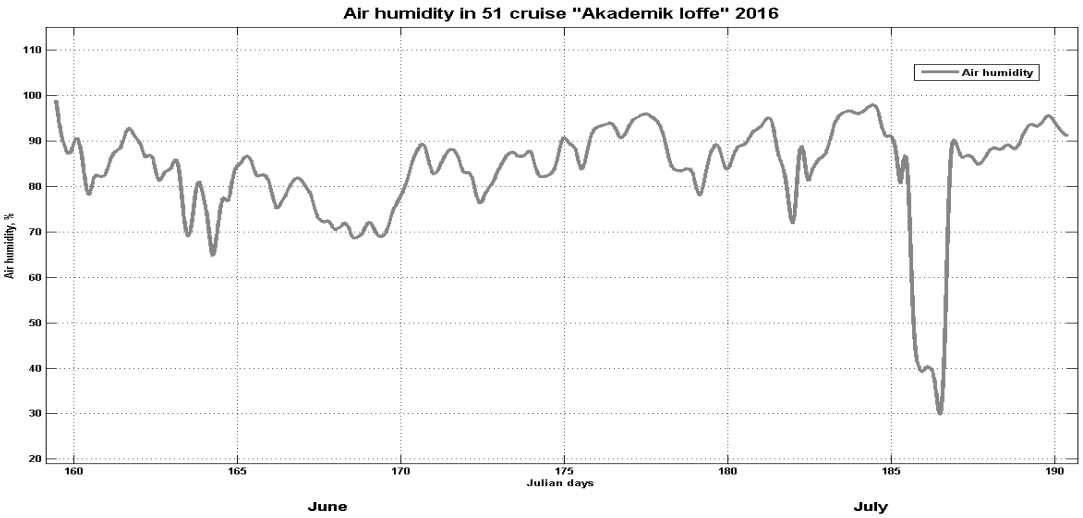

Figure 13. One-hour relative humidity (%) measured during 51 cruise of Akademik Ioffe.

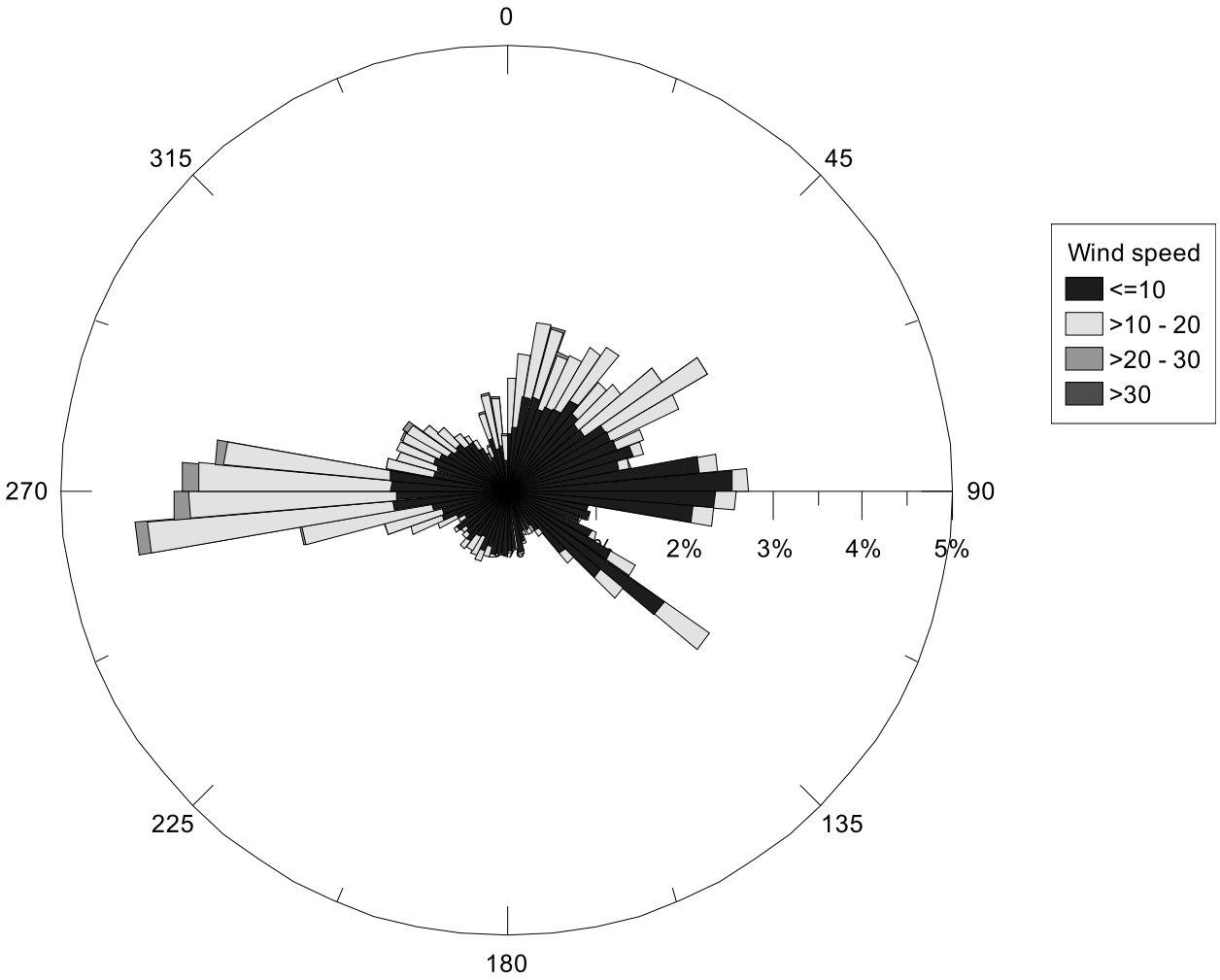

Figure 14. Wind speed and direction statistics during 51 cruise Akademik Ioffe.

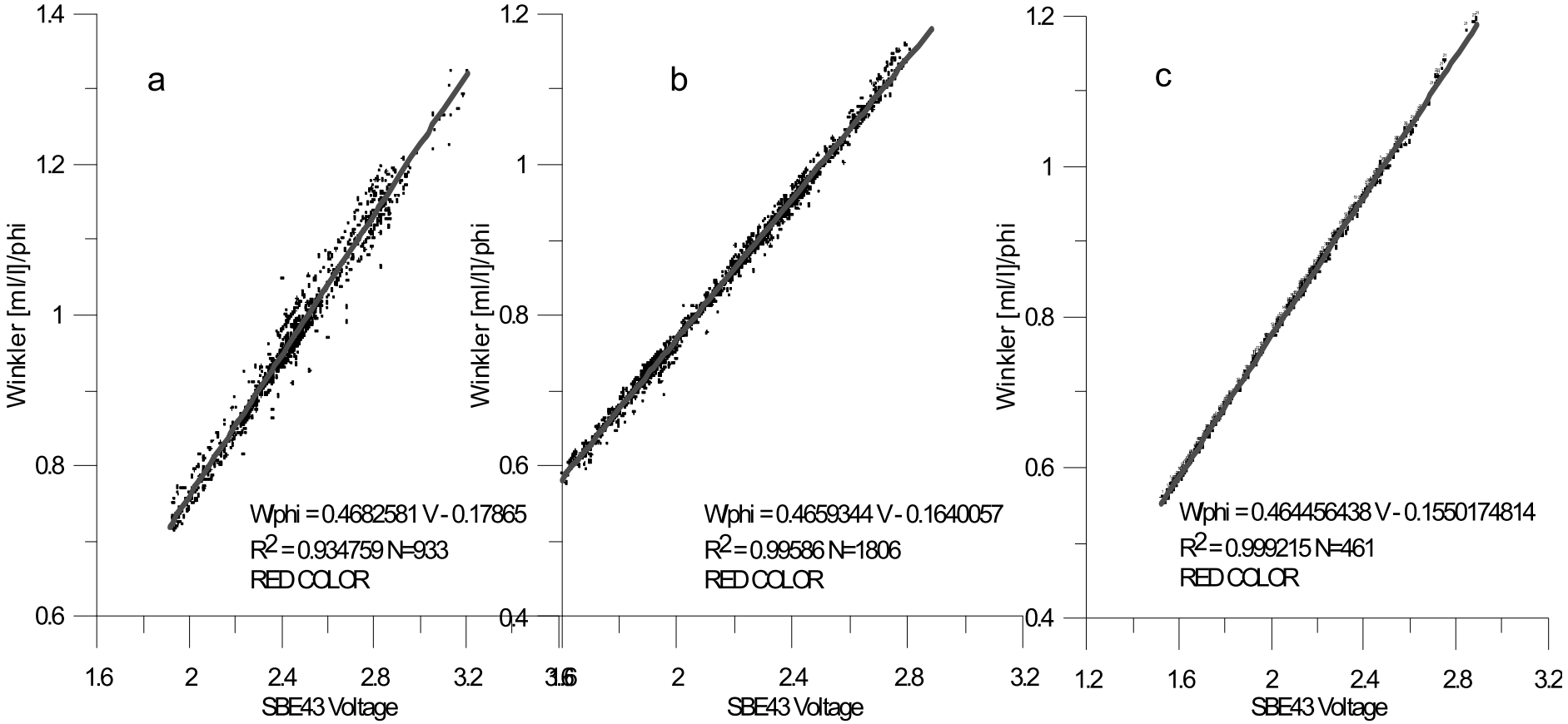

Figure 15 Regression lines for Winkler oxygen divided by φ versus SBE 43 output voltage for (a) sill sections (b) 59.5 section and (c) the Labrador Sea. Oxygen data collected at the East Greenland shelf is regressed separately.

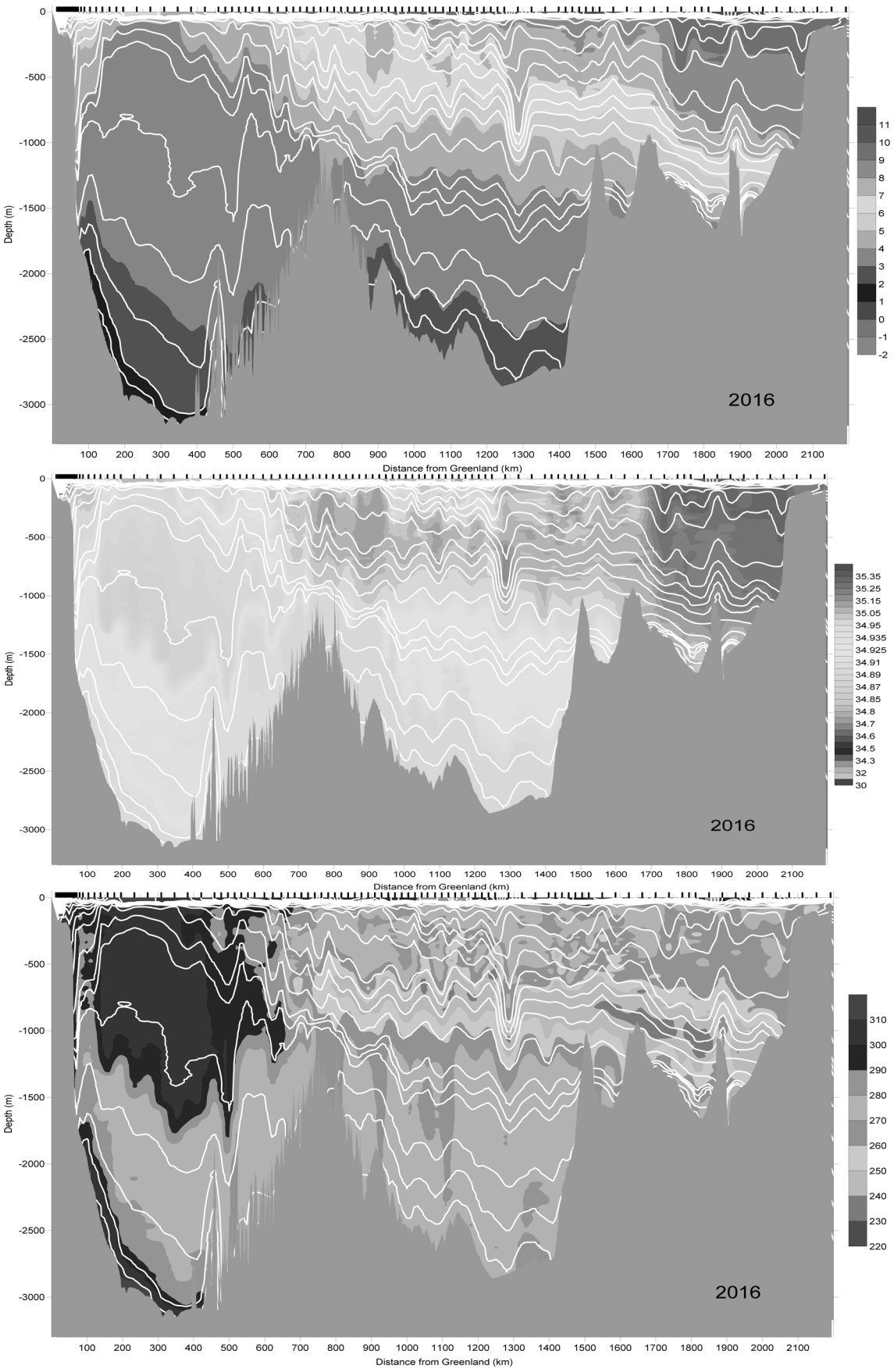

Figure 16 The vertical distribution of (a) potential temperature (°C) and (b) salinity and (c) CTD dissolved oxygen (μmol/kg) along 59.5 N in 16-29 June 2015. Density is shown in white. Station position is shown by vertical marks.

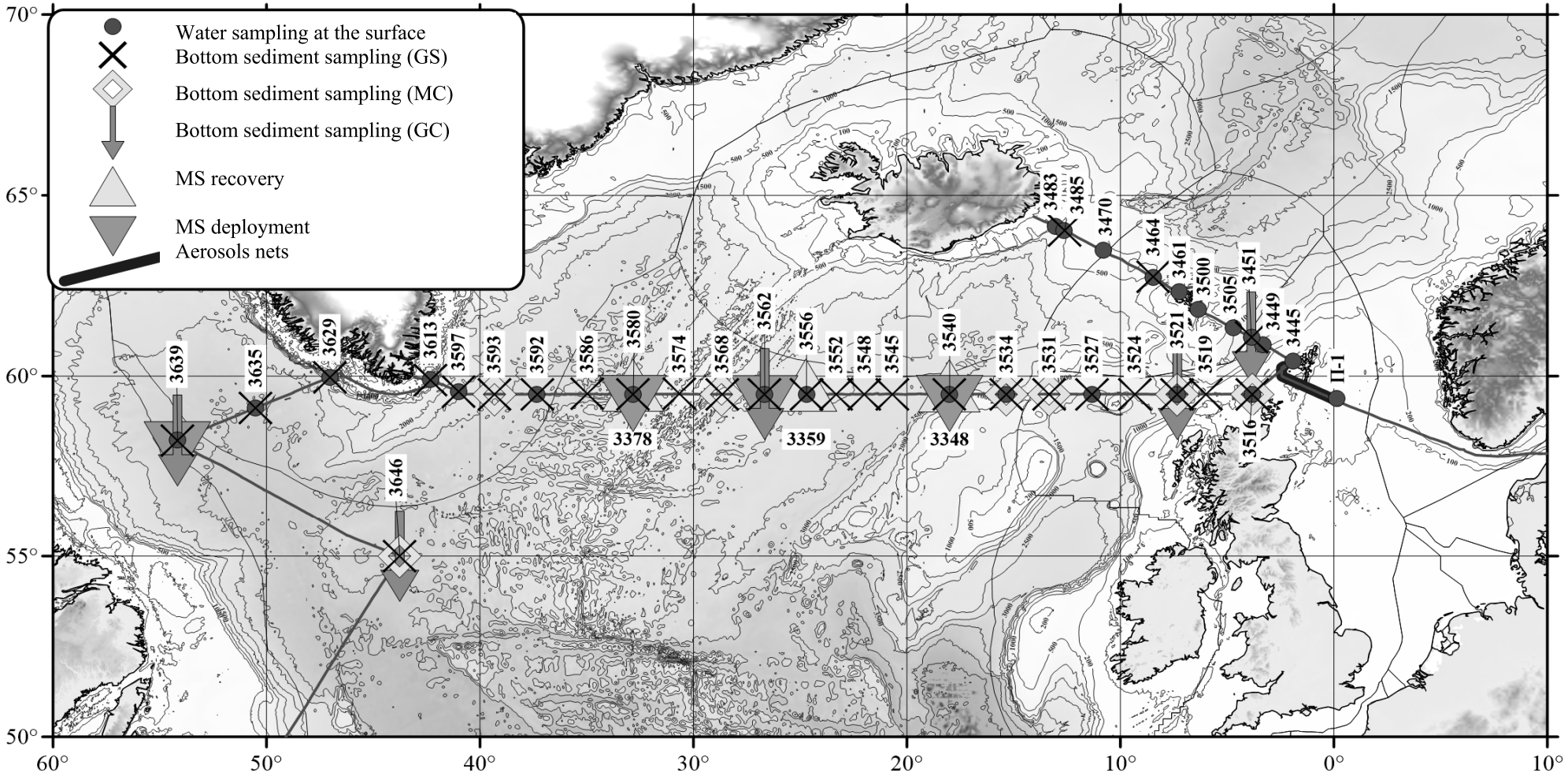

Figure 17. Chart of the geological stations in 51 cruise of RV Akademik Ioffe.

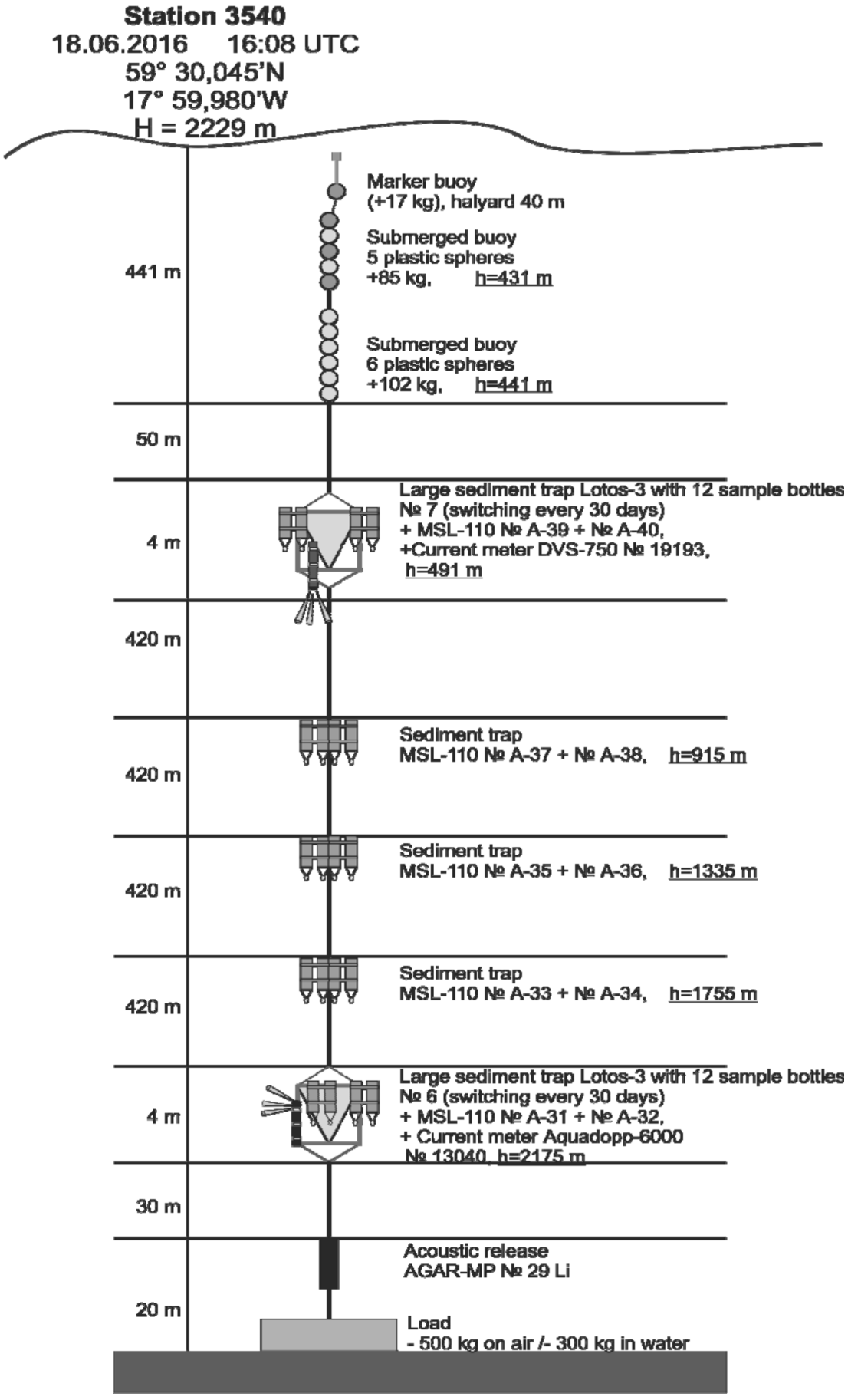

Figure 18. Mooring composition at sta. 3540.

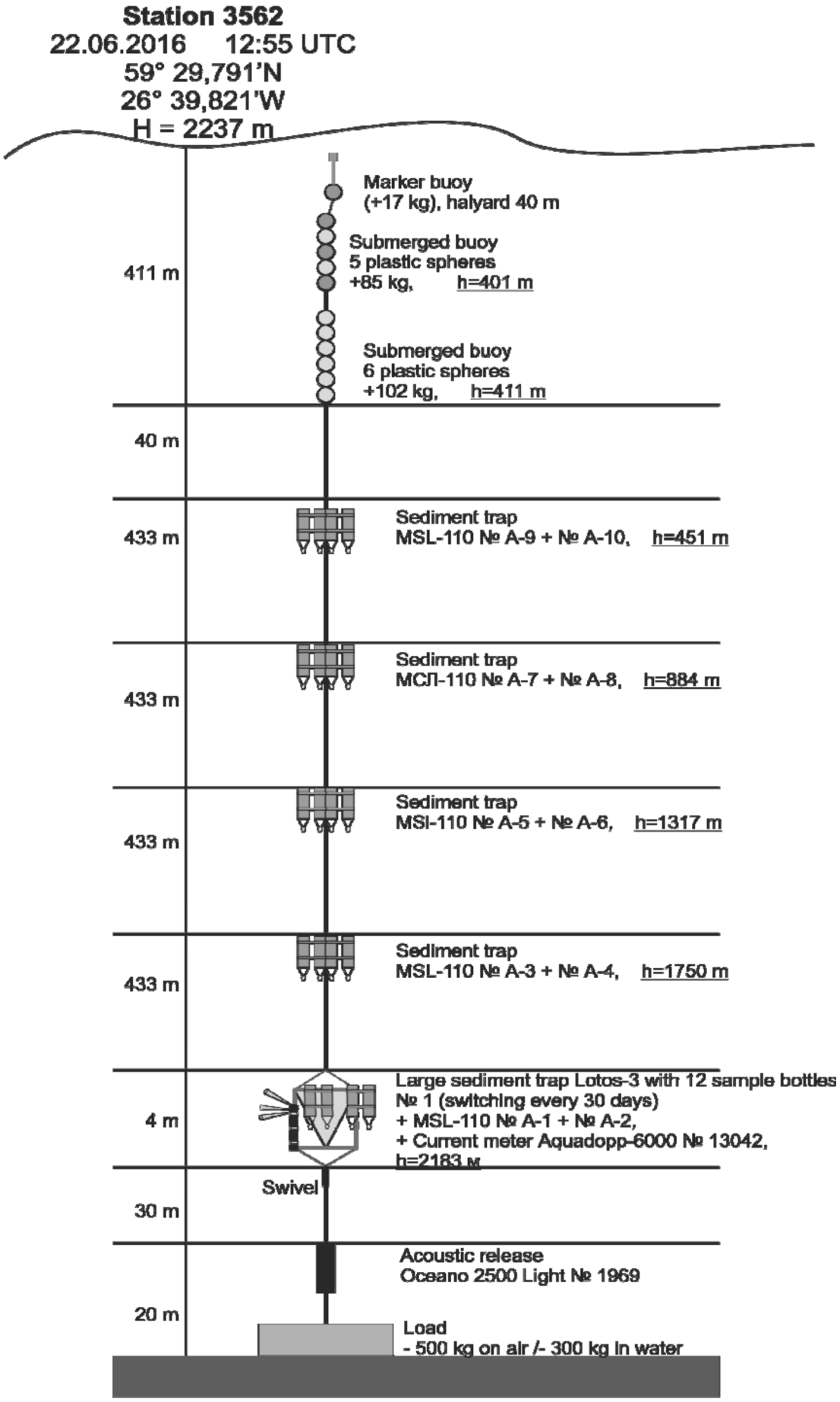

Figure 19. Mooring composition at sta. 3562.

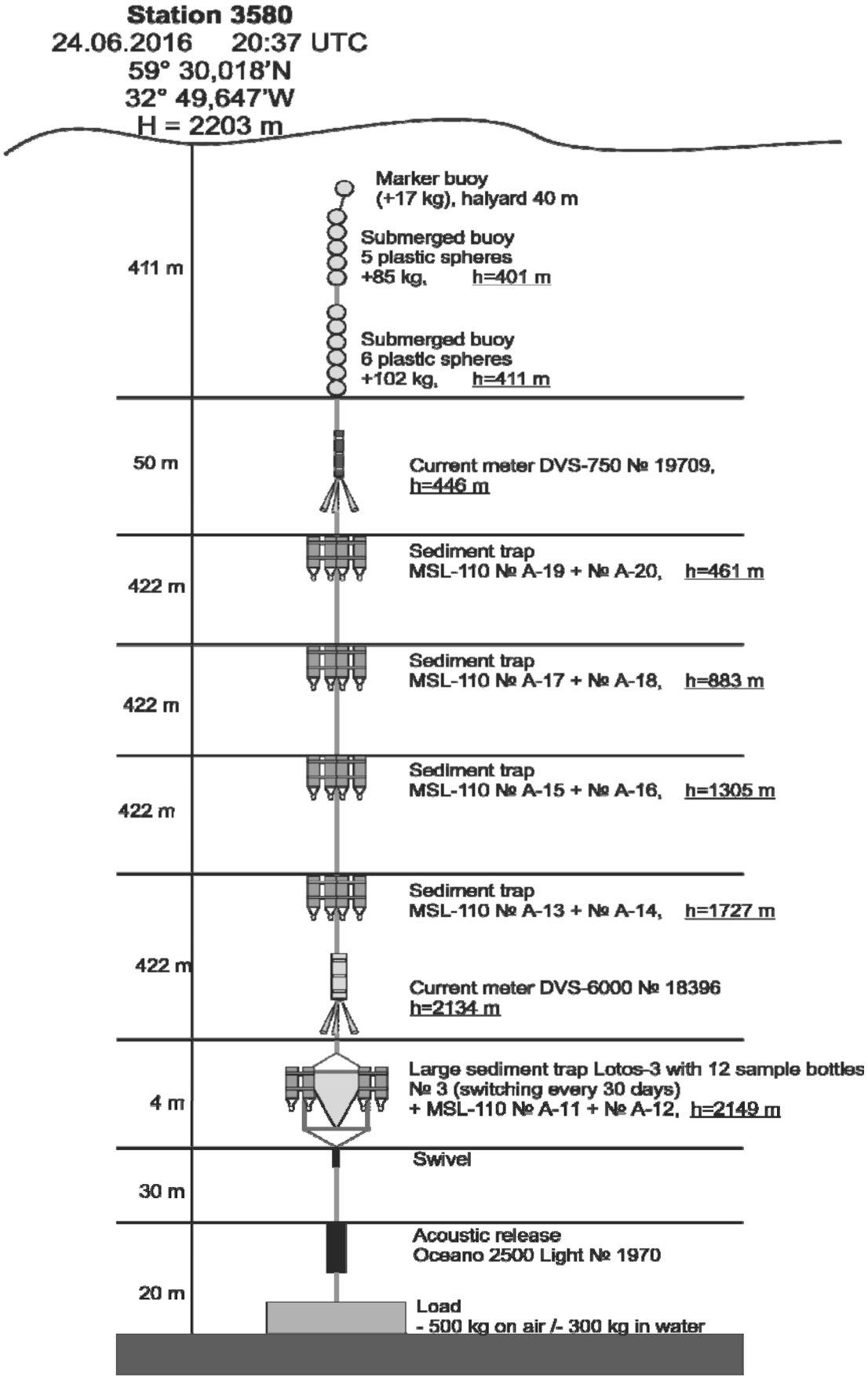

Figure 20. Mooring composition at sta. 3580.